

12-1995

## Geochemical evolution of a mid-miocene synextensional volcanic complex: The Dolan Springs volcanic field, northwestern Arizona

Scott Michael McDaniel  
*University of Nevada, Las Vegas*

Follow this and additional works at: <https://digitalscholarship.unlv.edu/thesesdissertations>

 Part of the [Geochemistry Commons](#), [Geology Commons](#), and the [Volcanology Commons](#)

---

### Repository Citation

McDaniel, Scott Michael, "Geochemical evolution of a mid-miocene synextensional volcanic complex: The Dolan Springs volcanic field, northwestern Arizona" (1995). *UNLV Theses, Dissertations, Professional Papers, and Capstones*. 1451.  
<http://dx.doi.org/10.34917/3434922>

This Thesis is protected by copyright and/or related rights. It has been brought to you by Digital Scholarship@UNLV with permission from the rights-holder(s). You are free to use this Thesis in any way that is permitted by the copyright and related rights legislation that applies to your use. For other uses you need to obtain permission from the rights-holder(s) directly, unless additional rights are indicated by a Creative Commons license in the record and/or on the work itself.

This Thesis has been accepted for inclusion in UNLV Theses, Dissertations, Professional Papers, and Capstones by an authorized administrator of Digital Scholarship@UNLV. For more information, please contact [digitalscholarship@unlv.edu](mailto:digitalscholarship@unlv.edu).

**Geochemical Evolution of a Mid-Miocene  
Synextensional Volcanic Complex: The  
Dolan Springs Volcanic Field,  
Northwestern Arizona**

by

Scott Michael McDaniel

A thesis submitted in partial fulfillment  
of the requirements for the degree of

Masters of Science

in

Geology

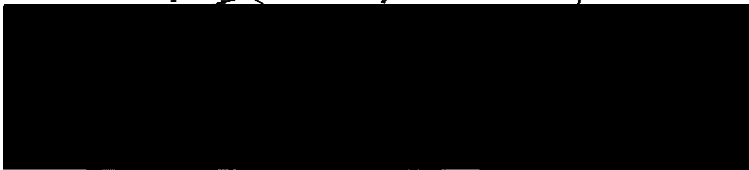
Department of Geoscience  
University of Nevada, Las Vegas  
December, 1995

© 1995 Scott Michael McDaniel  
All Rights Reserved

The thesis of Scott Michael McDaniel for the degree of Masters in Science in  
Geology is approved.



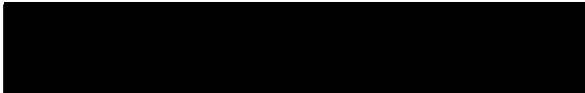
Chairperson, Rodney V. Metcalf, Ph.D.



Examining Committee Member, Eugene I. Smith, Ph.D.



Examining Committee Member, Wanda J. Taylor, Ph.D.



Graduate Faculty Representative, Donna Weistrop, Ph.D.

---

Interim Graduate Dean, Cheryl Bowles, Ed.D.

University of Nevada, Las Vegas  
December, 1995

## Abstract

The Dolan Springs volcanic field (DSV), of northwestern Arizona, is dominated by andesite and basaltic-andesite flows and breccias, with minor amounts of basalt, rhyolite, and ash-flow tuff. Geochemistry is used here as a tool to evaluate the roles and contributions of the lithospheric and asthenospheric mantles to magmatism related to Miocene extension in the Colorado River extension corridor (CREC). The majority of synextensional volcanic rocks in the DSV are geochemically similar to regional trends, but rare tholeiitic basalts erupted near the end of extension. The tholeiites have trace element signatures similar to ocean island basalt (OIB), but have isotopic values indicative of a source in the lithosphere. The tholeiites represent the endpoint in a progressive decrease in the depth of lithospheric melting (22-8 Ma) that occurs just prior to the onset of asthenospheric volcanism at 6 Ma. Using geochemical arguments, models are presented here for trace element stratification in the lithospheric mantle and magma genesis in the CREC.

## Table of Contents

Abstract.....	iii
List of Figures.....	vi
List of Tables.....	vii
List of Plates.....	vii
Acknowledgments.....	viii
CHAPTER 1 INTRODUCTION AND GEOLOGIC BACKGROUND .....	1
Introduction and Purpose.....	1
Location and Region Description.....	2
Geologic Background and Previous Work.....	3
CHAPTER 2 STRATIGRAPHY OF THE DOLAN SPRINGS	
VOLCANIC FIELD.....	9
Introduction and Methods.....	9
Stratigraphy of the Northern Dolan Springs Volcanic Field .....	10
Tertiary gravel conglomerate unit 1 .....	10
Tertiary andesite/tuff of Rodeo Grounds.....	11
Tertiary gravel conglomerate unit 2.....	13
Tertiary tuff of Table Mountain.....	14
Tertiary basalt of Table Mountain.....	15
Stratigraphy of the Southern Dolan Springs Volcanic Field.....	16
Culdesac rhyolite complex.....	16
Tertiary andesite of Alta Spring.....	20
Tertiary andesite of Powerline Road .....	20
Tertiary gravel unit 3 .....	21
DSV Chronology.....	22
CHAPTER 3 STRUCTURAL GEOLOGY OF THE DOLAN SPRINGS	
VOLCANIC FIELD.....	27
Tilted Strata and Angular Unconformities.....	27
Faults .....	28
CHAPTER 4 ERUPTIVE, DEPOSITIONAL AND TECTONIC HISTORY	
OF THE DOLAN SPRINGS VOLCANIC FIELD .....	31
Pre-extension History.....	31
Synextension History.....	33

A Possible Synextension Caldera Near DSV.....	35
Post-peak extension History .....	36
CHAPTER 5 GEOCHEMISTRY OF THE DOLAN SPRINGS VOLCANIC	
ROCKS.....	37
Introduction.....	37
Classification and Normative Mineralogy.....	37
Major Elements.....	39
Trace Elements .....	40
Isotopic Geochemistry.....	41
CHAPTER 6 MAGMATIC HISTORY OF THE DSV AND THE	
NATURE OF THE CREC MANTLE.....	51
Introduction.....	51
Introduction to DSV Magmatic History.....	53
Discussion of the Origin of Mafic Magmas .....	55
Synextensional Magmatism.....	55
Postextensional Magmatism.....	58
The Mt. Perkins Pluton - A Source for DSV?.....	71
Trace Element Enrichment and the Nature of the Lithospheric Mantle.....	74
Timing of Trace Element Enrichment and Model Ages.....	74
Stratification of Trace Element Abundances in the Mantle.....	77
Model for the Tectonic and Magmatic Evolution of the DSV and CREC .....	80
Model for Mantle Enrichment.....	80
Three Phase Model for CREC Magma Genesis.....	82
Phase I - Pre-extension Onset of Magmatism to 12 Ma.....	83
Phase II - Postextension 12-9 Ma.....	84
Phase III - Postextension 9-4 Ma.....	84
Summary.....	87
Appendix A.....	89
Appendix B.....	101
Analytical Techniques .....	101
References.....	106

## List of Figures

Figure 1-1.	General geologic Map of northwestern Arizona.	8
Figure 2-1.	Schematic stratigraphic cross-sections of the northern and southern Dolan Springs volcanic field (DSV).	25
Figure 2-2	Map delineating southern and northern sections of the DSV.	26
Figure 5-1.	Classification diagrams for the DSV volcanic rocks.	43
Figure 5-2	Na <sub>2</sub> O versus K <sub>2</sub> O diagram for the DSV volcanic rocks.	44
Figure 5-3	Harker variation diagrams for the DSV volcanic rocks.	45
Figure 5-4	Chondrite normalized REE diagrams for the DSV rocks.	46
Figure 5-5	Primordial mantle normalized trace element diagrams.	48
Figure 5-6	$\epsilon_{Nd}$ vs. $^{87}Sr/^{86}Sr_{(i)}$ diagram for the DSV rocks.	49
Figure 5-7	$\epsilon_{Nd}$ and $^{87}Sr/^{86}Sr_{(i)}$ vs. SiO <sub>2</sub> diagrams for the DSV rocks.	50
Figure 6-1	$\epsilon_{Nd}$ vs. $^{87}Sr/^{86}Sr_{(i)}$ diagram for the CREC.	65
Figure 6-2	Primordial mantle normalized trace element diagrams comparing synextensional CREC rocks.	66
Figure 6-3	$\epsilon_{Nd}$ vs. age for CREC rocks.	67
Figure 6-4	Primordial mantle normalized trace element diagrams of the CREC tholeiitic rocks.	68
Figure 6-5	Discrimination plot of CREC tholeiites.	69
Figure 6-6	Incompatible element plot of DSV, Golden Door volcanic section, and the Mt. Perkins pluton.	73
Figure 6-7	Total REE vs. age for CREC rocks.	79
Figure 6-8	Schematic three phase model for magma genesis in the CREC.	86



## List of Tables

Table 5-1	Isotopic variation for the DSV rocks.	47
Table 6-1	Summary of models for the CREC tholeiites.	70
Table 6-2	Averaged model mantle ages ( $T_{DM}$ ) for the DSV rocks.	76
Table A-1	Major and trace element analyses of the DSV rocks.	90
Table A-2	Analyses from Morikawa (1993 and unpublished data).	96
Table A-3	Normative mineralogy of the DSV rocks.	97
Table A-4	Normative mineralogy of Morikawa data (1993 and unpublished data).	100
Table B-1	Summary of analytical procedures by stratigraphic unit.	104
Table B-2	Accuracy of the XRF major elements.	104
Table B-3	Accuracy of the XRF trace elements.	104
Table B-4	Accuracy of the INAA trace elements.	105

## List of Plates

Plate I	Geologic map of the DSV.	in pocket
Plate II	Geologic cross-sections of the DSV.	in pocket
Plate III	Geochemical sample location map for the DSV.	in pocket

## Acknowledgments

I would like to thank my committee, Gene Smith, Wanda Taylor, and Donna Weistrop, for technical reviews and helpful discussions, and particularly Rod Metcalf for his extra time and willingness to help. I also appreciate Gene Yogodzinski for his helpful discussions on models. I am grateful for my friends Jim and Brinn Struthers and Maureen Stuart, who made it tolerable for me to stay and get this thing done during some hard times. Thanks to Shirley Morikawa for the radiometric date she obtained on a DSV tuff, and for helpful chemical analyses. I am indebted to Michael Wells for the use of his printer. I appreciate the financial support I received from Rod Metcalf, the Center for Volcanic and Tectonic Studies, the Geological Society of America, the Graduate Student Association, the Bernada E. French Scholarship Fund, and the Scroungers Scholarship Fund. A special thanks goes to Charlene Morrison who was a pleasant, though distracting encouragement in the final months of writing. She probably learned more about geology than she cared to while coloring my maps. And a final word to the wise... "Friends don't let friends do Grad school!"

# **CHAPTER 1**

## **Introduction and Geologic Background**

### **Introduction and Purpose**

Magmatism is associated with Cenozoic lithospheric extension in the Basin and Range Province. The geochemistry of synextensional magmatic rocks is key to understanding the relationship between magmatism and extension and magma genesis. In this study, the stratigraphy, structure, and geologic history of a Miocene volcanic complex provide a context in which to examine geochemical changes during the course of extension. In particular, this study focuses on the relative roles and contributions of the lithosphere and asthenosphere to synextensional magmatism.

In northwestern Arizona, volcanic rocks make up most of the accessible Miocene magmatic record. Exposures of synextensional plutons are rare except in the more highly dissected areas such as the Colorado River extensional corridor (CREC; Howard and John, 1987). This study investigates the Dolan Springs volcanic field (DSV) which lies in the northern part of the CREC in the southern White Hills, of northwestern Arizona (Fig. 1-1). The DSV is dominated by andesite and basaltic-andesite flows and breccias, with minor amounts basalt, rhyolite, and ash-flow tuff.

Synextensional rocks of the DSV share the trace element and isotopic characteristics of other CREC synextensional rocks that are thought to have an

origin in the lithospheric mantle. The DSV fits in a well established regional geochemical framework of synextensional volcanic rocks, but also includes a unique group of tholeiitic basalts that figure prominently into a model presented here for magma genesis during crustal extension. A literature survey identified other chemically and spatially similar tholeiitic basalts in the CREC which are also used in developing the model.

The first chapter of this thesis briefly describes the geologic background and previous work near the DSV. The second, third, and fourth chapters describe the stratigraphy, structure, and geologic history of the volcanic field. Major element, trace element, and isotopic geochemistry of the DSV rocks are presented in Chapter 5. Finally, chapter 6 discusses the origin of mafic magmas and the trace element character of the mantle. Chapter 6 finishes by presenting models for trace element enrichment of the lithospheric mantle and magma genesis in the CREC.

### **Location and Region Description**

The Dolan Springs volcanic field (DSV) is in the southern White Hills, northwestern Arizona, 50 km south of Lake Mead (Fig. 1-1). The study area is roughly defined by a triangle with legs along US Highway 93, the Pearce Ferry Road, and the White Hills Road (Fig 1-1, Plate I). North of the DSV is the central White Hills, an area dominated by Precambrian metamorphic basement. In the northern White Hills the Tertiary volcanic section crops out in the upper plate of a low-angle normal fault (Cascadden, 1991). The DSV is bordered to the west by Detrital Valley and the central Black Mountains. The

northern Black Mountains are dominated by Precambrian metamorphic rock. In the central Black Mountains the metamorphic basement is intruded by several Tertiary plutons and overlain by Tertiary volcanic rocks. To the south of the DSV are the Cerbat Mountains composed dominantly of Precambrian metamorphic rocks and Mesozoic intrusions. At the extreme northern end of the Cerbats, just south of the DSV, is a several kilometer thick section of Tertiary volcanic and volcanoclastic rocks. The dry Red Lake separates the eastern edge of the DSV from the Grand Wash Cliffs. The latter marks the eastern limit of extension and the edge of the Colorado Plateau and Paleozoic and Mesozoic sedimentary rocks.

### **Geologic Background and Previous Work**

The DSV lies on the eastern edge of the CREC, a 50-100 km wide zone of large magnitude mid-Miocene extension that follows the Colorado River from Lake Mead south to the Whipple Mountains (Howard and John, 1987; Weber and Smith, 1987; Duebendorfer et al., 1990; Faulds et al., 1990; Faulds et al., 1994). Regional-scale low-angle detachment faults, strike-slip faults, and associated upper plate high-angle normal faults accommodated extension across the CREC (e.g., Anderson, 1971; Meyers, 1984; Weber and Smith, 1987; Duebendorfer et al., 1990; Cascadden, 1991). The net displacement of the Colorado Plateau relative to the Sierra Nevada along a transect parallel to the direction of extension ( $S73^{\circ}\pm 12^{\circ}E$ ) has been estimated at  $247\pm 56$  km near the latitude of Las Vegas (Wernicke et al., 1988). This transect is presently 360 km wide. The stretching factor,  $\beta$  (extended length/original length), is approximately 3 for the entire transect with much higher  $\beta$  locally (Wernicke

et al., 1988).

In the Mt. Perkins block (Fig. 1-1), a portion of the Black Mountains west of the DSV and Detrital Valley, the age of extension is bracketed between 15.7 and 11.3 Ma with peak extension between 15.2 and 14.3 Ma (Faulds et al., 1995). The age and duration of extension in the DSV is similar to that in the Mt. Perkins block, though extension in the former appears to have begun slightly earlier, between 17.98 and 16.09 Ma (see Chapters 2 and 3).

Faulds et al. (1990) delineated a structural accommodation zone that begins in the northern Black Mountains and runs southeast through the DSV. In the northern Black Mountains the accommodation zone is a wide zone of complex splaying faults separating east-tilted strata and west dipping normal faults to the north from west-tilted strata and east dipping normal faults to the south. Where it intersects the western DSV the accommodation zone narrows to an anticlinal structure. In the DSV the division between these east and west tilted domains runs north-south through a wash in sections 19, 18, and 7, T.26N., R.19W. (Plate I). The DSV is almost entirely in the east tilted limb of the accommodation zone.

Previous work in the White Hills concentrated on the northern and central sections. Meyers (1984) mapped the regionally extensive Miocene Cyclopic Mine detachment fault in the central White Hills and documented two periods of gold mineralization in Precambrian rocks: one Precambrian in age and a second associated with the Tertiary detachment fault. In the northern White Hills, Cascadden (1991) described three coeval Miocene volcanic centers in the upper plate of the Salt Spring detachment fault, a

continuation of the Cyclopic Mine fault. These detachment complexes lie 20-30 km west of the Grand Wash Fault and represent the easternmost extensional allochthon of the Basin and Range Province.

Volcanic rocks dominate the Miocene depositional record in the CREC. In the CREC at least 27 Miocene volcanic centers and 10 plutons have been identified (Smith and Faulds, 1994). Volcanism swept northward through the CREC, beginning in the late Oligocene in the southern CREC and reaching the latitude of the DSV at approximately 20 Ma (Glazner and Bartley, 1984; Faulds et al., 1994; Faulds et al., 1995). Volcanism preceded the onset of extensional faulting by approximately 1-2 m.y. (Faulds et al., 1995).

As with most of the Miocene volcanic rocks in the Basin and Range Province, the CREC is dominated by intermediate calc-alkaline and alkalic-calcic suites. Primitive mafic rocks in these suites are typically alkali basalts. A number of recent studies of intermediate suites in the Basin and Range Province concluded that mixing of felsic crustally derived magmas and mafic mantle derived magmas was important to the production of intermediate rocks (Glazner, 1990; Larsen and Smith, 1990; Smith et al., 1990; Turner and Glazner, 1991). Magma mixing has been found to be a major process controlling the evolution of CREC calc-alkaline intrusive suites in the Wilson Ridge pluton (Larsen and Smith, 1990; Smith et al., 1990), the Mt. Perkins pluton (Metcalf et al., 1993; Metcalf et al., 1995), and the Aztec Wash pluton (Falkner, 1993; Falkner et al., 1995).

To understand the mechanisms of magma genesis and evolution, primitive basalts are often the focus of geochemical studies, because these

basalts are believed to be the parental mafic magmas which drive the processes forming the intermediate suites. Primitive basaltic volcanism in the CREC can be divided into two genetic and chronologic groups (Bradshaw, 1991; Fitton et al., 1991; Kempton et al., 1991, Bradshaw et al., 1993; Feuerbach et al., 1993). Pre-6 Ma basaltic volcanism which broadly coincides with extension is commonly alkalic, displays enriched isotopic ratios ( $\epsilon_{\text{Nd}} = -4$  to  $-11$ ;  $^{87}\text{Sr}/^{86}\text{Sr}_{(i)} = 0.705\text{-}0.710$ ), and has a source in the lithospheric mantle. A marked transition occurred at 6 Ma to asthenospherically derived alkali basalts with depleted isotopic ratios ( $\epsilon_{\text{Nd}} = -1$  to  $+7$ ;  $^{87}\text{Sr}/^{86}\text{Sr}_{(i)} = 0.703\text{-}0.705$ ). Fitton et al. (1991), Kempton et al. (1991), and Bradshaw et al. (1993) characterized the lithospherically derived basalts as having trace element signatures similar to that seen in subduction related settings. These rocks have large ion lithophile elements (LILE) and the light rare-earth elements (LREE) enriched relative to the high field strength elements (HFSE) and heavy rare-earth elements (HREE). In contrast, the basalts derived by melting of the asthenospheric mantle are less enriched in trace elements with less disparity between the LILE-LREE and HFSE-HREE, producing a signature typical of ocean island basalt (OIB). Although these patterns of volcanism are observed in the DSV, the DSV tholeiitic basalts constitute a previously unrecognized magma type in the CREC. These tholeiitic basalts, erupted during the latest phase of extension, have both an enriched isotopic signature denoting a source in the lithosphere, and OIB-like trace elements displayed by the later asthenospheric basalts. The geochemical characteristics outlined by other workers will be discussed in light of these new findings.

The volcanic history of the southern White Hills has not been studied



in detail. Chemical data from DSV rocks is restricted to several tuff analyses by Morikawa (1993) and a single basalt analysis by Bradshaw et al. (1993). During a regional study of the  $15.23 \pm 0.14$  Ma (Bridwell, 1991) tuff of Bridge Spring, Morikawa (1993) eliminated the possibility that a tuff in the DSV (named here tuff 2 of Culdesac Wash) was related to tuff of Bridge Spring. Morikawa (1993) based this observation on geochemistry, modal mineralogy, and radiometric dating. An  $^{40}\text{Ar}/^{39}\text{Ar}$  biotite age of  $16.09 \pm 0.15$  Ma was reported by Morikawa for pumice fragments of tuff 2 of Culdesac Wash (Sample Tct2-4.1, appendix A).

Morikawa (1990) suggested that tuff 2 of Culdesac Wash might be related to the  $15.96 \pm 0.06$  Ma Mt. Perkins pluton ( $^{40}\text{Ar}/^{39}\text{Ar}$ , biotite age; Faulds, 1993a) on the basis of the similar age and radiogenic isotope data. This proposed correlation is explored further here and is found to be permissive, but not compelling (Chapter 6). Faulds et al. (1995) suggested that the tilted Mt. Perkins block represents an exposed cross-section of a plutonic-volcanic system. Using geochemistry and field relationships, Faulds et al. (1995) correlated felsic phases in the Mt. Perkins pluton with the Golden Door volcanic rocks exposed to the west near the Colorado River (Fig. 1-1) structurally above the pluton.

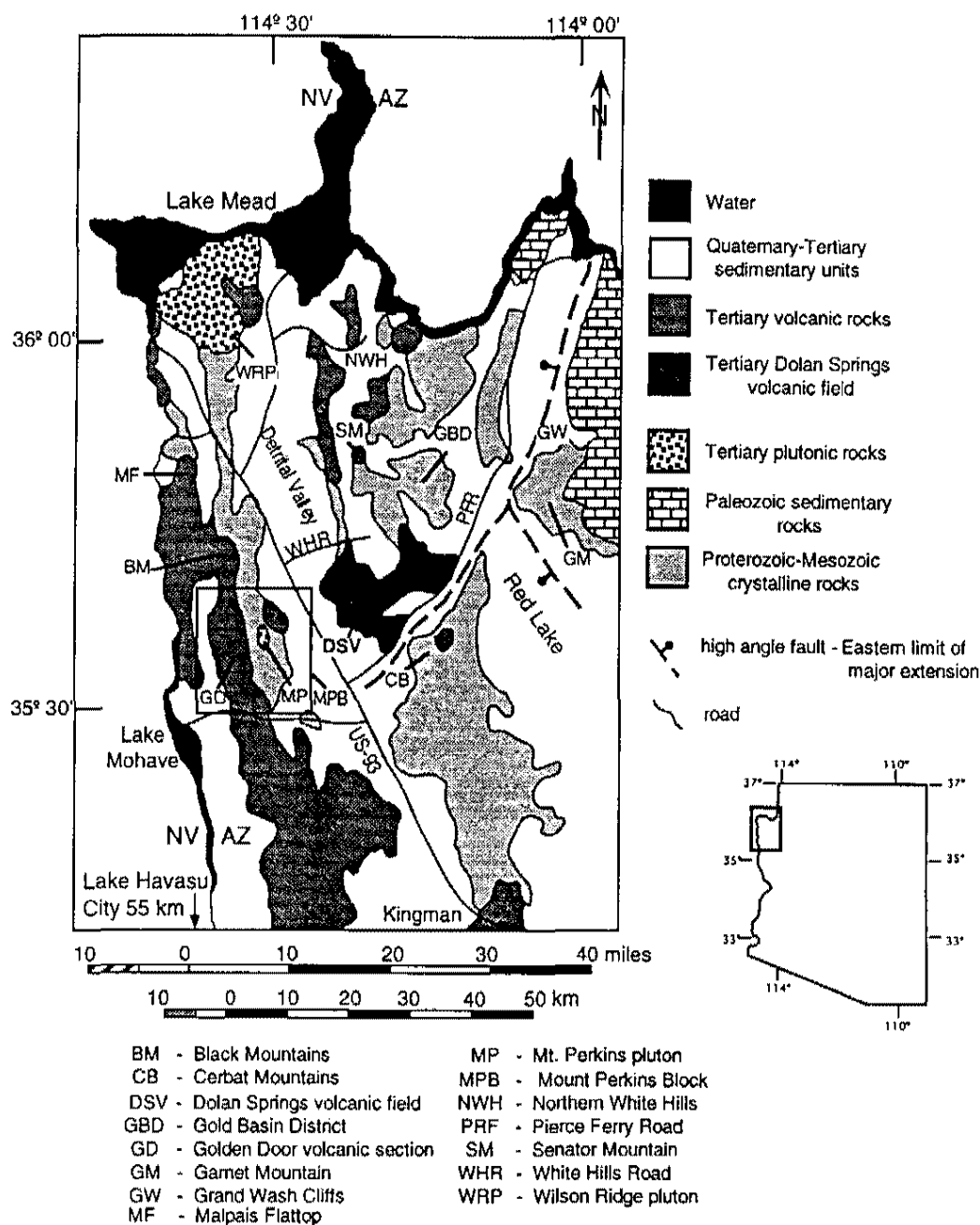


Figure 1-1. General geologic map of northwestern Arizona. Box outlines Mt. Perkins Block discussed in text. Modified from Reynolds et al. (1988), Faulds et al. (1990), and Faulds et al. (1995).

## **CHAPTER 2**

### **Stratigraphy of the Dolan Springs Volcanic Field**

#### **Introduction and Methods**

Miocene volcanic and sedimentary rocks in the Dolan Springs volcanic field (DSV) are divided here into nine stratigraphic units. Coarse-grained clastic sedimentary units both at the base and top of the section can not be dated but are inferred to be of Tertiary age. Quaternary deposits occupy modern drainages and contain detritus derived from the Tertiary section.

This chapter includes field and petrographic descriptions of the nine main units and their members. A total of 57 thin sections were examined and used to visually estimate the modal percentages of minerals and lithic fragments. Two different schematic stratigraphic columns are required because of differences in stratigraphy between the northern and southern parts of the study area (Fig. 2-1 & 2-2). A correlation between the two representative columns can be made for andesite of Rodeo Grounds based on field, petrographic and geochemical observations (Fig. 2-1). The stratigraphic sections are described in chronological order first for the northern section then the southern section. References to conformable contacts are based on the absence of angular unconformities and erosional features.

## Stratigraphy of the Northern Dolan Springs Volcanic Field

The northern DSV (Fig. 2-2) stratigraphic section is dominated by Tertiary conglomerates, including megabreccia blocks, and felsic to mafic lava flows.

### Tertiary gravel conglomerate unit 1 (Tg1)

The basal unit in the northern DSV is a poorly sorted, loosely to unconsolidated conglomerate named here the gravel conglomerate unit 1 (map unit Tg1, Plate I and Fig. 2-1). The conglomerate is composed primarily of sand and gravel, but also angular to rounded cobbles, boulders, and megabreccia clasts >30 m across. Clasts are exclusively Precambrian and Mesozoic(?) crystalline rocks including: quartzofeldspathic gneiss, muscovite-biotite schist, amphibolite, and Cretaceous(?) granitoids including muscovite-biotite granites (lithologically similar to nearby rocks radiometrically dated by Theodore et al., 1982). Gravel conglomerate unit 1 is distinguished from other DSV Tertiary sedimentary units based on the conspicuous absence of volcanic clasts.

Exposures of gravel conglomerate unit 1 are poor except where the megabreccia blocks provide large outcrops (30+ m across). Megabreccia blocks are sufficiently large to appear as outcrops of bedrock and are mapped as such on the Arizona Geological Survey's Geologic Map of Arizona (Reynolds, 1988). The megabreccia clasts are interpreted here as landslide blocks.

Gravel conglomerate unit 1 lies stratigraphically below the volcanic

rocks in the DSV. The only occurrence of volcanigenic rocks in gravel conglomerate unit 1 is a 3 m wide, 2 m thick channel fill of ash and small lithic fragments at 35°38'30" /114°20'00". The channel fill is graded and appears to be reworked rather than a primary volcanic rock. No other similar deposits were observed in gravel conglomerate unit 1.

The largest exposures of gravel conglomerate unit 1 are in the northern DSV south of the White Hills Road (Fig. 2-2). The upper contact of gravel conglomerate unit 1 appears to be conformable with the overlying andesite of Rodeo Grounds, but a lack of bedding makes it difficult to determine if dips fan below this contact. The total thickness of the unit is unknown because the lower contact is not exposed in the study area. If the dip is assumed to be the same as the overlying andesite ( $\approx 45^\circ$ ) then the exposed thickness is approximately 1400 m.

#### Tertiary andesite/tuff of Rodeo Grounds (Tra, Trt)

Overlying gravel conglomerate unit 1 is a set of dark-red to black and gray basalt, basaltic andesite, andesite, and dacite flows named here andesite of Rodeo Grounds (map unit Tra, Plate I and Fig. 2-1). The andesites and basaltic andesites are porphyritic (15-35% phenocrysts) with phenocryst assemblages dominated by plagioclase (10-30%) and clinopyroxene (5-15%), and by lesser amounts of orthopyroxene (<5%) and olivine (5-10%). Olivine is altered to reddish-brown iddingsite. In the andesites and basaltic andesites the amount of olivine increases inversely to the amount of clinopyroxene in the more mafic rocks while the amount of plagioclase phenocrysts remains fairly

constant relative to the ferromagnesian minerals. The matrix of these rocks is typically altered to fine-grained grayish opaque minerals. One sample of andesite contained abundant quartz xenocrysts and a xenolith of coarse-grained plagioclase and opaque oxides. Dacite flows are porphyritic (10-25 % phenocrysts) with plagioclase (10-20%) and hornblende (5-10%) with some clinopyroxene (<5%) and sanidine (0-10%) phenocrysts.

Lava flows are intercalated with reddish-brown debris flows containing exclusively volcanic clasts and matrix, and matrix-supported scoriaceous volcanic breccias. Breccia clasts are typically uniform in size (10-15 cm) while the debris flows have clasts up to 3 m in diameter. Three isolated lens (< .5 km<sup>2</sup>, 20 m thick) of a tan dacitic tuff were found only within the southern section of andesite of Rodeo Grounds (Fig. 2-2). These lens was mapped separately as tuff of Rodeo Grounds (map unit Trt, Plate I and Fig. 2-1). This tuff is bound above and below by debris flows that grade vertically up and down into lava flows (possibly auto-brecciated). The tuff is moderately welded, lithic-rich (dacite and andesite clasts), well-bedded, poorly sorted, and contains little pumice.

Andesite of Rodeo Grounds is the most voluminous and widespread unit in the study area. Individual lava flows and breccia rarely exceed 10-20 m in thickness and appear conformable but are laterally discontinuous. The estimated minimum total thickness of the andesite of Rodeo Grounds is 1400 m. The thickness was measured from the map across the largest continuous section where flow foliations allow attitude measurement, but is a minimum estimate because upper and lower contacts are not exposed in that section. The base of the andesite of Rodeo Grounds is only exposed in the northern

part of the study area where it conformably overlies the coarse gravels of the pre-volcanic gravel conglomerate unit 1. Andesite of Rodeo Grounds reaches its maximum exposed thickness ( $> 1$  km) in the southern part of the field area and thins to  $<20$  m near the Table Mountain Plateau to the north (Plate I). The thickness estimate of andesite of Rodeo Grounds in the southern section may be overestimated because the unit may be repeated by normal faults

### Tertiary gravel conglomerate unit 2 (Tg2)

Unconformably overlying the andesite of Rodeo Grounds is a conglomerate named here gravel conglomerate unit 2 (map unit Tg2, Plate I and Fig. 2-1). This unit includes two lithologically different sections. The first, making up the lower two-thirds of the unit is a poorly sorted, moderately to unconsolidated conglomerate composed primarily of sand and gravel, but also containing rounded to angular cobbles, boulders, and megabreccia clasts  $>20$  m across. The remaining approximately upper one-third of the unit, exposed below Table Mountain Plateau, is a cross-bedded, coarse sand and gravel conglomerate. Bedding within the upper portion strikes  $N12^{\circ}W$  to  $N15^{\circ}E$  and dips east, with dips decreasing up section from approximately  $30-40^{\circ}$  near the base to  $12^{\circ}$  below the capping basalt. A dark-red paleosol on top of the uppermost gravel directly underlies the basalt of Table Mountain. It is impossible to determine if the upper and lower portions of gravel conglomerate unit 2 are conformable due to the poor exposures below the cross-bedded sections.

Clasts in gravel conglomerate unit 2 are of both Precambrian and

Cretaceous(?) lithologies similar to gravel conglomerate unit 1, but also include andesitic rocks similar to the underlying andesite of Rodeo Grounds. Gravel conglomerate unit 2 is distinguished from gravel conglomerate unit 1 by the presence of these volcanic clasts. Megabreccias in gravel conglomerate unit 2 exhibit the same range of clasts lithologies and are interpreted as landslide deposits. Gravel conglomerate unit 2 is poorly exposed, except for the large megabreccia blocks and the upper cross-bedded conglomerate.

This unit crops out predominately in the northern DSV (Fig. 2-2) where it reaches an estimated maximum thickness of 1250 m (calculated assuming an average dip of 30°). The unit thins to the south. An isolated outcrop in the southern DSV that is approximately 80 m thick.

#### Tertiary tuff of Table Mountain (Ttmt)

Contained within the lower part of gravel conglomerate unit 2 is a lens of pale yellow to chalky white ash-flow tuff named here tuff of Table Mountain (map unit Ttmt, Plate I and Fig. 2-1). The lower half of the tuff is poorly to non-welded, and the upper portion is moderately-welded. The tuff contains small lithic fragments of andesite and rhyolite (<2 mm), abundant small pumice fragments (<4 mm), and phenocrysts of sanidine (15-20%) and biotite (<5%). This unit lies within gravel conglomerate unit 2 and forms a prominent north-south trending ridge in the extreme northern part of the field area that continues to the north of the mapped area (Plate I). Tuff of Table Mountain reaches a maximum thickness of 25 m in the study area, but pinches out south of the Table Mountain Plateau.



### Tertiary basalt of Table Mountain (Ttmb)

Overlying gravel conglomerate unit 2 and capping the northern DSV section (Fig. 2-2) are porphyritic (10-15% phenocrysts) vesicular tholeiitic basalt flows named here the basalt of Table Mountain. The basalt contains phenocrysts of olivine (5-8%), clinopyroxene (5-8%), and plagioclase (5-10%). The groundmass is made up of clinopyroxene, fine laths of plagioclase and opaque oxides. Both plagioclase phenocrysts and matrix crystals display a weak trachytic texture. Plagioclase and clinopyroxene phenocrysts are commonly found as glomerocrysts. Although the basalt of Table Mountain contains abundant amygdules filled with calcite, it is the least altered of any volcanic unit at the DSV.

Basalt of Table Mountain consists of 2-5 m thick flows with no intervening soil horizons. The minimum thickness of the basalt of Table Mountain was estimated in the field to be approximately 100 m suggesting the unit is composed of between 20-50 individual flows. The unit occurs only in the northwestern part of the study area forming the Table Mountain Plateau, the most physiographically prominent feature in the field area. Table Mountain Plateau should not be confused with the nearby Table Mountain which lies approximately 12 km east of the plateau on the east side of the Pearce Ferry Road (Plate I).

## Stratigraphy of the Southern Dolan Springs Volcanic Field

Two of the units present in the northern stratigraphic section correlate with units in the southern section, specifically gravel conglomerate unit 1 and andesite of Rodeo Grounds (Fig. 2-1). A description of these units is not repeated here. A major feature of the southern DSV (Fig. 2-2) is a package of rhyolitic lavas and pyroclastic flows collectively named here the Culdesac rhyolite complex.

### Culdesac rhyolite complex

A complete section of the Culdesac rhyolite complex crops out only in a single wash, here named Culdesac Wash, in sections 19 and 30, T.26N., R.19W. (Fig. 2-2 and Plate I), though individual tuff units continue outside the wash. The lower contact of the Culdesac rhyolite complex lies unconformably over tilted flows of andesite of Rodeo Grounds, but no angular unconformities are present between units of the complex.

### Tertiary tuff 1 of Culdesac Wash (Tct1)

The basal unit of the Culdesac rhyolite complex is a yellowish-gray, poorly-welded, pumice-rich, lithic tuff named here tuff 1 of Culdesac Wash (map unit Tct1, Plate I and Fig. 2-1). It contains abundant chalky-yellow zeolitized pumice fragments (< 2 cm) and abundant subangular lithic fragments (rhyolite and andesite). The matrix has eutaxitic ash shards and is moderately devitrified.

Phenocrysts phases include sanidine (1-3%), plagioclase (<2%), biotite

(<<1%), and opaque oxides (<1%). Tuff 1 of Culdesac Wash is approximately 30 m thick (estimated from the map). Tuff 1 of Culdesac Wash is distinguished from the tuff of Table Mountain by the presence of zeolitized pumice that the latter lacks.

### Tertiary rhyolite flows of Culdesac Wash (Tcr)

Discontinuous flows chemically transitional between rhyolite and dacite overlie tuff 1 and are named here the rhyolite flows of Culdesac Wash (map unit Tcr, Plate I and Fig. 2-1). The flows have a finger like morphology each consisting of (1) massive and flow-banded pinkish-gray stony rhyolite interiors, (2) a chilled margin of dark gray glassy vitrophyre surrounding the stony rhyolite, and (3) upper and lower bounding layers of breccia with angular clasts (up to 1 m) of rhyolite, vitrophyre, and pumice in a tuffaceous matrix. Perlitic alteration is present throughout the glass of the flows. Sanidine (2-4%), plagioclase (2-4%), biotite with rutile rims (<1%), hornblende (<1%), and opaque oxides (<2%) are phenocrysts in the vitrophyre, rhyolite, and pumice fragments. Also present in the rhyolites, vitrophyres, and tuff matrix are glomerocrystic xenocrysts of clinopyroxene (1-2%) and plagioclase. These minerals are designated xenocrysts because they are not present in pumice fragments. Pumice mineral phases probably represent the phases in the magma prior to eruption. The rhyolite flows reach a maximum estimated thickness of 90 m (estimated from the map).

### Tertiary surge of Culdesac Wash (Tcs)

Where rhyolite flows are not present, tuff 1 of Culdesac Wash is overlain by a well-bedded, lithic-dominated, yellow pyroclastic surge named the surge of Culdesac Wash (map unit Tcs, Plate I and Fig. 2-1). Individual beds range in thickness from 1-5 cm, are poorly graded, display bimodal sorting (lithics and phenocrysts are equigranular in a fine ash matrix), and are locally cross-bedded. The unit contains subrounded lithic clasts (rhyolite and andesite), minor pumice, and abundant angular broken fragments of sanidine and plagioclase. The unit is only associated with the rhyolite flows and has a maximum estimated thickness of 48 m (measured from the map).

The surge unit laps up onto the margins of rhyolite flows in Culdesac Wash, but do not appear on top of them. The surge may have either been eroded off the top, or the steep rhyolite flow fronts may have provided a topographic barrier to deposition.

### Tertiary tuff 2 of Culdesac Wash (Tct2)

The upper most unit of the Culdesac rhyolite complex is a rhyolitic tuff named here tuff 2 of Culdesac Wash (map unit Tct2, Plate I and Fig. 2-1). Tuff 2 is the thickest and most widespread of the Culdesac units and is present in both Culdesac Wash and to the north and west of the wash (Plate I). Tuff 2 overlies one of three units: surge of Culdesac Wash, rhyolite of Culdesac Wash, or andesite of Alta

Spring. Where tuff 2 overlies andesite of Alta Spring (described below), fragments of the andesite are incorporated into the lower part of tuff 2. In Culdesac Wash tuff 2 is composed of a dark-orange upper cooling unit of moderately-welded, lithic-rich, vitric tuff and a pale orange, poorly-welded lower cooling unit. The moderately-welded unit shows weak columnar jointing, and a eutaxitic fabric defined by black and brown glass fiammé (up to 2 cm in length) and the ash shards of the matrix. Both cooling units contain subangular lithic fragments (rhyolite, andesite, and basalt), large pumice clasts (up to 10 cm), and phenocrysts of sanidine (3-5%), plagioclase (1-4%), quartz (<2%), biotite (1-4%), and opaque oxides (2%). Clinopyroxene (2%), hornblende (<2%), and plagioclase grains are interpreted as xenocrysts, because they are present only in the tuff matrix and not in the pumice fragments. Pumice fragments contain phenocrysts of sanidine (<2%), plagioclase (<1%), biotite (<1%), and trace amounts of opaque oxides. Near the locality of Alta Spring (Fig. 2-2 and Plate I), tuff 2 grades into a breccia containing andesite clasts (up to 1.5 m in diameter) in an ash matrix. Tuff 2 of Culdesac Wash reaches its maximum thickness, approximately 70 m, in the north part of section 17, T.26N., R.19W. which lies approximately 2 km north of the Culdesac Wash. Morikawa (1993) reported an  $^{40}\text{Ar}/^{39}\text{Ar}$  biotite age of  $16.09 \pm 0.15$  Ma for pumice (sample Tct2-4.1) collected from this tuff near Culdesac Wash. Tuff 2 of Culdesac Wash is distinguished from the tuff of Table Mountain by the presence of large pumice fragments and glass fiamme that the latter lacks.

### Tertiary andesite of Alta Spring (Tasa)

A thin vesiculated A'a flow of andesite named here andesite of Alta Spring (map unit Tasa, Plate I and Fig. 2-1) lies conformably between the surge and tuff 2 of the Culdesac Wash. Andesite of Alta Spring is also found unconformably overlying tilted flows of andesite of Rodeo Grounds outside the Culdesac Wash near the locality of the Alta Spring (Fig. 2-2 and Plate I). Andesite of Alta Spring is porphyritic with 20-35% phenocrysts. Phenocrysts include biotite with rutile rims (5-8%), clinopyroxene (5-15%) and plagioclase (10-35%), with lesser amounts of iddingsite after olivine (0-10%) and orthopyroxene (<2%). The matrix is rich in fine grained opaque oxides, which appear to be in part alteration products. Flows of andesite of Alta Spring are thin and laterally discontinuous. It is deposited only in the southern DSV (Fig. 2-2) and pinches out in several places near the Culdesac Wash. The unit reaches a maximum estimated thickness of 20 m (measured from the map).

### Tertiary andesite of Powerline Road (Tpa)

Above tuff 2 of Culdesac Wash is a section of lava and debris flows ranging from basalt to andesite with basaltic andesite predominating. This unit is named here the andesite of Powerline Road (map unit Tpa, Plate I and Fig. 2-1). The lava flows are highly brecciated with intervening layers of monolithologic debris flows, matrix-supported scoriaceous breccias, and lesser amounts of intercalated coarse grained cross-bedded conglomerates. The conglomerates are dominated by Precambrian lithologies. The breccias and

debris flows are exclusively composed of volcanic clasts (basalt-andesite) and matrix. The lava flows are porphyritic, commonly vesicular, with 25-50% phenocrysts. Phenocrysts include plagioclase (15-35%), clinopyroxene (10-25%), orthopyroxene (<3%), and iddingsite after olivine (5-10%).

The basal flow of andesite of Powerline Road conformably overlies tuff 2 of Culdesac Wash. In Culdesac Wash, andesite of Powerline Road is found as small eroded remnants of a vesicular flow. Andesite of Powerline Road thickens to the north where it becomes brecciated and difficult to distinguish individual flows. Exposures in the northern part of the field area are poor and typically only occur as talus covered slopes. The poor exposure of andesite of Powerline Road makes it difficult to assess if dips fan internally within the unit. Gently dipping coarse grained, cross-bedded gravels are locally intercalated with the volcanic beds. Near Culdesac Wash a small ( $\approx 1$  m wide) dike cuts tuff 2 of Culdesac Wash and feeds the basal flow of andesite of Powerline Road. This dike was the only vent/dike identified in the study area. The maximum estimated thickness of the andesite of Powerline Road is 200-300 m. The thickness is estimated from topographic relief because it otherwise lacks clear bedding to estimate dip and flow thicknesses.

### Tertiary gravel unit 3 (Tg3)

Overlying andesite of Powerline Road is a poorly sorted, unconsolidated gravel and boulder deposit, with no internal bedding, named here gravel unit 3 (map unit Tg3, Plate I and Fig. 2-1). Clasts consist of both Precambrian and Cretaceous (?) crystalline rocks and Tertiary volcanic rocks

(andesite and basalt). Clasts are well rounded to angular and up to 1 m in diameter. Gravel unit 3 is the stratigraphically highest unit in the southern DSV (Fig. 2-2) and lies unconformably over tilted and faulted beds of gravel conglomerate unit 1, tuff 2 of Culdesac Wash, and andesite of Powerline Road. The thickness of gravel unit 3 estimated from topographic relief is 75 m.

### DSV Chronology

The chronology of the Dolan Springs volcanic field can not yet be rigorously constrained by radiometric dates, however sufficient data is presently available to establish a preliminary chronology of events. The only radiometric age in the DSV is a biotite  $^{40}\text{Ar}/^{39}\text{Ar}$  date of  $16.09 \pm 0.15$  Ma on tuff 2 of Culdesac Wash (sample Tct2-4.1; Morikawa, 1993) which lies in the middle of the southern DSV stratigraphic column (Fig 2-1). No angular unconformities are present within the Culdesac rhyolite complex so the age of tuff 2 is inferred to approximate the age of the entire complex.

The basal DSV unit, gravel conglomerate unit 1, cannot be dated directly but is inferred to be of Tertiary age based on the presence of probable Cretaceous clasts and the Miocene age of overlying beds. The oldest volcanic unit is andesite of Rodeo Grounds. Less than 12 km east of the northernmost DSV outcrop of andesite of Rodeo Grounds is an outcrop of andesite at Table Mountain (Plate I; sec. 19, T.27N., R.18W.) that was dated at approximately 17.98 Ma ( $^{40}\text{Ar}/^{39}\text{Ar}$  with no analytical uncertainty available; Gans and Faulds, unpublished data). The 17.98 Ma andesite at Table Mountain is the basal volcanic unit in that area and lies on coarse conglomerates that in turn lie on



Precambrian basement. The 17.98 Ma age will be adopted for andesite of Rodeo Grounds based the similar stratigraphic position, similar mineralogies, and close proximity to the DSV. Overlying the  $16.09 \pm 0.15$  Ma tuff 2 of Culdesac Wash is the andesite of Powerline Road (Fig 2-1). Because the Powerline Road unit overlies tuff 2 of Culdesac Wash it is younger than 16.09 Ma.

In the northern DSV (Fig. 2-2) tuff of Table Mountain lies within gravel conglomerate unit 2 which is capped by basalt of Table Mountain (Fig 2-1). Tuff of Table Mountain is younger than 17.98 Ma (the age assumed for the underlying andesite of Rodeo Grounds). Basalt of Table Mountain is the highest stratigraphic unit in the northern DSV stratigraphic section (Fig. 2-1). This coupled with the fact that it is the least tilted ( $<10^\circ$ ) of any DSV volcanic unit suggests that the basalt of Table Mountain is the youngest volcanic unit within the DSV. Basalt of Table Mountain has been previously reported as 8.5 Ma (Calderone, 1991) and 10.5 (Bradshaw et al., 1993). The 8.5 Ma age appears as a personal communication in Calderone (1991) and because the method was undisclosed this age will not be considered. The 10.5 Ma age reported by Bradshaw et al. (1993) is based on stratigraphic relationships that were not discussed. Thus, no reliable age is available for the basalt of Table Mountain.

As discussed later in Chapter 6, basalt of Table Mountain geochemically correlates with tholeiitic basalts of Senator Mountain (Cascadden, 1991) and Malpais Flattop (Feuerbach et al., 1993). These two CREC tholeiites are located less than 40 km from Table Mountain (Fig. 1-1). All three of them occur as 50-100 m thick lava capped mesas overlying coarse Tertiary gravels. The age of

the capping basalt flows of Malpais Flattop is well-constrained between  $11.88 \pm 0.15$  Ma and  $11.37 \pm 0.14$  Ma ( $^{40}\text{Ar}/^{39}\text{Ar}$ , Gans and Faulds, unpublished data). Senator Mountain has not been radiometrically dated, but Cascadden (1991) indicated that it is similar to a  $10.91 \pm 0.6$  Ma (K/Ar) basalt reported by Theodore et al. (1982) that lies in the central White Hills. Based on this data, basalt of Table Mountain is assigned an age of  $\sim 11$  Ma.

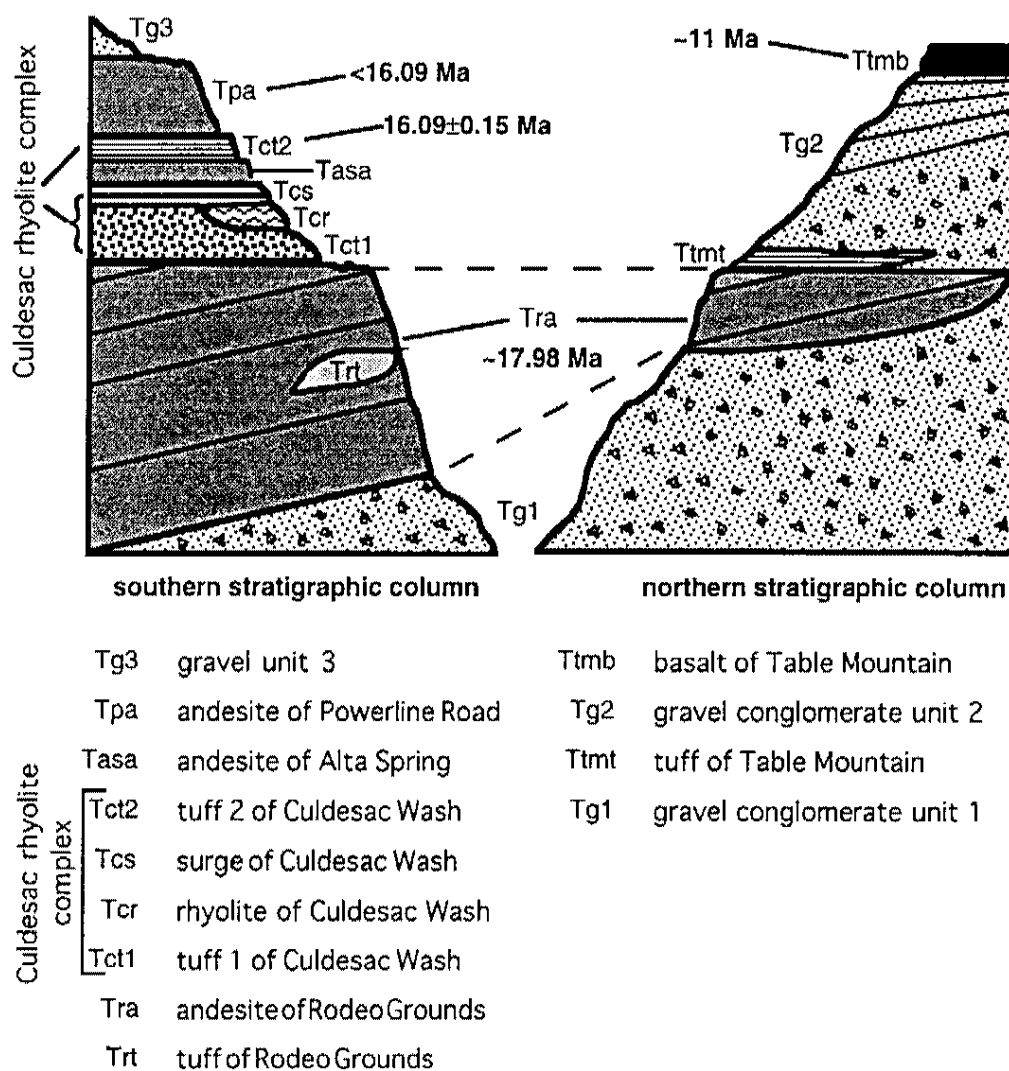


Figure 2-1. Schematic stratigraphic columns for the southern and northern Dolan Springs volcanic field showing inferred stratigraphic correlations and inferred ages. Note angular unconformity above the andesite of Rodeo Grounds.

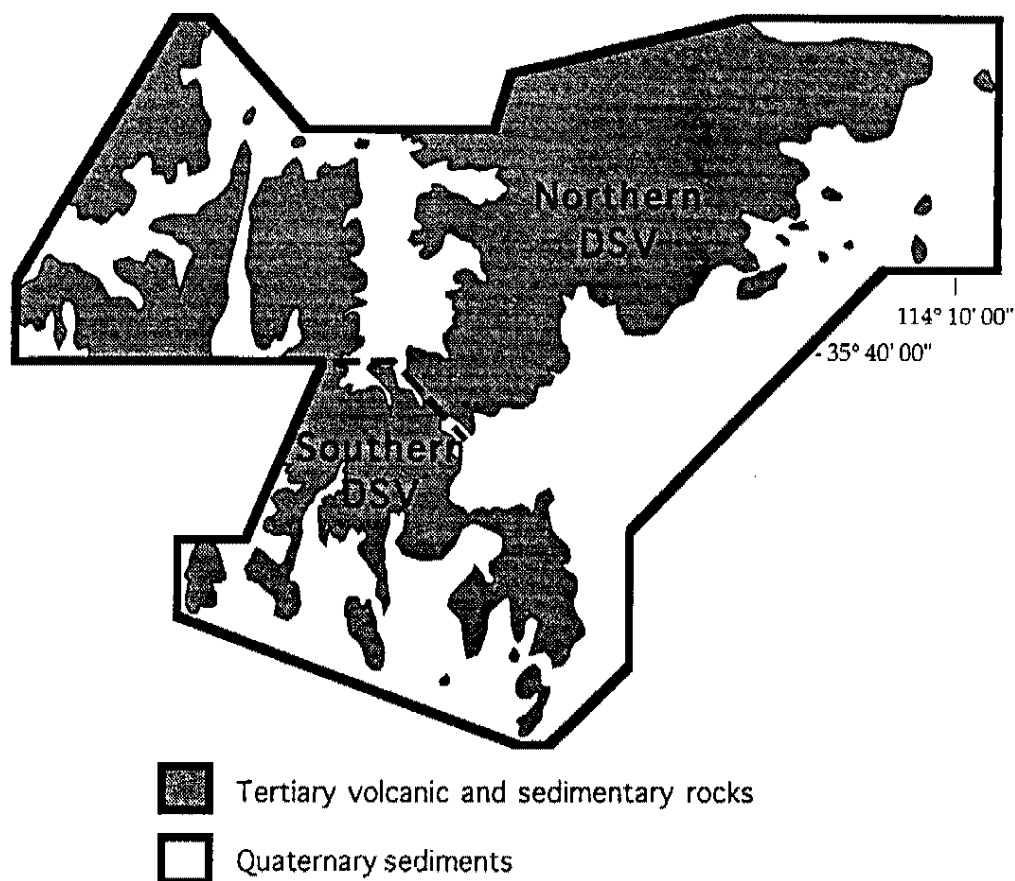


Figure 2-2. Schematic map of the Dolan Springs volcanic modified from Plate I. Dashed line indicates the division between the northern and southern sections of the study area mentioned in the text.

## CHAPTER 3

### Structural Geology of the Dolan Springs Volcanic Field

#### Tilted Strata and Angular Unconformities

The Dolan Springs volcanic field (DSV) was affected by large-scale Miocene crustal extension similar to most of the Colorado River extensional corridor (CREC). Geologic mapping confirmed that the majority of the DSV lies on the eastern side of the structural accommodation zone defined by Faulds et al. (1990). This section draws upon data primarily taken from the geologic map at a scale of 1:24,000 (Plate I) and the associated cross-sections (Plate II). Tertiary strata in the DSV have bedding and flow foliations that are dominantly tilted to the east between 9-45°. The only exception are west tilted beds in the extreme western ridge of the DSV (unmapped) at sec. 11, 12, and 13, T.26N., R.19W. (Plate I). Older units tend to dip more steeply than younger units.

Two lines of evidence indicate that a prominent angular unconformity exists at the top of the andesite of Rodeo Grounds (Fig. 2-1, Plate I). First, andesite of Rodeo Grounds generally has steeper dips (22-60°) than the overlying units (9-40°). Second, an angular unconformity is exposed between the andesite of Rodeo Grounds and the andesite of Alta Spring and tuff 2 of Culdesac Wash in a canyon exposure at sec. 16, T.26N., R.19W. (Plate I). The entire Culdesac rhyolite complex is assumed to be conformable, because no

angular unconformities or erosional surfaces were observed between contacts.

In the cross-bedded conglomerates that comprise the upper third of gravel conglomerate unit 2, dips progressively decrease up section. The fanning dips are compatible with a growth fault basin interpretation, therefore, this unit is inferred to have been deposited contemporaneously with extensional faulting. The youngest volcanic unit, basalt of Table Mountain, was deposited during the waning stage of extension as evidenced by its shallow dip ( $<9^\circ$ ) and small degree of fault displacement (10-20 m).

### Faults

All observed faults in the DSV are high angle normal faults that appear to be planar with depth. Fault orientations and stratigraphic separations suggest that the composite direction of maximum extension at the DSV is approximately east-west. Faults in the DSV are usually at a high angle to bedding although exceptions do exist. Faults in the DSV generally strike north, northeast, or northwest. Based on cross-cutting relationships, three generations of faults were identified in both the southern (S1-S3) and northern (N1-N3) DSV (Fig. 2-2).

The faults in the southern DSV (Fig. 2-2) are described first. The cross cutting relationships of the earliest faulting events are difficult to put in age context with each other because they are isolated from other faults. All of these earliest faults will be grouped under episode S1. All of the S1 faults cut units from the basal gravel conglomerate unit 1 up to andesite of Powerline Road (Fig. 2-1). S1 faults strike northwest and either (1) dip moderately to

steeply southwest (20-50°) with down to the west stratigraphic separation, or (2) dip moderately northeast with down to the northeast stratigraphic separation. A single fault apparently of this same generation strikes northeast and dips steeply northwest.

All the S1 faults are in turn cut by a series of north-south striking faults belonging to episode S2. The S2 faults dip steeply west and have down to the west stratigraphic separation. One exception is an S2 fault that dips moderately (30-45°) east and cuts bedding at a low-angle. Both the S1 and the S2 faults are covered by gravel unit 3.

The youngest fault in the southern DSV is assigned to episode S3. It is a single near vertical northeast striking fault that cuts gravel unit 3, the andesites of Powerline Road and Alta Spring, and tuff 2 of Culdesac Wash.

In the northern DSV (Fig. 2-2) the stratigraphy and faulting relationships are different from those in the south. The oldest faults in the northern DSV, referred to as N1, strike north-south, dip moderately west, and have apparent down to the west displacement. The current exposure level shows N1 faults cutting only the two lowest units of the northern stratigraphic section (Fig. 2-1), gravel conglomerate unit 1 and andesite of Rodeo Grounds.

The N1 faults are cut by episode N2 faults that strike east-west and dip steeply north to near vertical. At the current level of exposure, the N2 faults cut the two lowest stratigraphic units as well as gravel conglomerate unit 2 and tuff of Table Mountain.

The third generation of faults in the northern DSV, N3, cuts the youngest stratigraphic unit in the DSV, basalt of Table Mountain. The N3 faults strike north-northwest and dip steeply west, one exception strikes east-west and dips steeply north.



## **CHAPTER 4**

### **Eruptive, Depositional and Tectonic History of the Dolan Springs Volcanic Field**

The following model for the development of the eruptive, depositional, and tectonic history of the Dolan Springs volcanic field (DSV) is divided into pre-extension, synextension, and post-peak extension phases. Evidence for a possible caldera related to the Culdesac rhyolite complex is discussed in the synextensional section.

#### **Pre-extension History**

During the pre-extension stage of the DSV, gravel conglomerate unit 1 and andesite of Rodeo Grounds were deposited. Volcanic sediments do not make any substantial contribution to gravel conglomerate unit 1 (see Chapter 2), therefore, volcanism in the DSV had not yet begun at this time. Gravel conglomerate unit 1 includes megabreccia blocks of Precambrian basement rocks that are interpreted as landslides deposits, based on their size and angular nature.

Three modern locations of Precambrian highlands may have supplied the sediments and megabreccia blocks to the DSV. These are the central Black Mountains <15 km west of DSV, the Cerbat Mountains 10 km southeast of DSV, and Garnet Mountain 45 km northwest of DSV (Fig. 1-1). Another potential source for the Precambrian clasts and megabreccia blocks is the Gold

Basin District (Fig. 1-1) located less than 10 km north of the Table Mountain Plateau. The Gold Basin District is at present a low lying area of Precambrian basement exposed in the footwall of a low-angle detachment fault (Meyers, 1984). The detachment fault is exposed completely within the Precambrian basement rock but carries Tertiary strata in the hanging wall. The Northern White Hills volcanic field (NWH) contains similar megabreccia deposits that contain Precambrian clasts (Cassaden, 1991) and lies just north of the Gold Basin District. The Gold Basin District is the closest modern location of Precambrian basement to both the DSV and NWH. The Gold Basin District stands out in the White Hills as an isolated exposure of Precambrian basement surrounded by thick Tertiary volcanic and sedimentary cover. The pre-extension paleotopography may have been dramatically different from modern topography and the Gold Basin District might have had sufficient topographic relief to contribute debris to the northern and southern White Hills.

Further detailed work on the lithologies present in the megabreccias and the current exposures of Precambrian lithologies may constrain the location of the source of the megabreccia blocks. However, it should be noted that the source of the Precambrian clasts may now be buried beneath volcanic material or detritus and cannot be found.

The andesite of Rodeo Grounds eruptions began approximately 17.98 Ma (see Chapter 2 for explanation on age). The andesite is at its maximum thickness in the southern DSV (Fig. 2-2) which suggests a vent(s) near this location. Lava flows, debris flows, and ash-flow tuffs accumulated in thick discontinuous sheets. These eruptions were voluminous, producing a

package of intermediate composition volcanic rocks >1 km thick. No angular unconformities or contemporaneous faults were observed within andesite of Rodeo Grounds, therefore extensional faulting and block tilting appear to have begun after the cessation of these eruptions.

### Synextension History

Extensional faulting and block tilting began in the DSV before the deposition of gravel conglomerate unit 2 and tuff 1 of Culdesac Wash (Fig. 2-1). Both units overlie tilted flows of Rodeo Grounds. The faults that caused tilting of the andesite of Rodeo Grounds and the resulting unconformity were not identified in the field area. Even the oldest episodes of faults (S1 and N1) cut units younger than the angular unconformity.

The eruption of the Culdesac rhyolite complex, the andesite of Alta Springs and the basal flow of andesite of Powerline Road occurred before additional tilting, because no angular unconformities exists between these units. Andesite of Alta Spring, which like the Culdesac complex units, is confined to the southwestern part of the field area, probably erupted from a vent in the southern part of the DSV.

In the southern DSV (Fig. 2-2), faulting episodes S1 and S2 cut all the stratigraphy from gravel conglomerate unit 1 to the andesite of Powerline Road (Fig. 2-1). In the southern DSV (Fig. 2-2), gravel conglomerate unit 2 was deposited concurrently with extension and volcanism as evidenced by the decreasing dips up section of the conglomerate. The fanning dips are consistent with a growth fault basin interpretation for the depositional

environment. West dipping faults, between the DSV and the Grand Wash Cliffs (Fig. 1-1), may have been responsible for opening the basin and changing the depositional slope. An alternative hypothesis is that the fanning dips simply represent the progressive filling of a basin. Tuff of Table Mountain was erupted during the deposition of gravel conglomerate unit 2. Faulting episodes N1 and N2 cut stratigraphy from gravel conglomerate 1 to gravel conglomerate 2 (Fig. 2-1) and occurred prior to the eruption of basalt of Table Mountain.

The pre- and synextension volcanic rocks seem to be concentrated to the south and west whereas the sedimentary deposits are thickest in the northern DSV (Fig. 2-2). The maximum thickness of both gravel conglomerate units 1 and 2 occurs near Table Mountain Plateau. That suggests the existence of a long lived paleo-basin at that location. The southern and western DSV where the pre- and synextension volcanic rocks are concentrated may have been topographically higher and acted as a barrier to deposition of sedimentary rocks. Though it is speculative at best, the southwestern DSV may represent the flanks of an eroded and dissected stratovolcano with thick sequences of andesitic lavas and debris flows with lesser amounts of felsic lavas.

Notably absent from the DSV are two regional ash-flow tuffs, the Peach Springs tuff and the tuff of Bridge Spring. Peach Springs tuff (18.5 Ma) is older than andesite of Rodeo Grounds and may be lower in the section, but the 15.21 Ma (Faulds et al., 1995) tuff of Bridge Spring should be present. Tuff of Bridge Spring crops out in both the Northern White Hills less than 40 km to the north and in the central Black Mountains less than 15 km west. One

possible explanation for the lack of tuff of Bridge Spring is that topographic barriers existed preventing its deposition. These barriers may have been the same highlands that supplied the megabreccias to the DSV basin.

Alternatively there may not have been enough material in the tuff of Bridge Spring eruption to cover the southern White Hills.

### **A Possible Synextension Caldera Near DSV**

Several lines of evidence suggest that the Culdesac rhyolite complex represents a portion of a felsic eruptive center, perhaps a caldera margin. Caldera margins are characterized by the presence of pyroclastic surges, rhyolite flows and domes, and megabreccias (Fisher and Schmincke, 1984). Though no rhyolite domes occur at the DSV, rhyolite flows are abundant at the Culdesac Wash. These flows indicate a nearby vent because rhyolite is too viscous to travel far. Second, surge deposits, also present at Culdesac Wash, form near vents by collapse of plinian eruption clouds (Fisher and Schmincke, 1984). Finally, megabreccia blocks are contained in tuff 2 of Culdesac Wash near the Alta Spring locale. The breccia blocks are of andesite similar to andesite of Rodeo Grounds, which may have been eroded from a vent during an eruption. The area around Alta Spring is not a caldera margin, but large blocks such as these could not have traveled far in an ash-flow. These features suggest that the various units of the Culdesac rhyolite complex and specifically the Culdesac Wash locale, are associated with a caldera margin that is inferred to lie beneath Detrital Wash, south or west of the field area.

### **Post-peak extension History**

The youngest volcanic unit at the DSV is basalt of Table Mountain. The exposure of the basalt of Table Mountain is elongated east-west and appears to have flowed in the same basin that contained gravel conglomerate units 1 and 2. Table Mountain was cut by three faults (episode N3) towards the end of extension.

The youngest sedimentary unit in the DSV is gravel unit 3 which was deposited on highly tilted volcanic rocks and covers faults of episodes S1 and S2. Gravel unit 3 is cut by a single northeast striking fault (fault episode S3). No points of reference place gravel unit 3 in chronologic context with basalt of Table Mountain. Remnants of gravel unit 3 with boulder sized clasts of Precambrian basement appear on hill tops and in high saddles in many places in the DSV. The existence of these stranded gravels implies that parts or all of the DSV were previously buried in alluvium and then later exhumed.

## **CHAPTER 5**

### **Geochemistry of the Dolan Springs Volcanic Rocks**

#### **Introduction**

For the purpose of discussing the geochemistry, the Dolan Springs volcanic field (DSV) units are divided into two groups. The first group comprises the older, pre- to synextensional lavas and tuffs (17.98 to >11 Ma): the andesites of Rodeo Grounds, Alta Spring, and Powerline Road, the Culdesac rhyolite complex, and tuff of Table Mountain. The second much smaller group of rocks represents lavas erupted during the waning phase of extension (the  $\approx$ 11 Ma basalt of Table Mountain). Major, trace element, and isotopic analyses as well as rock norms are found in Appendix A. Analytical methods and analytical uncertainties are reported in Appendix B. Plate III is a sample location map.

#### **Classification and Normative Mineralogy**

Rocks of the Dolan Springs volcanic field are predominantly subalkaline. However four of the pre- and synextensional basalts are alkaline (Fig. 5-1a). Collectively the pre- and synextensional rocks are calc-alkaline (Fig. 5-1b & c). Basalt of Table Mountain is subalkaline (Fig. 5-1a) and is tholeiitic (Fig. 5-1b & c). Most of the DSV rocks underwent some degree of

secondary alteration as evidenced by the carbonate coatings in fractures and vesicles and the conversion of olivine to iddingsite. A plot of  $\text{Na}_2\text{O}$  versus  $\text{K}_2\text{O}$  (Fig 5-2) was used to evaluate the degree of alteration. Boxes on the plot represent the fields of "normal" (unaltered) igneous rocks from Carmichael et al. (1974) and Wilson (1989). All of the DSV rocks, except a few of the felsic rocks, are within one of these two "normal" fields. Therefore, metasomatism does not appear to have appreciably affected the DSV rocks.

The normative classification Color Index versus Anorthite % diagram (Fig. 5-1c) of Irvine and Baragar (1971) minimizes the effect of the alkali mobility and was used to assign rock names. The older pre- to synextensional mafic units, including the andesites of Rodeo Grounds, Alta Spring, and Powerline Road, range in composition from dacite to basalt, but are dominated by andesite and will be referred to collectively as andesites. The felsic rocks of the Culdesac rhyolite complex and tuff of Table Mountain (Ttmt) range from rhyolite to dacite and for simplicity will be referred to as rhyolite. Seven analyses from the Culdesac rhyolite complex included in this data set (Appendix A, Table A-2) are used with the permission of Morikawa (1993; & unpublished data).

All of the pre- to synextensional mafic rocks are hypersthene (3.6-12%) and quartz normative except for the least evolved (lowest  $\text{SiO}_2$ ) sample of each group, which are hypersthene and olivine normative. All samples of the basalt of Table Mountain are basalts (Fig 5-1d) and except for a single sample (Ttmb-16), all of the basalt of Table Mountain samples are olivine normative and generally are the most strongly hypersthene normative (7.4-18.5 wt.%).



## Major Elements

Harker variation diagrams (Fig. 5-3) show three groups: (1) the older mafic to intermediate rocks (andesite of Rodeo Grounds, andesite of Alta Spring, and andesite of Powerline Road), (2) the younger basalt of Table Mountain, and (3) the felsic rocks of the Culdesac rhyolite complex and the tuff of Table Mountain. All the mafic to intermediate rocks range in  $\text{SiO}_2$  from 49-60 wt.%. A pronounced compositional gap from 60-70 wt.%  $\text{SiO}_2$  occurs between the intermediate and felsic samples, with the exception of one Rodeo Grounds sample (Tra-33) at 66 wt.%  $\text{SiO}_2$ . The DSV felsic rocks range from 68-78 wt.%  $\text{SiO}_2$ . The range in  $\text{Al}_2\text{O}_3$  (13-18 wt%) is large for all the older intermediate and mafic rocks, but basalt of Table Mountain has the narrowest range (14.8-15.8%; Fig. 5-3a). Basalt of Table Mountain samples have the highest MgO,  $\text{FeO}^*$ ,  $\text{TiO}_2$ , and CaO, while having the lowest  $\text{SiO}_2$ ,  $\text{K}_2\text{O}$ , and  $\text{P}_2\text{O}_5$ . In addition, samples of basalt of Table Mountain contrast with the earlier rocks by having negative slopes for  $\text{Al}_2\text{O}_3$  and  $\text{Na}_2\text{O}$  and positive slopes on MgO and  $\text{TiO}_2$ . The andesites of Powerline Road and Alta Spring are more similar chemically than the earlier andesite of Rodeo Grounds.

The felsic rocks (Culdesac rhyolite complex and tuff of Table Mountain) range in  $\text{SiO}_2$  from 68-78 wt.%. Culdesac Wash rhyolite lava generally has lower  $\text{SiO}_2$  values than the tuffaceous samples: tuff 2 of Culdesac Wash and tuff of Table Mountain. Most tuff samples were sampled by extraction of pumice fragments, and thus more closely represent the composition of the magma at the time of eruption, than the lavas (see Appendix A for description of individual samples). The lavas and vitrophyres have lower

SiO<sub>2</sub> and high TiO<sub>2</sub>. The felsic rocks show a steep negative slope on Na<sub>2</sub>O that contrasts with the mafic rocks. The felsic rocks have lower concentrations of MgO, FeO\*, TiO<sub>2</sub>, CaO, and P<sub>2</sub>O<sub>5</sub> than the mafic rocks. Similar to the mafic rocks, Al<sub>2</sub>O<sub>3</sub> shows the most scatter in SiO<sub>2</sub>.

### Trace Elements

Trace element compositions display the same three groups as the major elements. For the mafic to intermediate rocks the sample with the lowest wt.% SiO<sub>2</sub> (range 49-53%) was chosen from each DSV unit to represent the most primitive member of that group. On chondrite normalized rare-earth element (REE) plots (Fig. 5-4a) the older rocks (andesites of Rodeo Grounds, Alta Spring, and Powerline Road) have similar, steep enriched patterns for the heavy rare-earth elements (HREE). Basalt of Table Mountain has the flattest profile and lowest REE concentrations (except Yb) of any unit. Figure 5-4b is a chondrite normalized REE plot of three felsic samples, a dacite lava from Culdesac Wash (Tcr-93-10), a pumice fragment from tuff 2 of Culdesac Wash (Tct2-37), and a whole rock analysis of tuff of Table Mountain (Ttmt-18). The Culdesac dacite lava has higher overall REE concentrations and does not have the Eu anomaly displayed by the tuffs. The whole rock sample of tuff of Table Mountain has higher REE concentrations and a sharp negative Eu anomaly.

Differences among the mafic units are seen clearly on a primordial-mantle normalized spider diagram (Fig. 5-5). The diagram is plotted with elements in order of increasing compatibility from the left using normalizing

values from Sun and McDonough (1989). The early pre- to synextensional rocks (andesites of Rodeo Grounds, Alta Spring, and Powerline Road) show similar patterns, characterized by large ion lithophile elements (LILE, i.e., Rb, Ba, & K) and the light rare-earth elements (LREE, i.e., La & Ce) enriched relative to the high field strength elements (HFSE, i.e., Ta, Nb, Zr, Ti, & Y) and HREE (i.e., Yb & Lu). The older mafic rocks reach their maxima at either Th (andesite of Rodeo Grounds) or Ba (andesite of Powerline Road and andesite of Alta Spring), and display a prominent trough at Nb-Ta and less prominent ones at P and Ti. There are sharp down steps in concentration for elements more compatible than Sr and then again at Ti.

The Table Mountain sample has a distinctly different pattern characterized by a smoother convex up mantle-normalized profile (Fig 5-5). These rocks have lower overall trace element abundances compared to the earlier mafic rocks. Basalt of Table Mountain reaches its maxima at Ba, but lacks the Nb, P, or Ti troughs and the steps down at Sr and Ti.

### Isotopic Geochemistry

All of the DSV rocks are isotopically enriched meaning that they are enriched in LILEs and LREE (i.e., Rb and Nd) and thus have higher Rb/Sr ratios and lower Sm/Nd than bulk earth (Faure, 1986). All of the DSV samples have lower than bulk-earth  $\epsilon_{Nd}$  and higher than bulk-earth  $^{87}Sr/^{86}Sr_{(i)}$  (Fig. 5-6). Basalt of Table Mountain has values closest to bulk-earth while the Culdesac rhyolite complex diverges the most. One pumice sample (Tct2-41) has a  $^{87}Sr/^{86}Sr_{(i)}$  of 0.719 which is shown with an arrow

designating its position off the plot. The  $^{87}\text{Sr}/^{86}\text{Sr}_{(i)}$  of the DSV rocks increases with increasing  $\text{SiO}_2$ , while the  $\epsilon_{\text{Nd}}$  uniformly decreases (5-7a&b). The similarity of the older mafic and intermediate rocks is again apparent while basalt of Table Mountain samples are distinctly different. Isotopic variation in the DSV suite is summarized in Table 5-1.

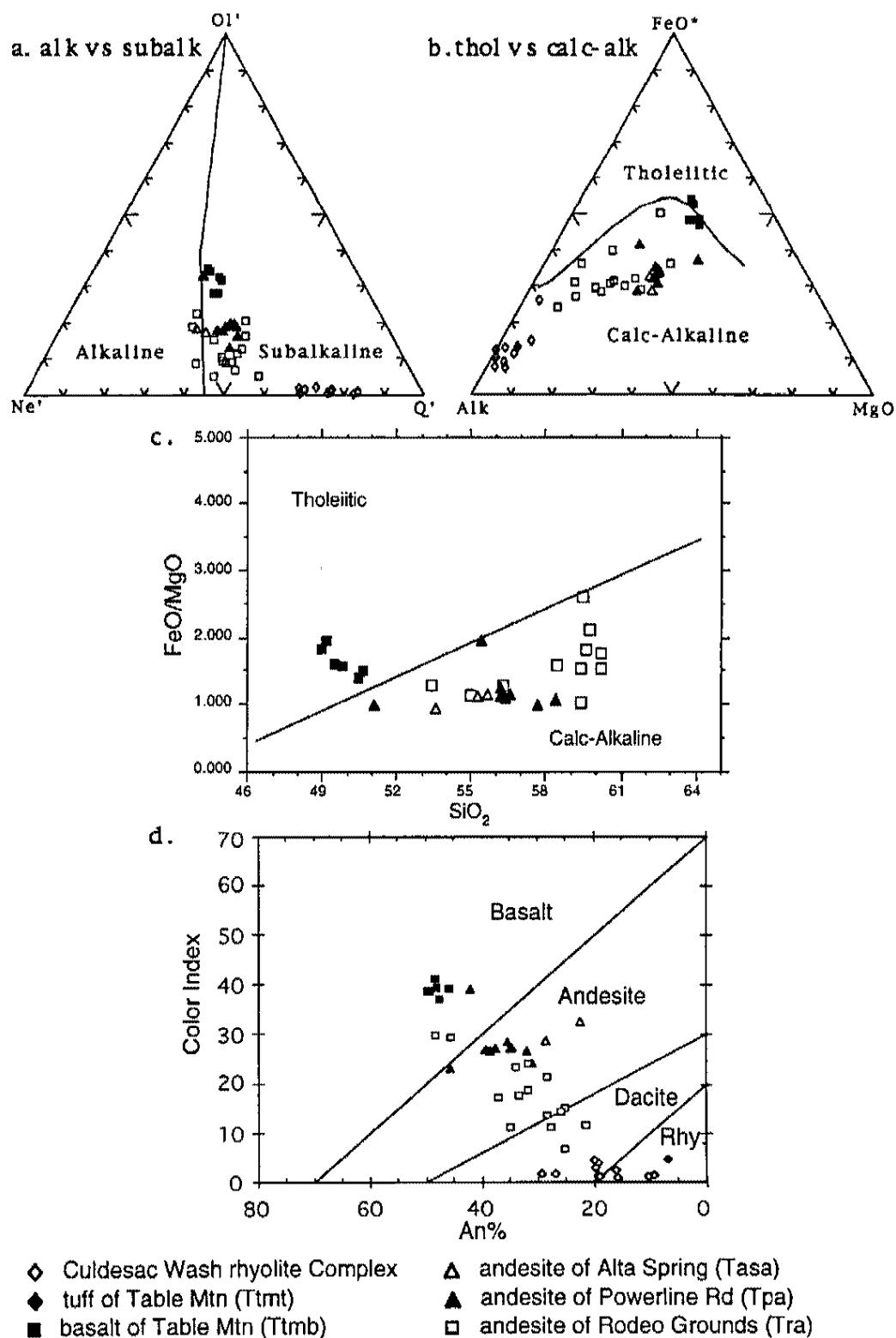


Figure 5-1a-d. Classification of Dolan Springs volcanic field rocks by geochemistry and normative mineralogy (Irvine and Baragar, 1971).  $An\% = 100 An/(An+Ab+(5/3Ne))$ , Color Index = ol + opx + cpx + mt + il + hm in wt.%,  $Ol' = Ol + 3/4 OPX$ ,  $Ne' = Ne + 3/5Ab$ ,  $Q' = Q + 2/5Ab + 1/4OPX$ .

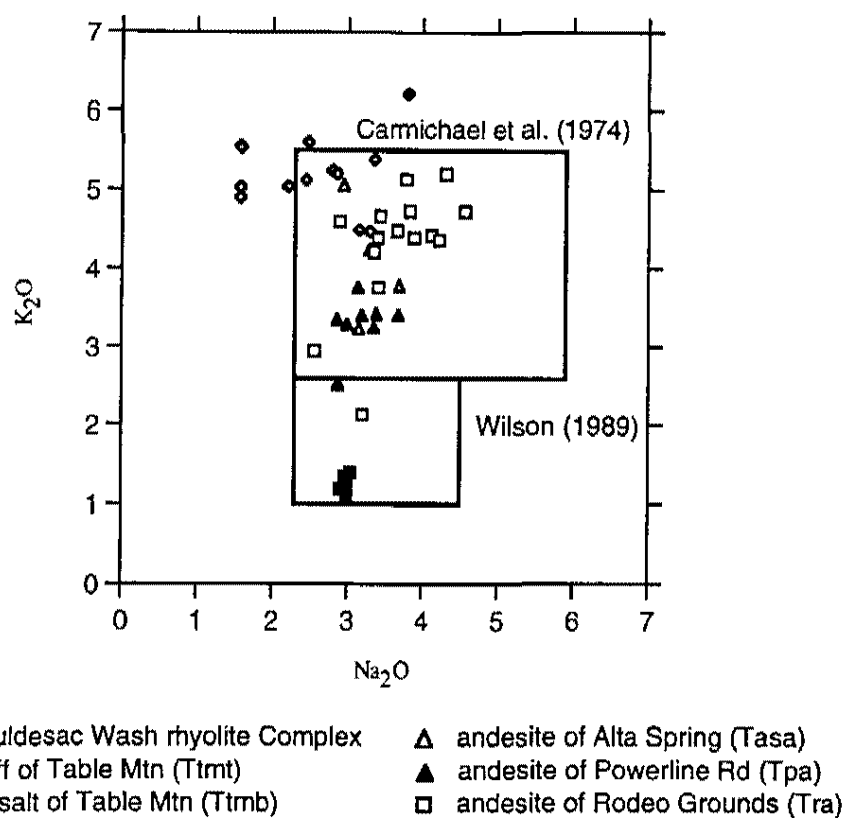


Fig. 5-2. Plot of  $\text{Na}_2\text{O}$  versus  $\text{K}_2\text{O}$  for DSV rocks. The boxes represent "normal" alkali contents of unaltered igneous rocks from Carmichael et al. (1974) and Wilson (1989).

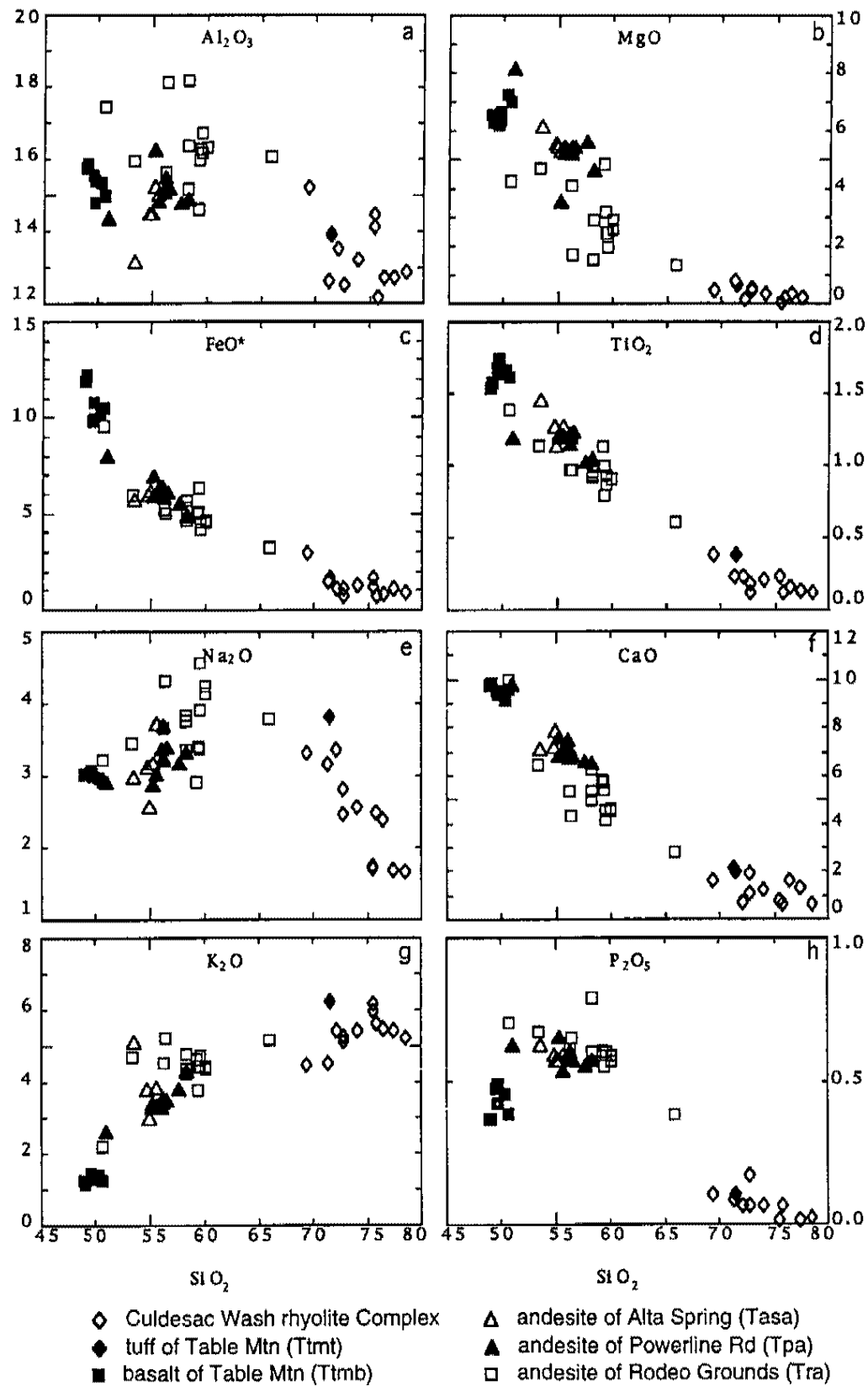
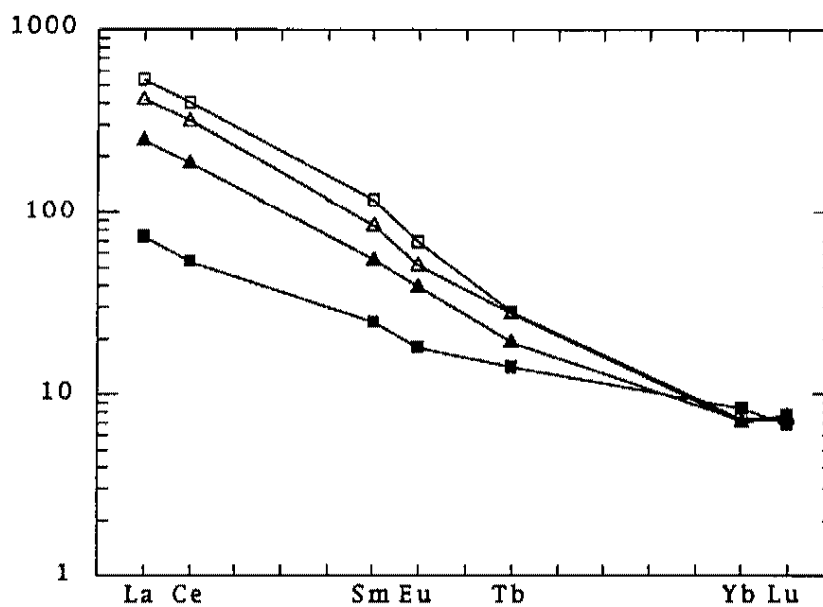
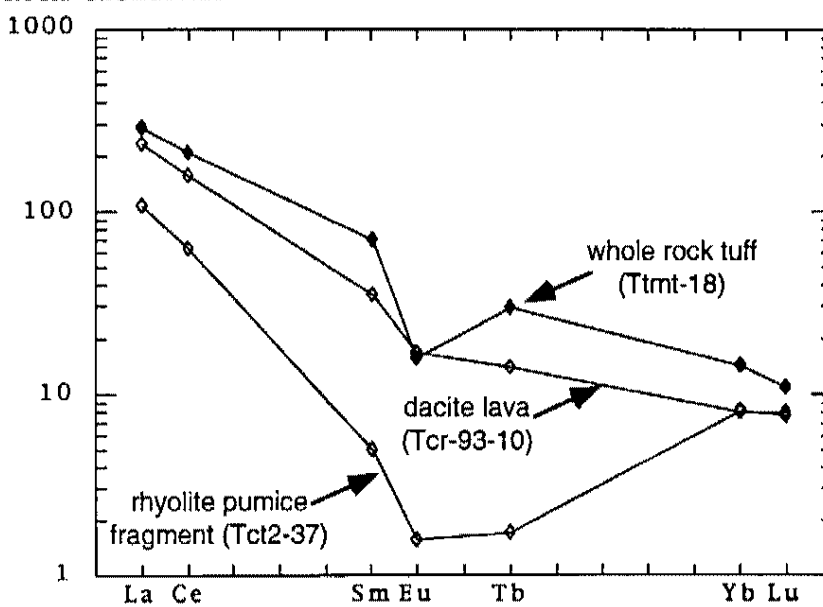


Figure 5-3a-h. Harker variation diagrams for the Dolan Springs volcanic field.

## a. Rock/Chondrites



## b. Rock/Chondrites



- ◇ Culdesac Wash rhyolite Complex
- ◆ tuff of Table Mtn
- basalt of Table Mtn (Tmb-25)

- △ andesite of Alta Spring (Tasa-83)
- ▲ andesite of Powerline Rd (Tpa-78)
- andesite of Rodeo Grounds (Tra72)

Figure 5-4a&b. Chondrite normalized rare earth element diagrams. a. DSV mafic samples (<54 wt.%  $\text{SiO}_2$ ). b. DSV felsic samples (>69 wt.%  $\text{SiO}_2$ ). Normalizing values from Nakamura (1974).



Table 5-1: Isotopic variation for the Dolan Springs volcanic field.

		Tmb	Tpa	Tasa	Culdesac Complex	Tmt	Tra
number analyzed		2	4	2	5	1	5
87/86 Sr(i)	min.	0.7053	0.7085	0.7086	0.7082		0.7086
	max.	0.7057	0.7088	0.7088	0.7193		0.7105
	avg.	0.7055	0.7086	0.7087	0.7114	0.7096	0.7097
epsilon Nd	min.	-4.26	-7.65	-7.28	-10.09		-9.20
	max.	-3.61	-7.91	-8.20	-9.42		-7.52
	avg.	-3.94	-7.57	-7.74	-9.83	-9.30	-8.26
206/204 Pb	min.	17.39	18.26	18.30	17.95		18.56
	max.	17.60	18.48	18.30	18.03		18.60
	avg.	17.50	18.35	18.30	18.02	18.03	18.58
207/204 Pb	min.	15.46	15.58	15.59	15.53		15.58
	max.	15.51	15.59	15.59	15.58		15.61
	avg.	15.48	15.58	15.59	15.56	15.54	15.60
208/204 Pb	min.	37.45	38.69	38.79	38.79		39.19
	max.	37.69	38.85	38.79	38.95		39.26
	avg.	37.57	38.75	38.79	38.85	38.96	39.23

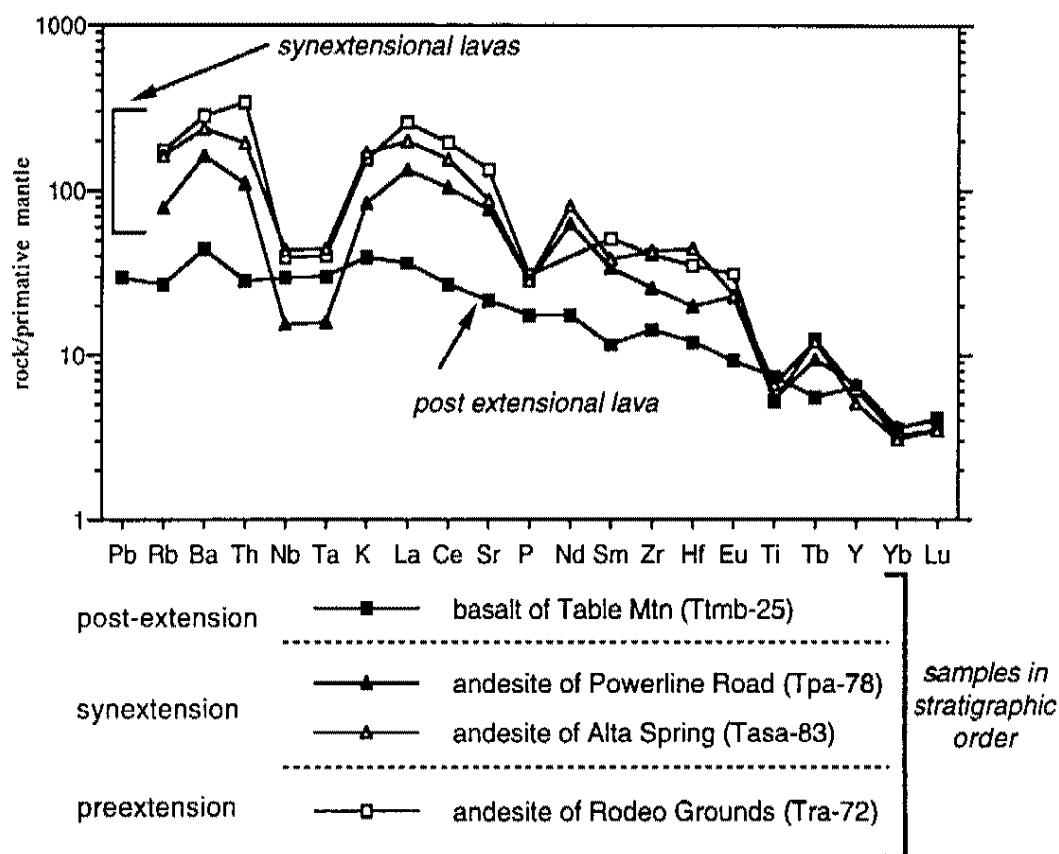


Figure 5-5. Primitive mantle normalized diagram comparing the most mafic samples from the DSV (<54 wt.%  $\text{SiO}_2$ ). Elements in order of increasing compatibility with normalizing values from Sun and McDonough (1989). Ta was assumed to be equal to Nb/17.

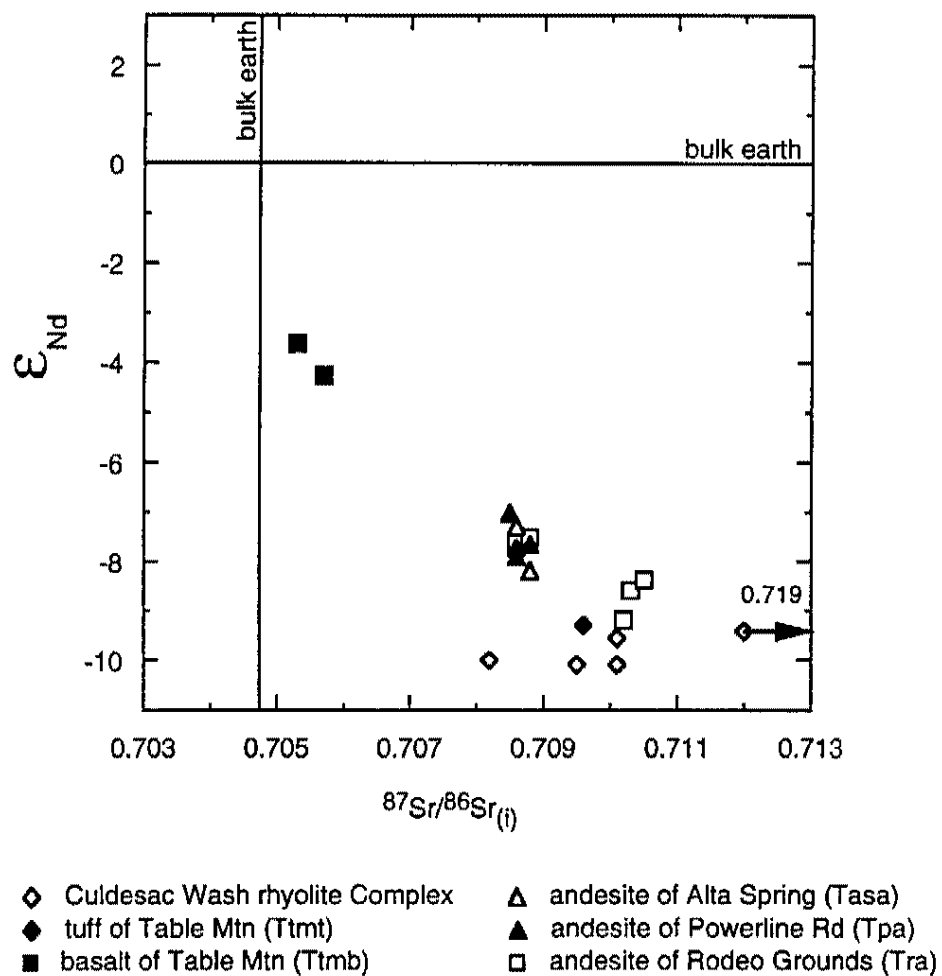


Figure 5-6.  $\epsilon_{Nd}$  and  $^{87}Sr/^{86}Sr(t)$  diagram for DSV rocks. Arrow indicates place of symbol off the graph.

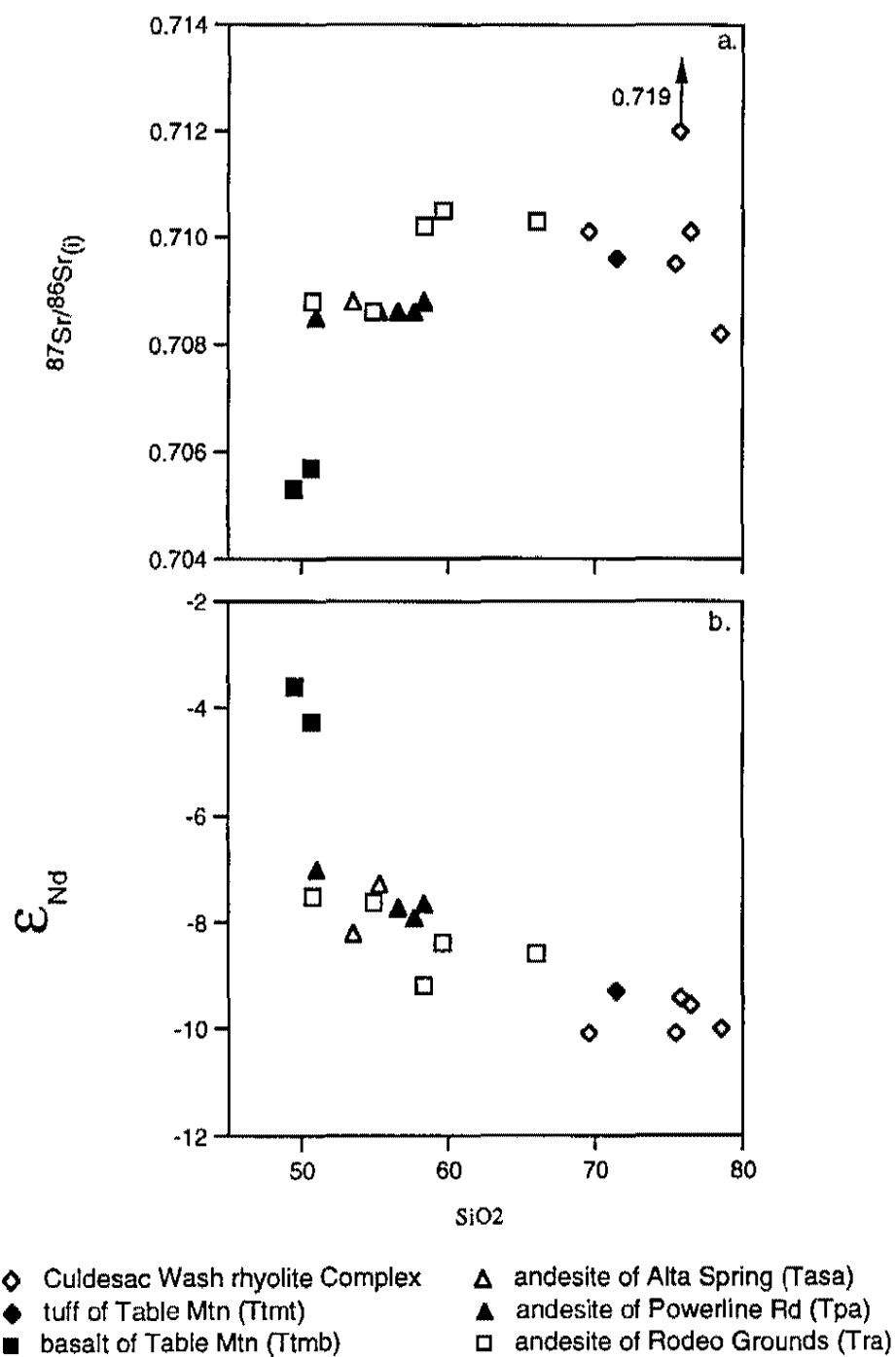


Figure 5-7.  $\epsilon_{\text{Nd}}$  and  $^{87}\text{Sr}/^{86}\text{Sr}(i)$  vs.  $\text{SiO}_2$  for DSV rocks. Arrow indicates place of symbol off the graph.

## CHAPTER 6

### Magmatic History of the DSV and the Nature of the CREC Mantle

#### Introduction

Previous work suggests that primitive basaltic magmatism during the Miocene in the CREC can be broadly divided into two genetically distinct groups (Bradshaw, 1991; Fitton et al., 1991; Kempton et al., 1991; Bradshaw et al., 1993; Feuerbach et al., 1993). The first group is mainly calc-alkaline intermediate rocks that were erupted between the onset of volcanism until 6 Ma. This first group broadly overlaps with extension in the CREC and represents approximately 95% of the volume of all CREC volcanism (Bradshaw et al., 1993). The pre-6 Ma mafic volcanism has been linked by numerous workers to a source in the lithospheric mantle (Glazner and Bartley, 1984; Smith et al., 1990; Bradshaw, 1991; Fitton et al., 1991; Kempton et al., 1991; Ormerod et al., 1991; Bradshaw et al., 1993; Feuerbach et al., 1993). These rocks have a wide range of enriched isotopic ratios (synextensional lavas on Fig. 6-1).

The majority of the pre-6 Ma rocks are enriched in LILE and LREE compared to HFSE and HREE producing the series of peaks and dips and the prominent Nb-Ta trough characteristic of Basin and Range synextensional magmatism (sample MO-2 in Fig 6-2). Such trace element signatures are

typical of subduction related settings (e.g., Yogodzinski et al., 1994), but in areas of continental extension they are unique to the lithosphere beneath the Basin and Range (cf. Fig. 10, p. 13,708, Western rift East Africa, in Fitton et al., 1991; Table 4, p. 241, Siberian Baikal rift, in Ionov et al., 1992). This 'subduction-type' signature is thought to be produced by ancient subduction related processes which chemically modify the overlying subcontinental lithospheric mantle (discussed later).

The second CREC group includes mafic alkali basalts of Miocene-Pliocene age (6-4 Ma). The post-6 Ma CREC basalts have asthenospheric isotopic signatures (Fig. 6-1;  $\epsilon_{Nd} = -1$  to  $+7$ ;  $^{87}Sr/^{86}Sr_{(i)} = 0.703-0.705$ ) with trace element patterns (i.e., low LILE/HFSE ratios, no Nb-Ta trough) similar to that of ocean island basalts (OIB). The change from lithospheric to asthenospheric magmatism is attributed to adiabatic melting of rising asthenosphere (Bradshaw, 1991; Fitton et al., 1991; Kempton et al., 1991; Daley and DePaolo, 1992; Bradshaw et al., 1993; Feuerbach et al., 1993). The abrupt transition to asthenospheric lavas is clear on a plot of age versus  $\epsilon_{Nd}$  (Fig. 6-3) where a sharp change is seen at approximately 6 Ma. No pre-6 Ma asthenospheric derived lavas are present at the DSV, but they are abundant near Lake Mead (e.g., Fortification Hill, Lava Cascade, Grand Wash Trough), 50 km to north of DSV. The distinction between lithosphere and asthenosphere in this study is made solely on the basis of geochemistry and does not rely on geophysical properties.

This chapter discusses the genesis and source of the mafic volcanic rocks of the Dolan Springs volcanic field (DSV) and places them in a regional context. Most of the DSV rocks are broadly similar to the regional

geochemical trends mentioned above, yet the youngest DSV basalts are tholeiitic and quite unique. The trace element character of the mantle is addressed and a hypothesis about stratification of trace element abundance will be presented. Additionally, a potential correlation between the Mt. Perkins pluton and the DSV is briefly explored. Finally, two models are presented, one for Basin and Range trace element enrichment and a second for magma genesis in the CREC.

### **Introduction to DSV Magmatic History**

Volcanism at the DSV began approximately at 17.98 Ma and lasted until about 11 Ma. Therefore, DSV rocks fall completely within the earlier CREC group mentioned above. The DSV volcanic rocks will be discussed in two groups, those erupted prior to and during extension, and those erupted after major extension ended. For simplicity the first group will be referred to as synextensional and the second as postextensional.

As a whole the DSV synextensional volcanic record (~17.98 Ma to ~16.09 Ma) is dominated by calc-alkaline intermediate compositions (i.e., andesite and basaltic-andesite, Fig. 5-1). However, the most primitive DSV synextension basalts (Fig. 5-1a) are alkalic and may be a closer representation of the parental magma from which the intermediate rocks evolved. None of the mafic rocks in the DSV probably represent unevolved mantle melts, but they are still the best source of information on the character of the mantle source.

The DSV synextensional rocks display isotopic variation with respect to

SiO<sub>2</sub> (Fig. 5-7) which suggests open system evolutionary processes. Other CREC calc-alkalic rocks with similar evidence for open system evolution have been effectively modeled by other workers with combinations of fractional crystallization and magma mixing (Feuerbach et al., 1986; Larsen and Smith, 1990; Smith et al., 1990; Cascadden, 1991; Falkner, 1993; Metcalf, et al. 1993; Metcalf, et al. 1995). The mafic end-members in these suites are mantle derived alkali basalts. Felsic end-members in such systems are thought to represent crustal melts. Rocks of the Culdesac rhyolite complex have trace element and isotopic compositions similar to the felsic end members used to model the petrogenesis of the Mt. Perkins (Metcalf et al., 1995), Wilson Ridge (Larsen and Smith, 1990, Feuerbach et al., 1993) and Aztec Wash plutons (Falkner, 1993; Falkner et al., 1995). Growing evidence suggests there is little variability in the CREC crustal source and that individual suites are most clearly discriminated by the mafic end-members that are driving the evolutionary processes (R.V. Metcalf, personal communication, 1995). The genesis of the most primitive rocks of the DSV and CREC is the primary interest here, so only the most mafic samples (< 55 wt.% SiO<sub>2</sub>) from any data set will be considered here.

The postextensional volcanic history of the DSV is uncommon for the CREC. Low volume tholeiitic basalts were erupted at approximately 11 Ma (age discussed in Chapter 2). No felsic or intermediate volcanism accompanied this tholeiitic pulse. The discussion of the DSV tholeiites is expanded to include other tholeiites identified elsewhere in the Colorado River extensional corridor (CREC).



## Discussion of the Origin of Mafic Magmas

### Synextensional Magmatism

The geochemical signature of synextensional basalts at the DSV is similar to basalts from other synextensional CREC volcanic fields. Figure 6-2 compares three DSV synextensional basalts with two synextensional basalts from Lake Havasu City, Arizona (Fig. 1-1), south of DSV (Bradshaw et al., 1993). The Lake Havasu City samples are representative of the regional CREC data set examined by Bradshaw et al. (1993).

Bradshaw et al. (1993) modeled the genesis of a large database of synextensional basalts from across the CREC (similar to DSV) with non-modal batch-melting of averaged lithospheric mantle compositions (from both Colorado Plateau mantle xenoliths and a modeled lithospheric source). Batch melts (1-25%) of a fertile garnet-bearing (2.5-4%) lherzolite explain most of the primitive basalts (i.e., MO-2 Fig. 6-2).

A subset of the Bradshaw et al. (1993) data contains basalts (referred to as group 2a) from Lake Havasu City, Arizona, erupted during the final stages of synextensional magmatism at that latitude (14-14.7 Ma). Lake Havasu City lies at the axis of the CREC in one of the most highly extended areas (Bradshaw et al., 1993). These rocks have a trace element pattern similar to the early synextensional rocks for elements more incompatible than the LREE's, but with lower overall abundances (Fig. 6-2). The young Lake Havasu City rocks, however, have a flatter profile for elements more compatible than La and higher abundances for elements more compatible than Ti (i.e., Y, Yb, Lu) than the older synextensional basalts (Fig 6-2). In addition larger degrees

of melting in the source can be invoked to create these more depleted signatures but that does not explain the higher Y and HREE (Yb & Lu) values. Larger degrees of melting are not intuitively consistent with the decreasing volume of volcanic material produced as extension waned.

An alternative method of producing the lower trace element abundances of the late extensional Lake Havasu City basalts is by melting a more depleted source. Bradshaw et al. (1993) modeled formation of the late extension Lake Havasu City basalts with 2-6% melting of a garnet absent, spinel bearing source. A spinel rather than garnet bearing source accounts for the higher Yb contents in the younger basalts. Ytterbium is incompatible in most mantle minerals (including spinel), with the exception of garnet which preferentially retains Yb ( $D_{Yb}^{garnet} > D_{Yb}^{spinel}$ ). Partial melting of a spinel-bearing source will release larger amounts of Yb than a garnet-bearing source. Xenoliths found within lavas are commonly garnet bearing peridotites, but depleted spinel lherzolite xenoliths have been found in the southern Arizona transition zone (Frey and Printz, 1978). Bradshaw et al. (1993) used the composition of a spinel bearing xenolith from the San Carlos volcanic field, Arizona (Frey and Printz, 1978) for their modeling of the late extension Lake Havasu City basalts. The San Carlos xenoliths have both a different modal mineralogy and different bulk composition from the garnet xenolith compositions used for modeling the earlier synextensional basalts. Bradshaw et al. (1993) suggest that the late synextensional basalts melted from a shallower source than the earlier synextensional basalts, because spinel is stable in the mantle at shallower pressures than garnet. Therefore, Bradshaw et al. (1993) concluded that the depth of melting decreased as extension

progressed based on the mineral stabilities of the changing sources modeled for the synextensional basalts.

Bradshaw et al. (1993) showed that rocks from all over the CREC share the same trace element traits as sample MO-2 (Fig. 6-2). The three DSV samples also share this trace element pattern further suggesting that synextensional volcanism across the CREC shared a source in the lithospheric mantle and similar history of melt generation.

Isotopes (Sm-Nd and Rb-Sr) lend support to the lithospheric mantle source hypothesis for CREC synextensional rocks. The mafic DSV synextensional rocks are isotopically enriched (Table 5-1, Fig. 5-5, Avg.  $\epsilon_{Nd} = -7.62$ ,  $^{87}Sr/^{86}Sr_{(i)} = 0.709$  for  $SiO_2 < 55$  wt.%). Two mechanisms may create isotopically enriched mantle reservoirs. The first mechanism creates intermediate isotopic ratios via mixing of less enriched primary magmas with highly enriched crustal material. The second mechanism, which is preferred here, assumes that primary magmas inherit their isotopic ratios from their source. The first path was explored by Daley and DePaolo (1992) and Bradshaw et al. (1993) and their modeling suggests that mixing of 55-65% felsic crust ( $\epsilon_{Nd} = -18.0$ ) is necessary to shift depleted isotopic values (asthenosphere  $\epsilon_{Nd} = +6.0$ ) to the observed values. Crustal contamination of this degree would elevate  $SiO_2$  wt.% much higher than observed in the DSV (e.g., sample Tasa-83 has  $\epsilon_{Nd} = -8.2$  &  $SiO_2 = 53.5$  wt. %).

Cryptic contamination by a mafic crustal source can produce changes in isotopic composition while leaving the major element composition unaffected. This model has been used to explain the systematic shift of three

$\epsilon_{Nd}$  units seen in successive flows at the Amboy crater field in the Mohave region (Glazner and Farmer, 1991; Glazner et al., 1991). This model seems thermodynamically unreasonable, however, because it requires the mixing of a 50% melt of Jurassic gabbro to change the isotopic signature of an asthenospheric basalt without affecting the major elements. The shift needed to account for CREC basalts would be much greater from  $\epsilon_{Nd} = +6$  (typical of asthenosphere) to  $\epsilon_{Nd} = -10$  (most enriched synextensional basalts).

In addition, it seems unlikely that contamination could produce large amounts of mafic magmas with such similar trace element signatures (Fig. 6-2) for a period of 10 my (20-10 Ma). It requires a crustal reservoir with rather uniform trace element composition. Therefore, the preferred hypothesis is that the enriched isotopic character of the synextensional basalts is inherited from their source region and any crustal contamination is minor. To create enriched isotopic reservoirs, the mantle source must be isolated from the convecting mantle for an extended period of time (>1 by). The age of lithosphere mantle beneath the CREC and the timing of the trace element enrichment is discussed in a later section.

### Postextensional Magmatism

The postextensional volcanism in the DSV is limited to the tholeiitic basalts of Table Mountain, which are volumetrically minor compared to the synextensional rocks, but mark a significant departure in chemical character from the earlier volcanism. On a primitive mantle normalized diagram (Fig 6-4a) the basalt of Table Mountain has a smoother convex up trace element

signature compared to a typical synextensional basalt and is similar to ocean island basalts (OIB). OIB magmas (e.g., Hawaii) originate in the convecting asthenosphere below the asthenospheric mid-ocean ridge basalt (MORB) source. Post-6 Ma basaltic rocks in the CREC also displays OIB like trace elements with isotopic ratios ( $\epsilon_{Nd} = -1$  to  $+7$ ;  $^{87}Sr/^{86}Sr_{(i)} = 0.703-0.705$ ) typical of asthenospheric derived magmas (Bradshaw, 1991; Fitton et al., 1991; Kempton et al., 1991; Bradshaw et al., 1993). Table Mountain, however, has an enriched isotopic signature suggestive of a source in, or contamination from, the lithosphere ( $^{87}Sr/^{86}Sr_{(i)} = 0.705-0.707$ ;  $\epsilon_{Nd} = -3.5$  to  $-4.5$ ).

In the CREC primitive basalts are almost ubiquitously alkalic; tholeiitic magmatism is rare. The only previously described occurrences of tholeiites in the CREC are at Malpais Flattop (Daley and DePaolo, 1992; Feuerbach et al., 1993) and upper basalt flows of Hamblin-Cleopatra volcano (Daley and DePaolo, 1992). Two additional previously unrecognized CREC tholeiitic basalts were identified from the literature: the basalt of Senator Mountain in the northern White Hills (Cascadden, 1991), and the basalt of Callville Mesa (Feuerbach et al., 1991; E.I. Smith, unpublished data).

Though not rigorously constrained, the CREC tholeiites appear to have erupted between approximately 12 Ma and 9 Ma. The age of the capping basalt flow at Malpais Flattop was reported as  $6.0 \pm 1.0$  Ma by Faulds (1993b) using the K/Ar whole rock analysis of Anderson et al. (1972) corrected with constants from Dalrymple (1979). Faulds and Gans (unpublished data) again dated capping flows of Malpais Flattop using whole rock  $^{40}Ar/^{39}Ar$  and obtained ages of  $11.88 \pm 0.15$  Ma and  $11.37 \pm 0.14$  Ma. The 11 Ma ages are preferred here because of the consistency and the minimized effects of sample

heterogeneities in  $^{40}\text{Ar}/^{39}\text{Ar}$  process. The upper flows of Hamblin-Cleopatra are reported to be 11.5 Ma (K/Ar; Thompson, 1985). The Callville Mesa flows erupted between  $10.46 \pm 0.23$  Ma and  $8.49 \pm 0.20$  Ma (K/Ar; Feuerbach et al., 1991). The basalt flows of Table Mountain and Senator Mountain have not been radiometrically dated but are also estimated to be approximately 11 Ma (see Chapter 2: Chronology)

The CREC tholeiites strongly contrast with the DSV calc-alkaline rocks (Figure 6-5). The tholeiites of Table Mountain, Senator mountain, and Malpais Flattop have  $\text{SiO}_2$  ranging from 47-51 wt.% (Fig. 6-5), while the Hamblin and Callville suites have a higher range of  $\text{SiO}_2$  (51-59 wt.%). Callville Mesa rocks are contaminated by felsic xenoliths. The contamination may account for deviation from the more primitive tholeiite compositions (Fig. 6-5). The Hamblin-Cleopatra rocks ( $\text{SiO}_2$  53-57 wt.%) also underwent some degree of contamination and/or fractionation (Fig. 6-5). Only the most primitive sample from any suite was used for comparison and analysis (all  $<53$  wt.%  $\text{SiO}_2$ ). All of the CREC tholeiites are strongly hypersthene normative (7.4-18.5 wt.%) and lack normative quartz. Similar to basalt of Table Mountain the other CREC tholeiites have an OIB like trace element signature (Fig. 6-4b). Notably the normalized patterns are smoother (Fig 6-4a&b), lack a Nb-Ta trough (minor trough on some samples may be transitional), and on average the tholeiites have lower overall trace element abundances than the synextensional rocks (Fig. 6-2). The OIB like trace element signature of the tholeiites is more similar to the post-6 Ma asthenospheric basalts than the earlier lithospherically derived synextensional basalts. In contrast, the CREC tholeiites ( $^{87}\text{Sr}/^{86}\text{Sr}_{(i)} = 0.705$ -

708;  $\epsilon_{Nd} = -3.5$  to  $-10.1$ ) share much the same range of isotopic values as the earlier synextensional rocks (Fig. 6-1). The enriched isotopic ratios of the tholeiites precludes a source in the asthenosphere.

Age constraints suggest that the CREC tholeiites occur at a time transitional between the clearly lithospherically derived synextensional rocks and the clearly asthenospherically derived post-6 Ma rocks. Geochemical modeling was undertaken to explain the lithospheric isotopic ratios and the OIB trace element signatures of the CREC tholeiites. Models are summarized in Table 6-1. Mixing of asthenospherically derived (MO-6; Bradshaw, 1993) and lithospherically derived magmas (various synextensional samples from DSV, Bradshaw et al., 1993, and Feuerbach et al., 1993) was dismissed on the grounds that to change asthenospheric isotopic ratios to the range exhibited by the tholeiites requires so large an addition (55-65%) of lithospheric magma as to impart the typical lithospheric trace element characteristics like the high Ba and Nb-Ta trough.

Batch melting calculations were performed using the median composition of 375 spinel peridotite xenoliths (McDonough, 1990), and individual xenolith compositions of garnet amphibolite, granulite, eclogite, and paragneiss from the Colorado Plateau (Wendlandt et al., 1993). All models proved to inaccurately model the trace elements, produce an overly felsic composition, and/or have completely unsuitable isotopic compositions. A cryptic crustal contamination approach was attempted with an amphibolite from Saddle Island, Lake Mead which has trace elements broadly similar to OIB (E.I. Smith, unpublished data; Duebendorfer et al., 1990). A depleted mantle melt was used as the parent in order to allow the smallest amount of

the assimilant to impart the OIB like signature to the melt. To approximate the tholeiitic trace element signature, 40% whole rock assimilation of the amphibolite was required, which does not seem reasonable in terms of a heat budget. A partial melt of the amphibolite mixed with a mantle melt was also tried, but failed to produce acceptable concentrations of Nb, Ta, or Sr as did whole rock assimilation. The only model that accurately produced the trace element pattern of the basalt of Table Mountain or any of the tholeiites was a mixture (80:20) of a 10% partial melt of spinel peridotite (median of 375 world wide samples; McDonough, 1990) with an average of the andesite of Alta Spring (the latest synextensional rock). This mixture could also produce the observed isotopic variation of the tholeiites, because both sources are lithospheric. This model seems too contrived because it requires the mixture of two distinct types of lithospheric melts, one typical of the Basin and Range (with a Nb-Ta trough, etc.) and one typical of world wide lithospheric mantle (no Nb-Ta trough).

The unique character of the tholeiitic rocks may be related to melting of a shallow, previously untapped portion of the lithospheric mantle. Experimental melting of a spinel lherzolite (Takahashi and Kushiro, 1983) under dry conditions established that alkali basalts are derived by melting at 15-25 kb, while olivine tholeiites are created from larger degrees of partial melting at the same pressures or smaller degrees of melting at lower pressures (8-15 kb). The higher pressure tholeiites differ from the lower pressure tholeiites in having lower normative hypersthene contents. Twenty five tholeiites melted between 5-15 kb have an average normative hypersthene content of 13.8% and six tholeiites melted between 20-25 kb have

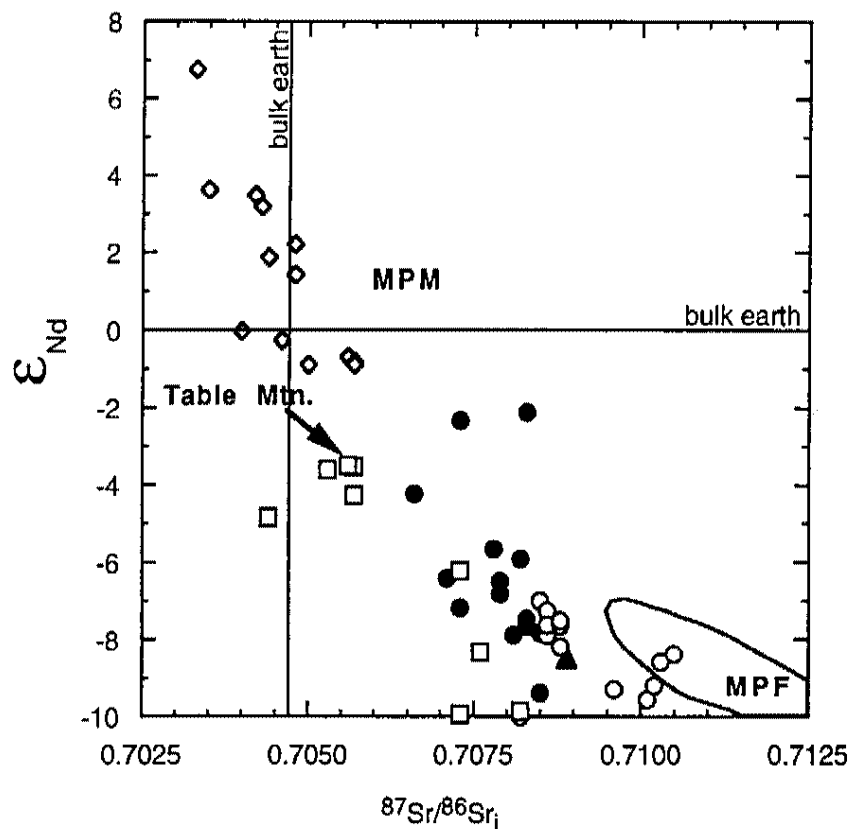


an average hypersthene content of 3.3%. The average normative hypersthene for the Table Mountain tholeiites is 13.6 versus an average of 8.9 for the DSV synextensional rocks  $\leq 56$  wt.%  $\text{SiO}_2$  (Appendix A, Table A-3). Higher normative hypersthene combined with the low volume of tholeiitic basalt (e.g., basalt of Table Mountain  $\approx 10 \text{ mi}^2 \times 300 \text{ ft} = 8.4 \times 10^{10} \text{ ft}^3$ ) suggest that they were produced by low degrees of partial melting at shallow depths (35-50 km assuming the crust is 30 km thick and  $\rho = 2.8 \text{ g/cm}^3$  and the lithosphere is 70 km thick  $\rho = 3.3 \text{ g/cm}^3$ ; Daley and DePaolo, 1992).

As discussed previously, primitive basalts erupted prior to the tholeiitic episode are entirely alkalic and are produced at depths of 50-70 km (Takahashi and Kushiro, 1983). The implication for the CREC is that the depth of melting became shallower during extension and entered the range of tholeiite production by  $\approx 12$  Ma. This observation agrees with the previous interpretation by Bradshaw et al. (1993) that the depth of melting decreased in the lithosphere as a transition was made from a higher pressure garnet source to a lower pressure spinel source.

The source for the tholeiites is interpreted here to be in the uppermost part of the lithospheric mantle (35-50 km) with a depleted trace element signature that lacks the features usually associated with Basin and Range lithosphere (i.e., high Ba, Nb-Ta trough, etc.). No obvious crustal contamination was observed in petrographic analysis of basalt of Table Mountain. Although there are probably few rocks in the CREC that represent unevolved mantle melts, the trace element patterns of the tholeiites probably reflect the composition of the mantle source. The origin and evolution of this unique lithospheric source is still debatable.

The importance of the tholeiites as a unique CREC volcanic episode generated from a distinctly different lithospheric source was previously unrecognized. Basalt of Table Mountain was misinterpreted earlier as an asthenospheric basalt on the basis of its OIB like trace element signature (Bradshaw et al., 1993). Therefore, it is important to avoid the discrimination of asthenospheric and lithospheric sources based purely on trace element compositions (e.g., Bradshaw, 1991; Fitton et al., 1991; Bradshaw et al., 1993).



- DSV synextensional alkalic to calc-alkalic lavas (Tra, Tasa, Tpa).
- CREC synextensional alkalic to calc-alkalic lavas (Cascadden, 1991; Daley and Depaolo, 1992; Bradshaw et al., 1993; Feuerbach et al., 1991; Feuerbach et al., 1993; E.I. Smith, unpublished data).
- Tholeiitic basalts (Cascadden, 1991; Daley and DePaolo, 1992; Bradshaw et al., 1993; Feuerbach et al., 1993; E.I. Smith, unpublished data, P.B. Gans and J.E. Faulds, unpublished data, and Ttmb from the DSV).
- ▲ Calville Mesa, may represent crustally contaminated tholeiite (E.I. Smith, unpublished data). (Feuerbach et al., 1993).
- ◇ Post extensional asthenospheric alkali basalts (Daley and Depaolo, 1992; Bradshaw et al., 1993; Feuerbach et al., 1991; Feuerbach et al., 1993; E.I. Smith, unpublished data).

Figure 6-1. Isotopic plot for CREC rocks. Arrow points to the basalt of Table Mountain tholeiites. MPM is the mafic end-member in the Mt. Perkins plutonic suite and MPF is the range of felsic end-members in that suite. Data from Daley and DePaolo (1992), Bradshaw et al. (1993), Feuerbach et al. (1993), Metcalf et al. (1993), Metcalf et al. (1995), E.I. Smith, unpublished data, and current study. All samples <60 wt. %  $SiO_2$  most <55 %.

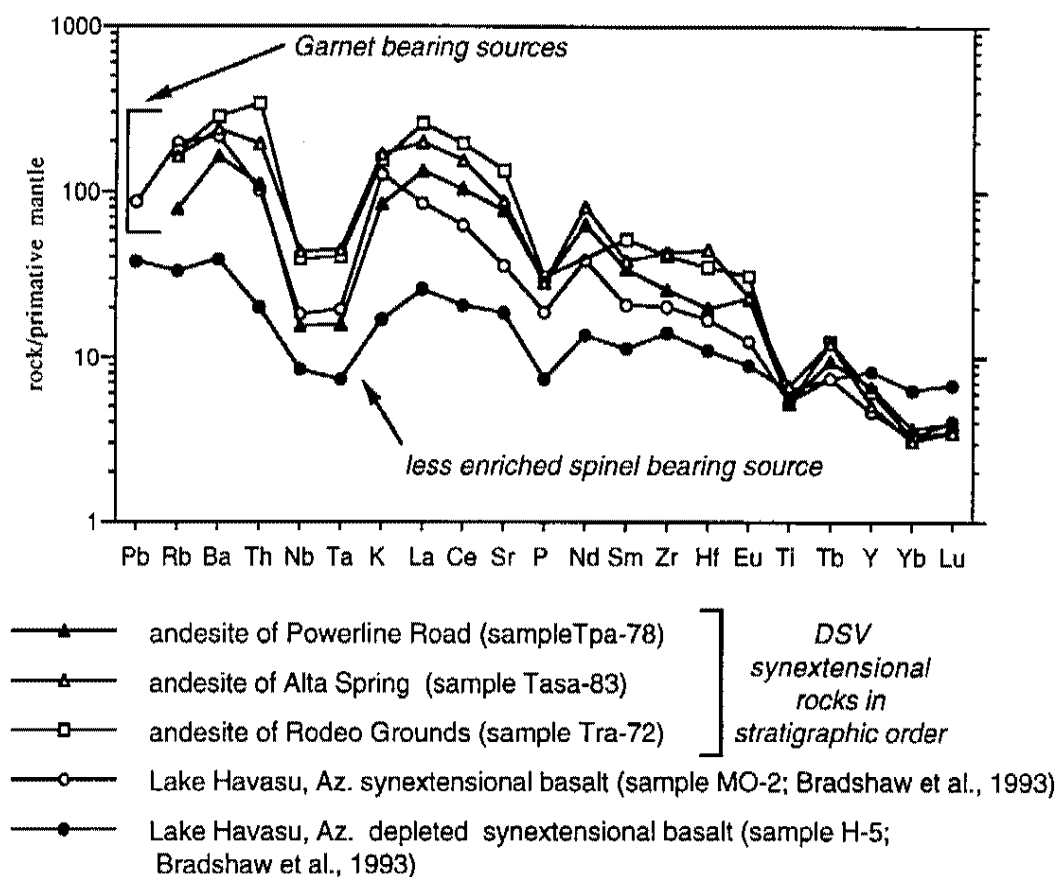
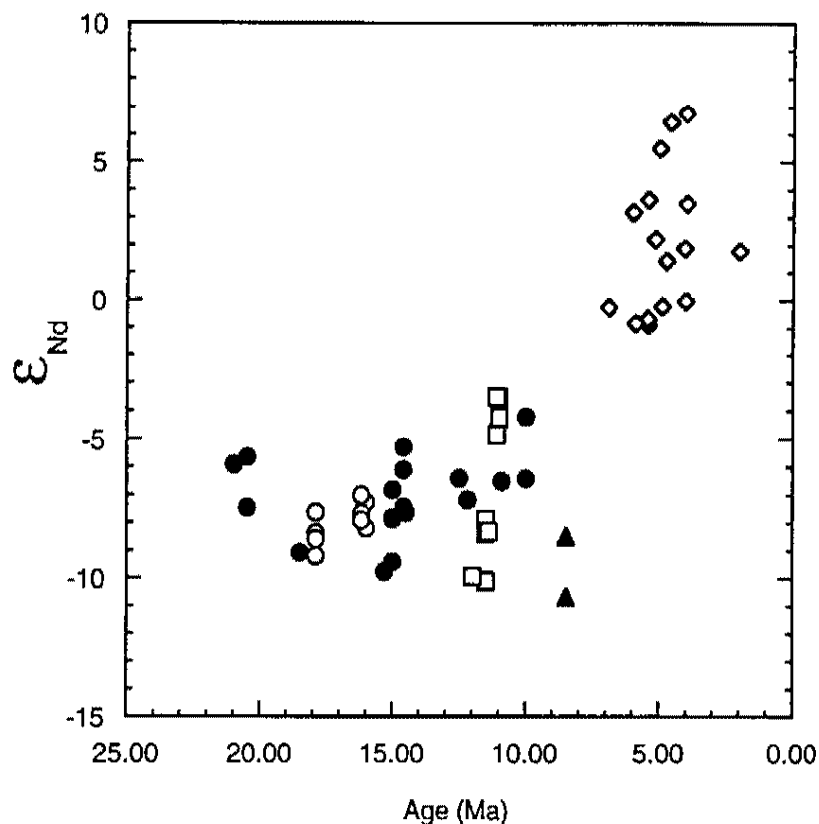


Figure 6-2. Primitive mantle normalized diagrams. Three of the most mafic synextensional samples from the DSV (<54 wt.%  $\text{SiO}_2$ ) compared to two other CREC samples. Elements in order of increasing compatibility with normalizing values from Sun and McDonough (1989). When Nb or Ta were unavailable the ratio  $\text{Ta} = \text{Nb}/17$  was used.



- DSV synextensional alkalic to calc-alkalic lavas (Tra, Tasa, Tpa).
- CREC synextensional alkalic to calc-alkalic lavas (Cascadden, 1991; Daley and Depaolo, 1992; Bradshaw et al., 1993; Feuerbach et al., 1991; Feuerbach et al., 1993; E.I. Smith, unpublished data).
- Tholeiitic basalts (Cascadden, 1991; Daley and DePaolo, 1992; Bradshaw et al., 1993; Feuerbach et al., 1993; E.I. Smith, unpublished data, P.B. Gans and J.E. Faulds, unpublished data, and Ttmb from the DSV).
- ▲ Calville Mesa, may represent crustally contaminated tholeiite (E.I. Smith, unpublished data). (Feuerbach et al., 1993).
- ◇ Post extensional asthenospheric alkali basalts (Daley and Depaolo, 1992; Bradshaw et al., 1993; Feuerbach et al., 1991; Feuerbach et al., 1993; E.I. Smith, unpublished data).

Figure 6-3. Epsilon Nd vs. age for CREC rocks. Notice the change to asthenospheric values at approximately 6 Ma. Data from Daley and DePaolo (1992), Bradshaw et al. (1993), Feuerbach et al. (1993), E.I. Smith, unpublished data, and current study. All samples <60 wt. % SiO<sub>2</sub> most <55 %.

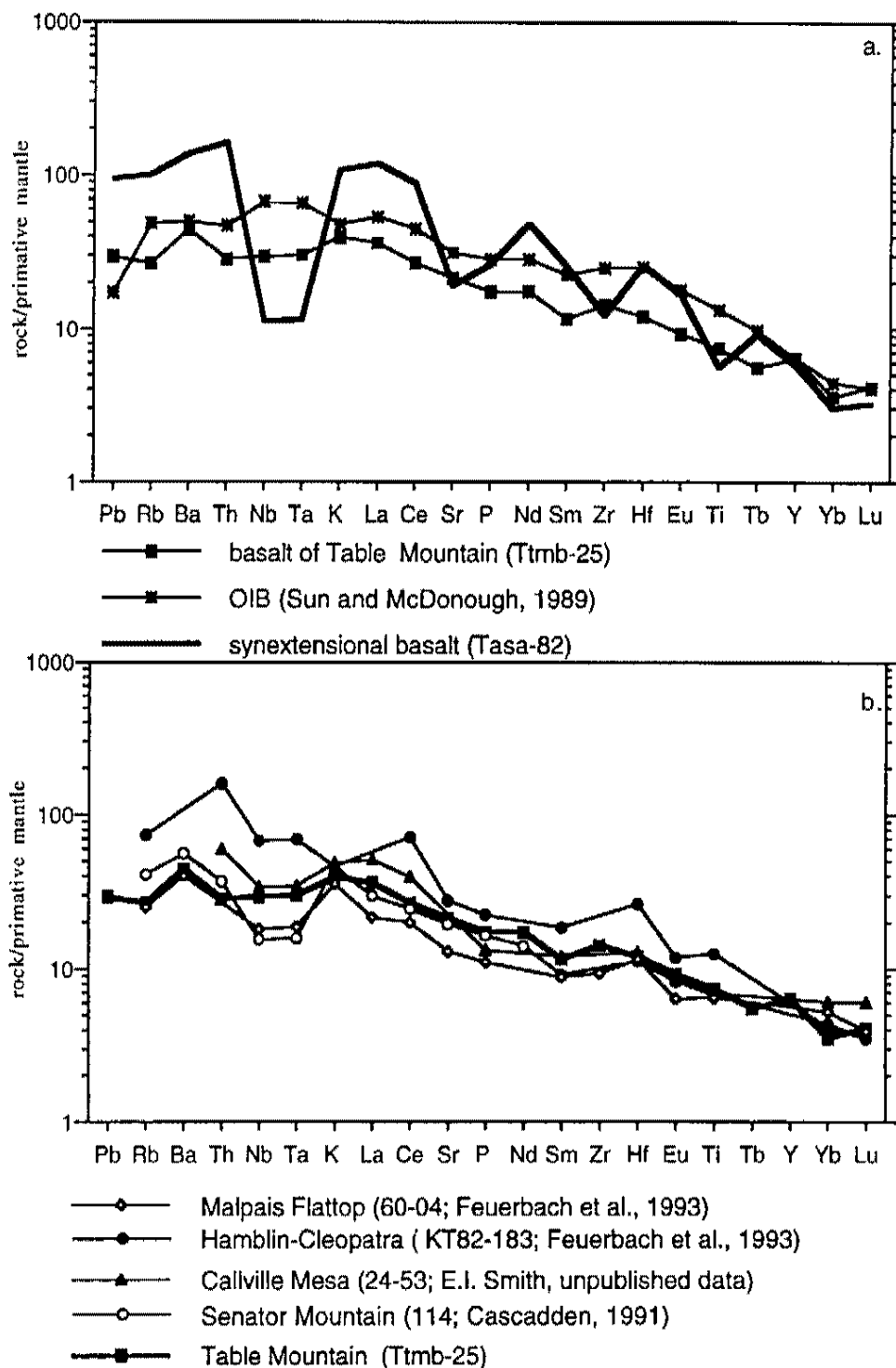


Figure 6-4. Primitive mantle normalized diagrams. a. Ttmb compared to OIB and a DSV synextensional basalt. b. Four other CREC basalts of approximately the same age as Ttmb that also have OIB like patterns. Elements in order of increasing compatibility with normalizing values from Sun and McDonough (1989). When Nb or Ta were unavailable the ratio  $Ta = Nb/17$  was used.

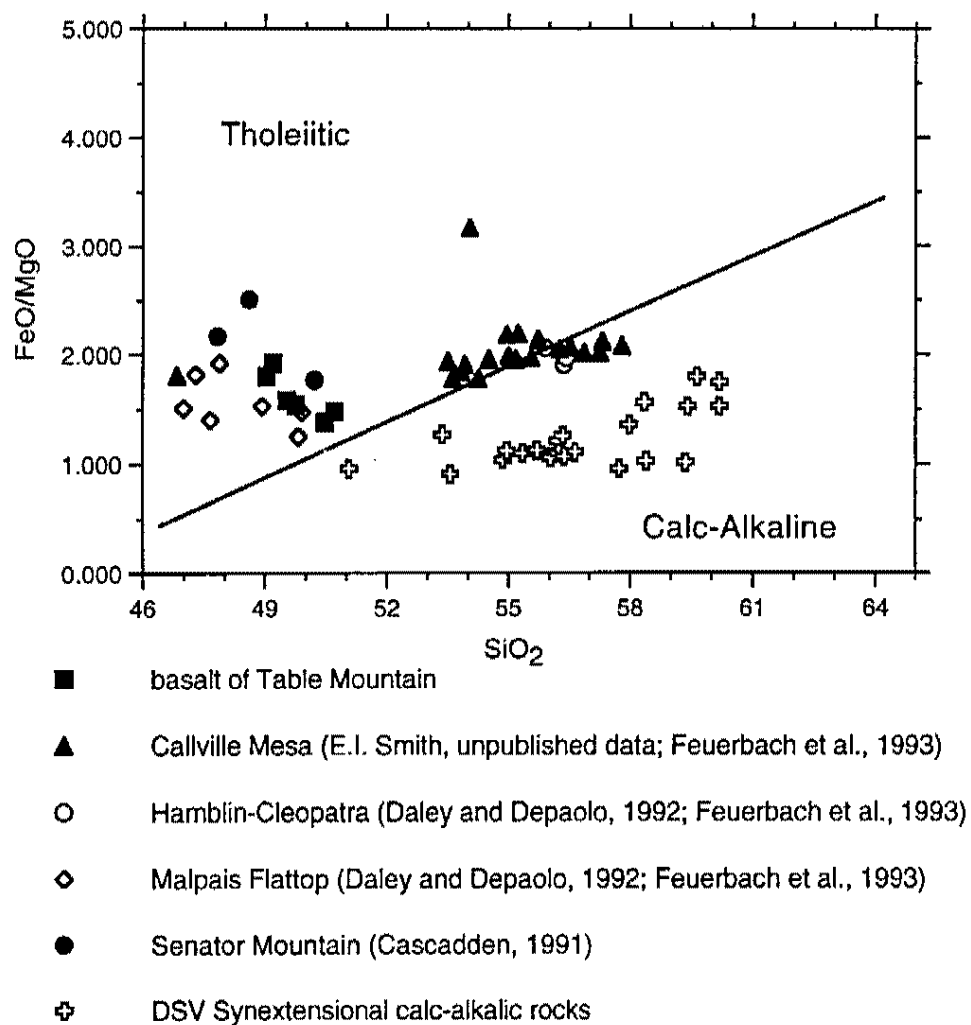


Figure 6-5. Plot discriminating tholeiites from calc-alkalic rocks (Irvine and Baragar, 1971). All of the tholeiites were erupted from 12-9 Ma in the CREC.

Table 6-1: Summary of models for the CREC tholeiites.

<u>Model</u>	<u>Sources</u>	<u>Problem</u>
Mixing of lithospheric and asthenospheric magmas	Asthenosphere (MO-6) from Bradshaw et al. (1993) Lithospheric samples from all DSV units Bradshaw et al. (1993) Feuerbach et al. (1993)	SiO <sub>2</sub> values too high. Ba, Nb, and Ta do not match basalt of Table Mountain (Ttmb).
Batch melting	Median composition of 365 spinel peridotite xenoliths from McDonough (1990)	Failed to match trace element compositions of Ttmb.
Batch melting	Xenolith compositions: garnet amphibolite granulite eclogite paragneiss from Wendlandt et al. (1993)	Failed to match trace element compositions of Ttmb.
40% whole rock assimilation by depleted mantle melt	Saddle Island amphibolite from E.I. Smith, unpublished data and Duebendorfer et al. (1990) Mantle compositions from Hofmann (1988) McDonough (1990) Bradshaw et al. (1993) Yogodzinski et al. (1994)	Broadly similar trace element values, but deemed thermodynamically unreasonable.
Mixing of a batch melt of amphibolite and mantle batch melts	Compositions same as above	Failed to match trace element compositions of Ttmb, especially Nb-Ta trough and Sr.
Mixing 10% batch melt of lithospheric mantle with average of andesite of Alta Spring in proportions 80:20	Lithospheric compositions from median composition of 365 spinel peridotite xenoliths, McDonough (1990) Andesite of Alta Spring from this study.	Appropriate trace element and isotopic values, but deemed unreasonable. Discussed in text.



### The Mt. Perkins Pluton - A Source for DSV?

The Mt. Perkins pluton is a  $15.96 \pm 0.04$  Ma (Faulds, 1993a) granitoid intrusion in the central Black Mountains approximately 15 km west of the DSV (Fig. 1-1). The intermediate rocks of the pluton were derived through a complex history of mixing of asthenospheric basaltic magma ( $^{87}\text{Sr}/^{86}\text{Sr}_{(i)} = 0.7056$ ;  $\epsilon_{\text{Nd}} = +1.2$ ) with a crustal felsic melt ( $^{87}\text{Sr}/^{86}\text{Sr}_{(i)} = 0.7086$  to  $0.7127$ ;  $\epsilon_{\text{Nd}} = -7.82$  to  $-12.5$ ; Metcalf et al., 1995). The pluton lies in the west tilted Mt. Perkins structural block (MPB) that exposes both the pluton and overlying volcanic cover, the Golden Door volcanic rocks (Faulds et al., 1995). Faulds et al. (1995) interpret the MPB as an exposed cross-section of a volcanic-plutonic complex. Faulds et al. (1995) used geochemistry to compare the Mt. Perkins pluton to the Golden Door volcanic section. Incompatible trace elements and isotopes in both suites were found to be similar, making a correlation geochemically permissive. Faulds et al. (1995) support the geochemical correlation with field relationships, including synplutonic dikes traced from the pluton to the volcanic flows.

Morikawa (1993) proposed that the Mt. Perkins pluton might be the source of the DSV volcanic rocks based on similar isotopic ratios and radiometric ages. Morikawa (1993) analyzed a pumice from tuff 2 of Culdesac Wash and reported isotopic ratios ( $^{87}\text{Sr}/^{86}\text{Sr}_{(i)} = 0.7082$ ;  $\epsilon_{\text{Nd}} = -10.0$ ) similar to felsic samples of the Mt. Perkins pluton (Fig. 6-1). The  $^{40}\text{Ar}/^{39}\text{Ar}$  biotite age of  $16.09 \pm 0.15$  (Morikawa, 1993) indicated that the two suites were similar in age.

Lacking any modern physical linkages to the pluton, geochemistry was used to further explore the relationship between the pluton and the DSV.

Isotopic analysis of the DSV mafic rocks (Appendix A, Table A-1) indicate that none of them have the appropriate isotopic values for asthenospheric melts, thereby eliminating them from any correlation with the Mt. Perkins mafic end-member (Fig. 6-1). It should be noted that asthenospheric basalts prior to 6 Ma, such as that at Mt. Perkins, are extremely rare. Incompatible trace elements and isotopes of the DSV felsic rocks were compared to the Mt. Perkins pluton felsic rocks, but the relationships were more ambiguous. Figure 6-6 is an incompatible element diagram used by Faulds et al. (1995) to support the geochemical correlation of the Golden Door volcanic section and the Mt. Perkins pluton. Figure 6-6 is representative of comparisons performed here for the felsic members of these three suites. Felsic rocks from the DSV plot within the fields of both the Mt. Perkins pluton and the Golden Door volcanic section (Fig. 6-6). A correlation between the Mt. Perkins pluton and the DSV is permissive based on the geochemical data, but it is neither unique nor compelling without physical links of dikes or conduits.

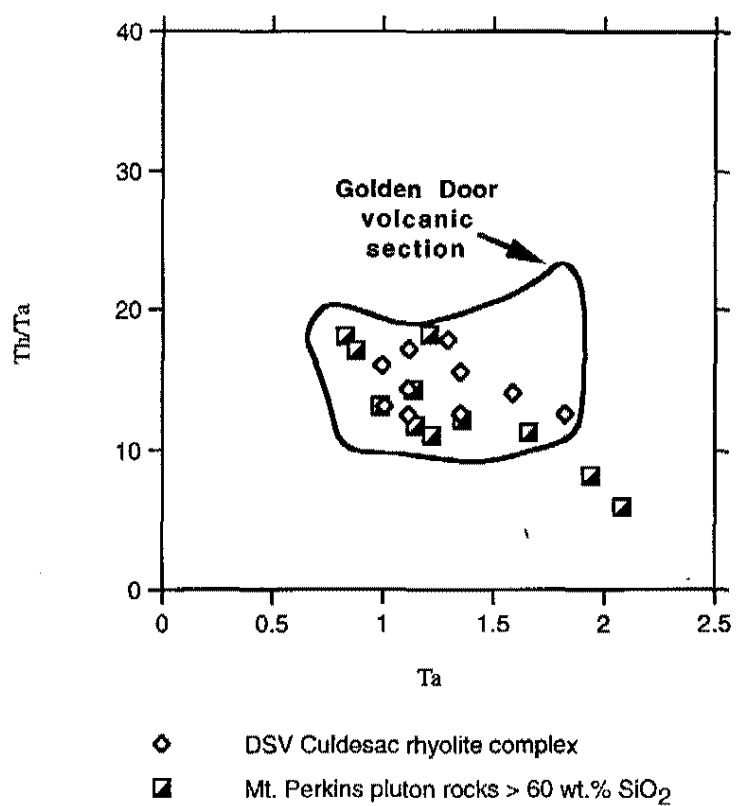


Figure 6-6. Incompatible element diagram for rocks of the DSV and Mt. Perkins pluton (Metcalf et al., 1993; Metcalf et al., 1995) plotted within the field of the Golden Door volcanic rocks (Faulds et al., 1995).

## Trace Element Enrichment and the Nature of the Lithospheric Mantle

### Timing of Trace Element Enrichment and Model Ages

Many previous studies point out that the Basin and Range lithospheric mantle (and the CREC in particular) must have undergone an episode of trace element enrichment, based on the enriched abundances of trace elements in the lithospherically derived basalts (Bradshaw, 1991; Bradshaw et al., 1993; Kempton et al., 1991; Fitton et al., 1991; Ormerod et al., 1991). A previous section demonstrated that the mafic synextensional DSV lavas have trace element signatures similar to the other CREC volcanic rocks (Fig. 6-2). If the subcontinental lithosphere beneath the southwestern United States has seen a metasomatic enrichment event, when did it occur? Intuitively the enrichment event must have been ancient, given the significant time needed to mature the isotopic ratios found in the synextensional basalts. Tertiary subduction of the Farallon plate off the western margin of the United States is too young to account for the isotopic signatures of the synextensional basalts. Bradshaw et al. (1993) argued that  $^{207}\text{Pb}/^{204}\text{Pb}$  and  $^{206}\text{Pb}/^{204}\text{Pb}$  data from CREC synextensional basalts forms a secondary isochron of 1.57 Ga that may represent the age of trace element enrichment. Bradshaw et al. (1993) reported that the 1.57 Ga age is consistent with the age of a lithospheric heating event in the western United States (Dudas et al., 1987). The 1.57 Ga age for the enrichment is somewhat different than the 1.8 Ga Pb/Pb isochron age from synextensional basalts proposed by Kempton et al. (1991) for the entire southwestern United States. The range of the DSV Pb data was not

sufficient to independently assess a secondary isochron age.

Another way to address the timing of enrichment is by placing a minimum age on the lithosphere with Sm/Nd depleted mantle model ages,  $T_{DM}$  (DePaolo, 1981; Bennet and DePaolo, 1987). When applied to basalts the  $T_{DM}$  ideally represents the age when the source of the basalt (i.e., the lithosphere) became separated from mantle that had seen a previous melt extraction. The validity of any model age rests on the assumption that evolution of the Sm-Nd system in the source rock is a simple single-stage closed-system process (McDonough, 1990). Any subsequent melt extraction or enrichment events will decouple the  $^{147}\text{Sm}/^{144}\text{Nd}$  from the radiogenic  $^{143}\text{Nd}/^{144}\text{Nd}$  and impart a new slope to the Nd decay curve. A melt enrichment event will have the effect of making the decay curve shallower and the  $^{143}\text{Nd}/^{144}\text{Nd}$  will increase more slowly, because any melt will have a smaller Sm/Nd ratio than the rock it is intruding (Nd is more incompatible than Sm and will preferentially enter the melt). Therefore, a source that has been melt enriched will produce melts with an artificially low  $T_{DM}$ . If subsequent enrichment episodes occurred in the mantle below the CREC, then the model age reflects only the minimum age when the source of the basalts separated from the depleted mantle. Any young (i.e., Tertiary or later) enrichment events would have not had a significant effect on the  $T_{DM}$  because they are too recent to be resolved in the radiogenic decay.

Table 6-2 displays stratigraphically averaged  $T_{DM}$  model ages for the DSV mafic and intermediate units (personal communication, D. Walker). The lithospheric source of the DSV rocks is at a minimum 1.1 Ga if no ancient enrichment events have occurred. Since some form of an

enrichment event is well established it has probably forced the  $T_{DM}$  to younger values, therefore the age of the lithosphere and the enrichment event are probably greater than 1.1 Ga. An age of trace element enrichment greater than 1.1 Ga age is compatible with the Proterozoic ages proposed by Bradshaw et al. (1993) and Kempton et al. (1991).

Table 6-2: Average depleted mantle model ages ( $T_{DM}$ ) for DSV.

DSV units in stratigraphic order	# in Average	Average Depleted Mantle Age (Ma)
basalt of Table Mountain	2	1053
andesite of Powerline Road	4	1054
andesite of Alta Spring	2	1031
andesite Rodeo Grounds	5	1049

Variable melt enrichment and depletion can also account for the isotopic heterogeneity of the synextensional magma source. DSV mafic lavas have  $^{87}\text{Sr}/^{86}\text{Sr}_{(i)} = 0.708$  to  $0.710$  and  $\epsilon_{\text{Nd}} = -7.0$  to  $-9.2$  while synextensional samples from the CREC have an even larger range (Fig. 6-1 and 6-3). Prolonged periods of enrichment for example would impart various Sm/Nd ratios to the invaded mantle thereby creating pockets of metasomatised mantle with different  $^{143}\text{Nd}/^{144}\text{Nd}$  ratios. An inconsistency with this hypothesis, not resolved here, is that the least trace element enriched basalts, the tholeiites, have the same range of isotopic variability as the earlier enriched rocks (Fig. 6-1 and 6-3).

### Stratification of Trace Element Abundances in the Mantle

As stated earlier, the decreasing depth of melting can be tracked up through the lithosphere during and after extension until ~8 Ma based on two arguments: (1) sources modeled for synextension melt generation change from garnet to spinel-bearing and (2) postextension tholeiitic basalts are likely generated at shallower depths than alkali basalts.

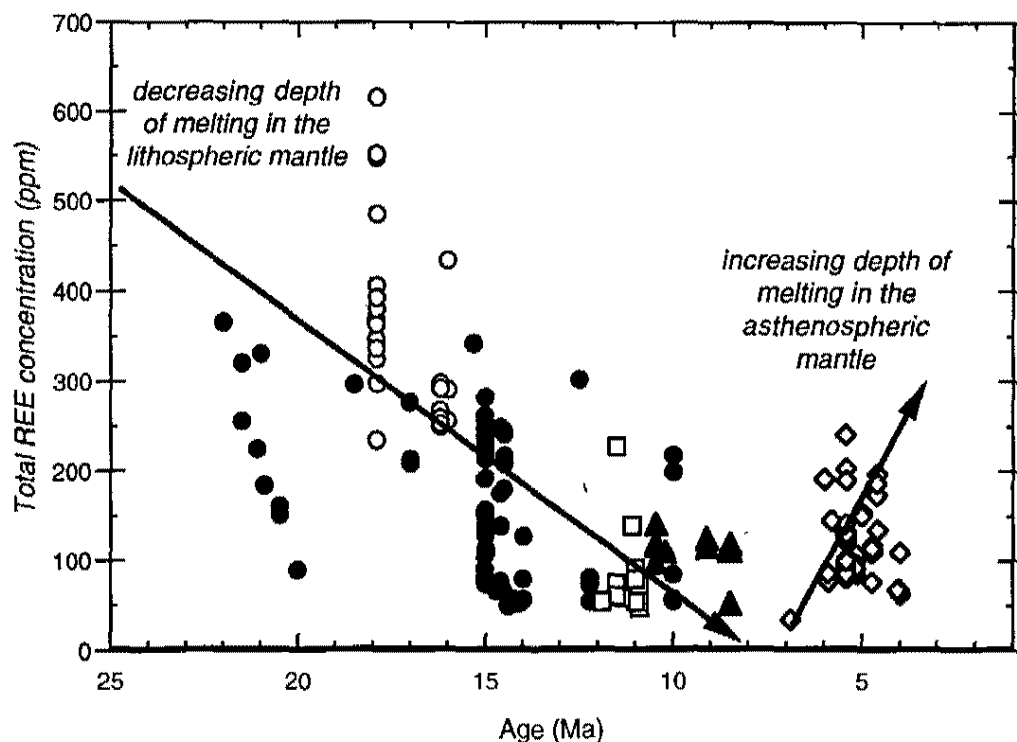
On a diagram of total REE (sum of La, Ce, Sm, Eu, Tb, Yb, Lu) versus age (Fig. 6-7) the general trend is toward decreasing total abundances with age from the period 22-8 Ma. The REE are used to represent trace elements in the source because as a group they demonstrate very similar behavior during melting and they were available in most of the data sets examined. The decrease in REE abundances can be argued to be the result of increasing degrees of partial melting, but this is inconsistent with the decreasing volume of volcanic products as extension progressed (Bradshaw et al., 1993). The hypothesis preferred here is that the lower lithospheric mantle is more enriched in trace elements and the effects of this enrichment decreases upward toward the crust.

At approximately 6 Ma the change to asthenospherically derived basalts occurred in the CREC, though none of these are found at the DSV. Feuerbach et al. (1993) reported that in the Lake Mead area from 6 to 4 Ma basaltic volcanism shifted towards increasingly primitive asthenospheric compositions with higher positive  $\epsilon_{Nd}$  values and an increasing high U/Pb (HIMU) component. Feuerbach et al. (1993) suggested that this shift is due to

the depth of melting increasing between 6 to 4 Ma.

Incompatible trace element abundances are thought to increase with depth from the top of the asthenosphere down, because of the depleting effect of prior melt extraction. Therefore, if the depth of melting was increasing, the 6 to 4 Ma basalts should also show a trend of increasing trace element abundances. This is confirmed by the diagram of total REE versus age (Fig. 6-7) which shows a distinct trend toward increasing REE during this time period. In summary, the mantle may have a bimodal distribution of trace elements with the most enriched compositions in the lower lithosphere. Abundances decrease upward in the lithospheric mantle toward the crust, and increase downward in the asthenospheric mantle toward undepleted regions.





- DSV synextensional alkalic to calc-alkalic lavas (Tra, Tasa, Tpa).
- CREC synextensional alkalic to calc-alkalic lavas (Cascadden, 1991; Daley and Depaolo, 1992; Bradshaw et al., 1993; Feuerbach et al., 1991; Feuerbach et al., 1993; E.I. Smith, unpublished data).
- Tholeiitic basalts (Cascadden, 1991; Daley and DePaolo, 1992; Bradshaw et al., 1993; Feuerbach et al., 1993; E.I. Smith, unpublished data, P.B. Gans and J.E. Faulds, unpublished data, and Ttmb from the DSV).
- ▲ Calville Mesa, may represent crustally contaminated tholeiite (E.I. Smith, unpublished data). (Feuerbach et al., 1993).
- ◇ Post extensional asthenospheric alkali basalts (Daley and Depaolo, 1992; Bradshaw et al., 1993; Feuerbach et al., 1991; Feuerbach et al., 1993; E.I. Smith, unpublished data).

Figure 6-7. Total REE content (La, Ce, Sm, Eu, Tb, Yb, Lu) vs. age for basalts of the CREC. Arrows indicate the decrease in total REEs from 22-8 Ma and then an increase after 6 Ma. See text for discussion related to depth of melting. All samples <60 wt. %  $\text{SiO}_2$  most <55 %. Vertical linear trends are due to limited age data.

## Model for the Tectonic and Magmatic Evolution of the DSV and CREC

### Model for Mantle Enrichment

Though many workers agree that the lithospheric mantle below the Basin and Range underwent trace element enrichment (Dudas et al., 1987; Bradshaw, 1991; Fitton et al., 1991; Kempton et al., 1991; Ormerod et al., 1991; Bradshaw et al., 1993; Wendlandt et al., 1993), little information is known about the process of this enrichment. Fitton et al. (1991) and Kempton et al. (1991) have suggested that fluids expelled by a subducting oceanic plate imparted the subduction-type signature (high Th-Ba, Nb-Ta trough) to the Basin and Range lithospheric mantle. The idea of subducting slab interaction with the overlying mantle is developed further below.

A plausible mechanism for trace element enrichment can be borrowed from Yogodzinski et al. (1994) who modeled the genesis of the modern Piip volcano in the western Aleutians. Piip lavas display the characteristic subduction signature (Fig. 15, p.185, in Yogodzinski et al., 1994) shared by the CREC synextensional basalts (Fig. 6-2). Piip volcano occurs in an ocean-ocean subduction setting, but the conceptual model for trace element enrichment of overlying mantle is still applicable. In this model a trace element enriched slab melt is added to a highly depleted MORB source (N-MORB normalized REE's  $\ll 0.1$ ) in the proportions 4% melt/96% MORB source. Rutile is stabilized in the downgoing slab which preferentially retains Ti, and

therefore, Nb and Ta as well. The effect of even this small amount of enriched melt with a Nb-Ta trough overwhelms the MORB source and results in a trace element signature that mimics the slab melt. Yogodzinski et al. (1994) then in turn effectively model the subduction-type trace element signature of the Piip lavas with a 15% batch melt of this slab/MORB source.

Over the long life of a subduction zone, a melt enrichment process such as this could have potentially imparted the trace element subduction signature to the lithospheric mantle beneath the CREC. If a slab driven process imparted the subduction-type trace element signature to the CREC lithosphere, it may also account for the decreasing trace element abundance with decreasing depth. The mantle nearer the downgoing slab may have been affected to a larger degree. A low degree partial melt from a subducting slab would be silicic with a relatively low temperature and would crystallize as it ascended. Therefore the trace element enriched melt would not likely penetrate the entire pre-extension lithospheric thickness (probably 100 km inferred from unextended Colorado Plateau, (Smith et al., 1989) and the melts should have a decreasing trace element enrichment effect on the lithosphere with decreasing depth. Inherent in this model is the assumption that the mantle prior to enrichment had such depleted trace element abundances that the invading slab melt was able to overwhelm its signature. The CREC tholeiitic basalts interpreted to be the shallowest lithospheric melting event do not display the subduction-type trace element signature and were presumably not affected by the slab melts. The tholeiites' trace element signature is similar to OIB, but it is not known whether this represents the pre-enriched mantle composition or whether this source has undergone a

unique enrichment history. At present no information exists about the composition of the native Proterozoic lithospheric mantle.

### Three Phase Model for CREC Magma Genesis

Using the geochemical observations made in the previous sections, a model has been developed relating Miocene magmatism to crustal extension in the CREC. The model presented here borrows heavily from previous work (Daley and DePaolo, 1992; Bradshaw et al., 1993; Feuerbach et al., 1993; Faulds et al., 1995).

Figure 6-8 schematically depicts a three phase model showing a progression of changing magma sources and depths as extension proceeds. The horizontal lines in the diagram,  $S_{p1}$  and  $S_{p2}$ , represent the solidii of garnet and spinel peridotite at their respective pressures ( $p_1$  &  $p_2$ ). The arched dashed lines,  $G_{t1}$  and  $G_{t2}$ , are schematic geotherms meant to represent the temperatures at which the mantle at a given depth will melt as extension progresses and the depth of melting decreases. Melting will occur when the "melting geotherm" intersects the appropriate solidus. The implication in this model is that the hot rising asthenosphere is forcing the "melting geotherms" to shallower depths by advectively heating the overlying lithospheric mantle. The temperature of the geotherm at time 2 (late extension) is not as high as at time 1 (early extension) because the depth is shallower.

No temperatures are attached to the solidii or geotherms because of the poor constraints on the effects of volatiles in CREC magma genesis. For an

examination of mantle melting with temperature and pressure constraints under dry conditions see McKenzie and Bickle (1988) and Arndt and Christensen (1992), and under wet conditions see Gallagher and Hawkesworth (1992) and Bradshaw et al. (1993).

#### Phase I - Pre-extension Onset of Magmatism to 12 Ma

The first phase of the model encompasses the onset of CREC Miocene magmatism at approximately 22 Ma up to the end of major extension at 12 Ma. During this period alkalic basaltic magmas were generated in the lithospheric mantle between depths of 50-70 km (Takahashi and Kushiro, 1983). Basalts formed early in Phase I are generated from an enriched garnet bearing source ( $S_{p1}$  and  $G_{t1}$ ) which changes to a depleted spinel source ( $S_{p2}$  and  $G_{t2}$ ) as the depth of melting decreases. Trace element content of basalts decreased during Phase I (Fig. 6-7) and, therefore, the bulk trace element abundance of the lithosphere is inferred to decrease upward. The mantle derived alkali basalts ponded in the crust or at its base where open system assimilation-fractional crystallization type processes formed the intermediate compositions that dominate the magmatism of this period (Larsen and Smith, 1990; Smith et al., 1990; Falkner, 1993; Falkner et al., 1995; Metcalf et al., 1993; Metcalf et al., 1995). Heat exchanged between basaltic reservoirs and the crust was probably responsible for crustal melting and CREC felsic volcanism.

## Phase II - Postextension 12-9 Ma

The second phase of this model includes the brief pulse of tholeiitic volcanism in the CREC (Fig. 6-8b). Melting reached its shallowest depth 35-50 km, and exploited a previously untapped source capable of producing OIB like trace element patterns (Fig. 6-4a). The tholeiites appear to be the end point in a progressive decreasing depth of melting. The tholeiites have the same enriched isotopic signature found in the earlier synextensional basalts (Figs. 6-1 and 6-3), therefore the source continued to remain within the lithosphere during Phase II. Given the constraints on the depth of tholeiite production, the melting of the lithosphere can not simply be an adiabatic process. If melting were triggered by decompression melting of lithosphere rising in response to extension, then the tholeiites should display the earlier synextensional trace element signature (i.e., Nb-Ta trough, etc.). Therefore, an advective heating process that triggers melting at shallow levels is preferred here. The probable heat source driving this process is in the asthenosphere. The model is valid whether the asthenosphere is rising actively as a plume or passively due to extension.

## Phase III - Postextension 9-4 Ma

The final phase marks the transition in the CREC to asthenospheric magmatism at about 6 Ma (Fig. 6-8c). The asthenospheric melts are alkaline, thus the depth of melting is deeper (50-70 km) than the Phase II tholeiitic basalts. No concurrent tholeiitic volcanism has been identified for this period, therefore, the geotherms relaxed so that melting was no longer

possible at depths of 35-50 km. The melting in the asthenosphere was accomplished through an adiabatic process bringing it into the range of alkali basalt production (50-70 km). The depth of melting decreased from 6 to 4 Ma as evidenced by the increasing HIMU component (Feuerbach et al., 1993),  $+ \epsilon_{Nd}$  (Fig. 6-3), and REE content (Fig. 6-7).

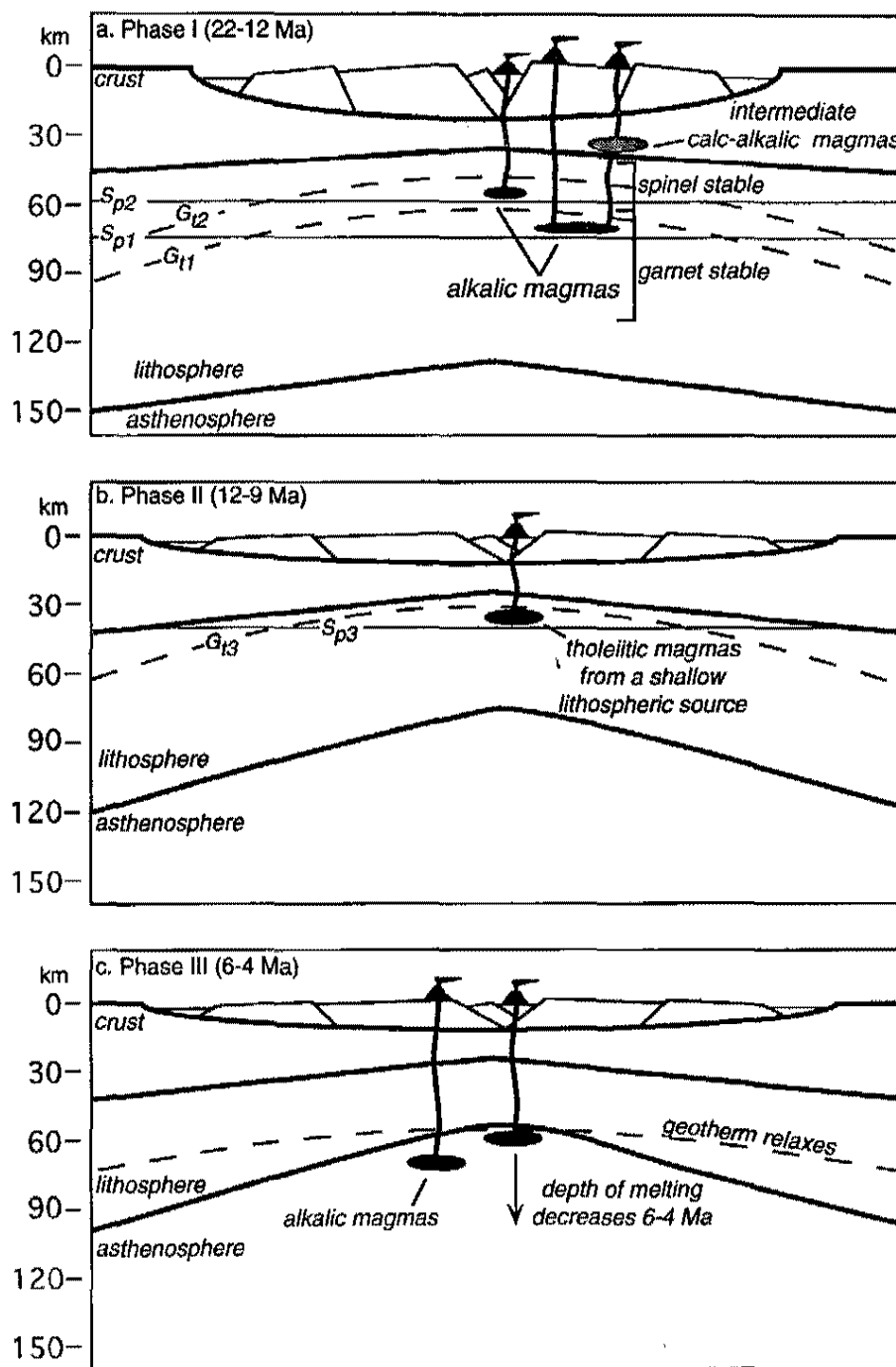


Figure 6-8. Three phase schematic diagram of magma genesis model for the CREC. Model diagram depicts pure shear extension only for the sake of simplicity.  $S_{p1,2,3}$  = peridotite solidus at pressures  $p1-3$ .  $G_{t1,2,3}$  = melting geotherm at time  $t1-3$ . See text for discussion.



### Summary

- 1) Volcanism at the DSV began at approximately 17.98 Ma and ended at approximately 11 Ma. Therefore, it falls completely within the pre-6 Ma volcanic group of the CREC.
- 2) Early pre- and synextensional volcanism in the CREC and at the DSV is dominated by intermediate compositions that evolved from alkali basalts. The most primitive rocks of the DSV share a close chemical affinity to other CREC volcanic rocks of this period (20-12 Ma). The source of the early CREC synextensional rocks (inferred for DSV as well) was a garnet peridotite in the lithospheric mantle. As extension proceeded, the depth of melting decreased and in some of the most highly extended areas a depleted spinel bearing source was tapped late in extension (cf., Bradshaw et al., 1993).
- 3) The synextensional basalts are isotopically enriched and heterogeneous. The preferred hypothesis is that the isotopic signature is inherited from the source, therefore, the source of the pre-6 Ma basalts is inferred to be within the lithospheric mantle.
- 4) A postextension episode of tholeiitic volcanism in the CREC occurred from approximately 12-9 Ma. It includes the DSV basalt of Table Mountain. The CREC tholeiites do not have the trace element features usually associated with Basin and Range synextensional basalts (i.e., high LILE/HFSE ratios), but rather have signatures similar to that seen in OIB (low LILE/HFSE ratios). The tholeiites have the same isotopic variation as the earlier synextensional basalts, therefore, they are also inferred to have a source within the

lithospheric mantle. The depth of tholeiite production (35-50 km) is shallower than that of alkali basalt (50-70 km), which is consistent with the decreasing depth of melting inferred from the synextensional basalts.

5) The decreasing depth of melting in the lithosphere is coincident with decreasing total REE concentrations in basalts from 22 to 12 Ma. Therefore, trace element abundances are believed to be stratified in the lithospheric mantle decreasing upwards.

6) A Proterozoic subduction related process is probably responsible for the enriched arc-like trace element signature of the CREC synextensional basalts. Enriched slab melts penetrating the overlying mantle wedge may have overprinted the native Basin and Range lithospheric geochemical signature.

7) Advective heating of the lithosphere by rising asthenosphere may have initiated synextensional magmatism. As extension progressed from 22 to 12 Ma the depth of melting decreased culminating in the CREC tholeiitic episode which tapped the shallowest level in the lithosphere.

8) At 6 Ma the asthenosphere reached a depth that initiated the production of alkali basalts. The depth of melting decreased from 6 to 4 Ma (Feuerbach et al., 1993).

## **Appendix A**

### **Geochemical Analyses and Rock Norms**

The major and trace element analyses of DSV rocks performed for this study are presented in Table A-1. The method of analysis is in parentheses next to the element in the table: X-ray Fluorescence (XRF), Instrumental Neutron Activation Analysis (INAA), isotope dilution (ID). LOI stands for loss on ignition. The major and trace element analyses on several units of the Culdesac rhyolite complex performed by Morikawa (1994 and unpublished data) are included in Table A-2 with permission of the author. CIPW normative mineralogies for the analyses of this study and from Morikawa (1994 and unpublished data) are presented in Tables A-3 and A-4 respectively. A map of sample locations is on Plate III. All analytical procedures are presented in Appendix B.

Table A-1: Major and trace element analyses of the DSV rocks.

sample#	Tra-3	Tra-4	Tra-57	Tra-31	Tra-43	Tra-6	Tra-27
type	lava	lava	lava	lava	lava	lava	lava
SiO <sub>2</sub>	50.79	58.39	59.35	54.96	59.41	59.46	60.19
Al <sub>2</sub> O <sub>3</sub>	17.40	18.15	14.62	14.43	15.95	16.24	16.31
Fe <sub>2</sub> O <sub>3</sub>	10.56	6.28	5.51	6.79	5.47	6.99	4.97
CaO	9.87	4.94	5.78	7.78	5.42	5.72	4.59
MgO	4.17	1.47	4.80	5.40	3.19	2.42	2.89
Na <sub>2</sub> O	3.20	3.83	2.89	2.56	3.40	3.41	4.22
K <sub>2</sub> O	2.13	4.73	4.60	2.95	4.39	3.76	4.36
TiO <sub>2</sub>	1.37	0.92	1.12	1.12	0.99	0.79	0.90
MnO	0.14	0.09	0.08	0.10	0.08	0.08	0.08
P <sub>2</sub> O <sub>5</sub>	0.70	0.79	0.59	0.57	0.60	0.55	0.59
LOI							1.38
Total	100.33	99.59	99.34	96.66	98.90	99.42	100.48
Pb(ID)		33.20					
Rb(XRF)	49	132	120	55	77	91	123
Ba(XRF)	1180	1623	1143	1047	1255	1148	1159
Th(INAA)		28.53	14.44	10.31	21.75	14.38	25.42
Nb(XRF)	13	34	19	16	19	17	25
La(INAA)		138.8	110.7	74.8	112.9	99.2	119.3
Ce(INAA)		248.4	197.7	144.7	213.9	183.2	230.6
Sr(XRF)	1262	1861	1285	1455	1769	1638	1611
Nd(ID)	63.71	97.71		64.38			
Sm(INAA)		14.42	11.67	10.87	14.04	11.23	13.80
Zr(XRF)	280	606	363	319	362	386	408
Hf(INAA)		11.46	9.92	7.65	8.77	7.86	10.55
Eu(INAA)		3.15	2.73	2.45	3.13	2.47	3.08
Y(XRF)	26	26	21	26	24	24	22
Yb(INAA)		0.62	1.73	0.92	1.58	0.65	1.08
Lu(INAA)		0.10	0.25	0.18	0.16	0.13	0.15
Sc(INAA)		6.8	11.8	14.6	10.3	10.2	8.3
Tb(INAA)		0.84	0.68	0.85	0.92	0.72	0.83
Cr(INAA)		57	173	204	42	140	64
Ni(INAA)		70	139	122	68	89	49
<sup>87</sup> Sr/ <sup>86</sup> Sr <sub>(i)</sub>	0.70882	.71016		.70857			
<sup>143</sup> Nd/ <sup>144</sup> Nd	0.512242	0.512154		0.512236			
<sup>147</sup> Sm/ <sup>144</sup> Nd	0.10	0.09		0.10			
ε Nd	-7.52	-9.20		-7.63			
T <sub>DM</sub>	1093	1078		1045			
<sup>206</sup> Pb/ <sup>204</sup> Pb		18.57					
<sup>207</sup> Pb/ <sup>204</sup> Pb		15.61					
<sup>208</sup> Pb/ <sup>204</sup> Pb		39.19					

Table A-1: Major and trace element analyses of the DSV rocks, continued.

sample#	Tra-52	Tra-54	Tra-55	Tra-38	Tra-66	Tra-60	Tra-72
type	lava	lava	lava	lava	lava	lava	lava
SiO <sub>2</sub>	56.34	59.64	60.19	58.35	56.45	59.65	53.36
Al <sub>2</sub> O <sub>3</sub>	15.61	16.17	16.29	15.15	18.11	16.70	15.89
Fe <sub>2</sub> O <sub>3</sub>	5.75	4.97	5.06	5.11	5.54	4.54	6.58
CaO	5.36	4.47	4.51	6.19	4.25	4.10	6.41
MgO	4.06	2.46	2.58	2.90	1.68	1.92	4.61
Na <sub>2</sub> O	3.66	3.89	4.12	3.35	4.31	4.56	3.43
K <sub>2</sub> O	4.48	4.39	4.42	4.21	5.20	4.72	4.66
TiO <sub>2</sub>	0.96	0.86	0.90	0.91	0.96	0.93	1.13
MnO	0.08	0.07	0.07	0.09	0.10	0.08	0.09
P <sub>2</sub> O <sub>5</sub>	0.61	0.59	0.57	0.57	0.65	0.60	0.67
LOI							
Total	96.91	97.51	98.71	96.83	97.25	97.80	96.83
Pb(ID)						43.26	
Rb(XRF)	154	129	123	115	139	173	110
Ba(XRF)	1297	1310	1191	1323	1164	1064	1967
Th(INAA)	53.90	22.90	25.97	22.47	42.71	68.36	28.80
Nb(XRF)	34	24	25	18	43	60	28
La(INAA)	156.8	123.2	126.2	107.9	212.3	178.7	175.9
Ce(INAA)	304.1	220.5	234.6	209.8	379.6	346.6	345.6
Sr(XRF)	1617	1812	1650	1628	2353	1222	2823
Nd(ID)						111.85	
Sm(INAA)	17.85	14.12	14.26	13.43	16.98	16.39	22.79
Zr(XRF)	512	428	416	341	558	598	459
Hf(INAA)	14.78	9.52	10.54	8.60	14.70	19.80	10.85
Eu(INAA)	3.93	2.95	3.23	3.10	4.01	3.48	5.21
Y(XRF)	25	20	23	22	22	22	28
Yb(INAA)	1.68	1.27	1.38	1.73	1.56	1.66	1.61
Lu(INAA)	0.26	0.21	0.19	0.16	0.23	0.25	0.26
Sc(INAA)	11.6	8.2	8.2	10.0	6.4	6.9	11.4
Tb(INAA)	1.16	0.92	0.97	0.99	1.17	1.10	1.34
Cr(INAA)	123	59	62	39	16	43	104
Ni(INAA)	136	52	86	50	59	44	102
<sup>87</sup> Sr/ <sup>86</sup> Sr <sub>(i)</sub>						0.71055	
<sup>143</sup> Nd/ <sup>144</sup> Nd						0.512196	
<sup>147</sup> Sm/ <sup>144</sup> Nd						0.08	
ε Nd						-8.38	
T <sub>DM</sub>						1003	
<sup>206</sup> Pb/ <sup>204</sup> Pb						18.60	
<sup>207</sup> Pb/ <sup>204</sup> Pb						15.60	
<sup>208</sup> Pb/ <sup>204</sup> Pb						39.24	

Table A-1: Major and trace element analyses of the DSV rocks, continued.

sample#	Tra-33	Tasa-82	Tasa-83	Tasa-74	Ttmt-18	Tcr-93-10	Tcr-80
type	lava	lava	lava	lava	tuff	vitro.	vitro.
SiO <sub>2</sub>	66.05	55.34	53.55	55.70	71.49	69.57	72.20
Al <sub>2</sub> O <sub>3</sub>	16.07	15.18	13.10	15.01	13.91	15.22	13.50
Fe <sub>2</sub> O <sub>3</sub>	3.58	6.49	6.21	6.81	1.80	3.19	1.10
CaO	2.79	6.72	7.04	6.93	1.96	1.55	0.69
MgO	1.29	5.27	6.08	5.38	0.60	0.44	0.11
Na <sub>2</sub> O	3.78	3.15	2.94	3.69	3.81	3.29	3.35
K <sub>2</sub> O	5.13	3.24	5.06	3.78	6.21	4.47	5.38
TiO <sub>2</sub>	0.60	1.21	1.44	1.26	0.37	0.38	0.23
MnO	0.06	0.10	0.10	0.10	0.05	0.06	0.05
P <sub>2</sub> O <sub>5</sub>	0.38	0.57	0.62	0.59	0.10	0.10	0.06
LOI						2.69	
Total	99.73	97.27	96.14	99.25	100.30	100.96	96.67
Pb(ID)	37.67	17.53			29.76	25.82	
Rb(XRF)	220	64	103	99	226	136	158
Ba(XRF)	931	958	1649	1100	0	709	192
Th(INAA)	67.88	13.77	16.40	15.25	41.49	19.17	
Nb(XRF)	32	8	31	21	48	19	21
La(INAA)	133.1	81.6	136.1	89.3	95.8	76.7	
Ce(INAA)	242.9	157.3	273.8	182.5	182.1	135.7	
Sr(XRF)	1013	403	1853	1517	77	230	83
Nd(ID)	82.96	65.72	109.33		73.85	42.51	
Sm(INAA)	11.91	11.30	17.10	12.54	13.55	6.71	
Zr(XRF)	141	137	480	349	265	210	169
Hf(INAA)	12.70	8.04	13.75	8.25	11.19	6.86	
Eu(INAA)	2.28	2.81	3.91	3.02	1.21	1.29	
Y(XRF)	16	26	23	23	36	23	29
Yb(INAA)	1.57	1.49	1.52	1.65	3.15	1.77	
Lu(INAA)	0.27	0.24	0.26	0.26	0.37	0.27	
Sc(INAA)	5.1	15.6	13.8	16.5	2.6	3.7	
Tb(INAA)	0.83	0.99	1.31	0.96	1.38	0.66	
Cr(INAA)	24	182	349	205	13	25	
Ni(INAA)	31	161	317	125	<20.35	23	
<sup>87</sup> Sr/ <sup>86</sup> Sr <sub>(i)</sub>	0.71031	0.70855	0.70883		0.70956	0.71006	
<sup>143</sup> Nd/ <sup>144</sup> Nd	0.512184	0.512254	0.512206		0.512152	0.512109	
<sup>147</sup> Sm/ <sup>144</sup> Nd	0.09	0.10	0.09		0.11	0.09	
ε Nd	-8.59	-7.28	-8.20		-9.30	-10.09	
T <sub>DM</sub>	1027	1039	1022		1269	1143	
<sup>206</sup> Pb/ <sup>204</sup> Pb	18.56	18.30			18.03	17.95	
<sup>207</sup> Pb/ <sup>204</sup> Pb	15.60	15.59			15.54	15.53	
<sup>208</sup> Pb/ <sup>204</sup> Pb	39.26	38.79			38.96	38.80	

Table A-1: Major and trace element analyses of the DSV rocks, continued.

sample#	Tct2-37	Tct2-41	Tpa-78	Tpa-931	Tpa-46	Tpa-69	Tpa-48
type	pumice	pumice	lava	lava	lava	lava	lava
SiO <sub>2</sub>	72.88	75.79	51.06	55.40	56.21	56.37	56.64
Al <sub>2</sub> O <sub>3</sub>	11.52	12.15	14.28	16.21	15.05	15.44	15.16
Fe <sub>2</sub> O <sub>3</sub>	0.70	0.73	8.74	7.60	7.01	6.40	6.72
CaO	1.84	0.59	9.71	7.47	7.41	6.68	6.75
MgO	0.41	0.19	8.08	3.52	5.16	5.34	5.38
Na <sub>2</sub> O	2.44	2.47	2.87	2.86	3.35	3.68	3.38
K <sub>2</sub> O	5.12	5.60	2.53	3.35	3.25	3.41	3.43
TiO <sub>2</sub>	0.11	0.11	1.17	1.19	1.19	1.19	1.22
MnO	0.04	0.05	0.13	0.11	0.10	0.11	0.10
P <sub>2</sub> O <sub>5</sub>	0.17	0.06	0.62	0.65	0.58	0.59	0.57
LOI	4.99				0.86		
Total	100.22	97.74	99.19	98.36	100.17	99.21	99.35
Pb(ID)		28.67					17.69
Rb(XRF)	192	204	50	88	59	76	84
Ba(XRF)	0	0	1130	1280	1165	1026	1005
Th(INAA)	22.27		9.34		11.06	11.85	13.60
Nb(XRF)	27	29	11	19	17	19	18
La(INAA)	34.8		91.3		81.5	83.5	79.6
Ce(INAA)	53.6		184.5		158.8	168.3	157.8
Sr(XRF)	50	20	1632	1307	1452	1353	1316
Nd(ID)		11.27	85.57				72.78
Sm(INAA)	1.41		15.16		11.48	11.02	11.17
Zr(XRF)	73	76	286	364	328	322	329
Hf(INAA)	3.70		6.12		8.10	8.60	8.15
Eu(INAA)	0.12		3.79		2.80	2.66	2.59
Y(XRF)	16	14	30	24	26	25	27
Yb(INAA)	1.79		1.80		1.30	1.48	1.33
Lu(INAA)	0.26		0.29		0.16	0.24	0.22
Sc(INAA)	1.3		24.4		15.2	15.4	15.7
Tb(INAA)	<0.08		1.02		0.88	0.67	0.82
Cr(INAA)	3		233		190	179	190
Ni(INAA)	<15.36		171		133	114	136
<sup>87</sup> Sr/ <sup>86</sup> Sr <sub>(i)</sub>		0.71929	0.70849				0.70862
<sup>143</sup> Nd/ <sup>144</sup> Nd		0.512143	0.512273				0.512236
<sup>147</sup> Sm/ <sup>144</sup> Nd		0.08	0.10				0.09
ε Nd		-9.42	-7.01				-7.72
T <sub>DM</sub>		1040	1036				986
<sup>206</sup> Pb/ <sup>204</sup> Pb		18.01					18.29
<sup>207</sup> Pb/ <sup>204</sup> Pb		15.56					15.56
<sup>208</sup> Pb/ <sup>204</sup> Pb		38.79					38.72

Table A-1: Major and trace element analyses of the DSV rocks, continued.

sample#	Tpa-11	Tpa-68	Tpa-51	Tpa-50	Ttmb-7	Ttmb-8	Ttmb-25
type	lava	lava	lava	lava	lava	lava	lava
SiO <sub>2</sub>	56.23	55.68	58.39	57.73	49.04	49.19	50.70
Al <sub>2</sub> O <sub>3</sub>	15.21	14.82	14.87	14.74	15.72	15.79	14.94
Fe <sub>2</sub> O <sub>3</sub>	6.62	6.52	5.33	6.03	13.14	13.47	11.56
CaO	6.92	6.82	6.48	6.49	9.67	9.74	9.51
MgO	5.38	5.19	4.59	5.59	6.48	6.23	6.96
Na <sub>2</sub> O	3.19	2.99	3.29	3.14	2.99	2.99	2.90
K <sub>2</sub> O	3.40	3.29	4.24	3.76	1.18	1.10	1.19
TiO <sub>2</sub>	1.21	1.20	1.04	1.01	1.52	1.56	1.60
MnO	0.10	0.01	0.08	0.10	0.17	0.17	0.17
P <sub>2</sub> O <sub>5</sub>	0.60	0.53	0.57	0.55	0.36	0.36	0.38
LOI							
Total	98.86	97.05	98.88	99.14	100.27	100.60	99.91
Pb(ID)			22.64	21.80			5.44
Rb(XRF)	82.	85	82	83	16.	15	17
Ba(XRF)	944	1096	1323	1427	490	778	309
Th(INAA)	13.11	13.85	14.84	13.05	2.48		2.41
Nb(XRF)	20	18	17	14	21	21	21
La(INAA)	81.7	81.5	92.1	82.0	23.9		24.9
Ce(INAA)	152.1	160.5	181.9	153.3	45.8		47.7
Sr(XRF)	1297	1283	1589	1717	469	494	451
Nd(ID)			73.35	68.32			23.64
Sm(INAA)	11.05	11.27	12.65	11.55	4.86		5.15
Zr(XRF)	321	319	370	350	161	169	160
Hf(INAA)	7.50	7.85	9.41	7.85	3.61		3.72
Eu(INAA)	2.45	2.97	2.94	2.53	1.40		1.55
Y(XRF)	26	24	25	24	20	22	29
Yb(INAA)	1.40	1.56	1.28	1.62	1.83		1.75
Lu(INAA)	0.19	0.25	0.17	0.17	0.23		0.30
Sc(INAA)	15.0	15.8	11.3	14.0	24.9		25.1
Tb(INAA)	0.74	0.91	0.78	0.88	0.66		0.60
Cr(INAA)	170	181	171	154	289		261
Ni(INAA)	101	177	175	82	84		70
<sup>87</sup> Sr/ <sup>86</sup> Sr <sub>(i)</sub>			0.70882	0.70862			0.70567
<sup>143</sup> Nd/ <sup>144</sup> Nd			0.512241	0.512227			0.512416
<sup>147</sup> Sm/ <sup>144</sup> Nd			0.11	0.10			0.12
ε Nd			-7.65	-7.91			-4.26
T <sub>DM</sub>			1129	1064			1076
<sup>206</sup> Pb/ <sup>204</sup> Pb			18.26	18.48			17.60
<sup>207</sup> Pb/ <sup>204</sup> Pb			15.58	15.59			15.51
<sup>208</sup> Pb/ <sup>204</sup> Pb			38.69	38.85			37.69



Table A-1: Major and trace element analyses of the DSV rocks, continued.

sample#	Ttmb-14	Ttmb-15	Ttmb-16
type	lava	lava	lava
SiO <sub>2</sub>	50.45	49.54	49.75
Al <sub>2</sub> O <sub>3</sub>	15.32	15.52	14.75
Fe <sub>2</sub> O <sub>3</sub>	11.14	10.85	10.98
CaO	9.09	9.44	9.32
MgO	7.19	6.12	6.33
Na <sub>2</sub> O	2.96	3.04	3.00
K <sub>2</sub> O	1.34	1.39	1.34
TiO <sub>2</sub>	1.65	1.66	1.72
MnO	0.16	0.16	0.16
P <sub>2</sub> O <sub>5</sub>	0.45	0.47	0.49
LOI			
Total	99.75	98.19	97.84
Pb(ID)		4.94	
Rb(XRF)	20	24	19
Ba(XRF)	944	195	271
Th(INAA)	2.67		
Nb(XRF)	24	24	26
La(INAA)	27.0		
Ce(INAA)	54.1		
Sr(XRF)	486	467	517
Nd(ID)		24.35	
Sm(INAA)	5.38		
Zr(XRF)	171	168	180
Hf(INAA)	4.13		
Eu(INAA)	1.63		
Y(XRF)	32	33	34
Yb(INAA)	2.07		
Lu(INAA)	0.25		
Sc(INAA)	25.7		
Tb(INAA)	0.59		
Cr(INAA)	261		
Ni(INAA)	106		
<sup>87</sup> Sr/ <sup>86</sup> Sr <sub>(i)</sub>		0.70527	
<sup>143</sup> Nd/ <sup>144</sup> Nd		0.512449	
<sup>147</sup> Sm/ <sup>144</sup> Nd		0.13	
ε Nd		-3.61	
T <sub>DM</sub>		1029	
<sup>206</sup> Pb/ <sup>204</sup> Pb		17.39	
<sup>207</sup> Pb/ <sup>204</sup> Pb		15.46	
<sup>208</sup> Pb/ <sup>204</sup> Pb		37.45	

Table A-2: Analyses from Morikawa (1993 and unpublished data).

sample#	Tct2-1.1	Tct2-5.1	Tcr-6.5	Tct2-6.6	Tct2-7.1	Tct2-7.2	Tct2-7.3	Tct2-4.1
type	pumice	pumice	lava	pumice				pumice
SiO <sub>2</sub>	70.63	72.20	70.19	68.39	72.91	71.45	72.91	74.33
Al <sub>2</sub> O <sub>3</sub>	11.72	11.83	13.13	13.08	12.50	12.61	12.60	12.15
Fe <sub>2</sub> O <sub>3</sub>	0.81	1.10	1.63	1.09	1.18	1.60	1.56	0.93
CaO	1.46	1.17	0.68	0.66	1.05	2.13	2.50	0.56
MgO	0.34	0.17	0.00	0.01	0.51	0.75	0.46	0.00
Na <sub>2</sub> O	2.20	1.57	1.58	1.57	2.79	3.15	2.85	1.57
K <sub>2</sub> O	5.04	5.03	5.54	5.55	5.24	4.49	5.20	4.90
TiO <sub>2</sub>	0.14	0.12	0.20	0.20	0.18	0.23	0.23	0.10
MnO	0.04	0.04	0.05	0.04	0.04	0.05	0.06	0.05
P <sub>2</sub> O <sub>5</sub>	0.00	0.01	0.00	0.01	0.06	0.08	0.12	0.02
LOI								
Total	92.37	93.25	92.99	90.60	96.46	96.54	98.49	94.60
Pb(ID)								
Rb(XRF)	149	156	160	143	143	124	108	
Ba(XRF)	236	169	582	678	240	356	331	11
Th(INAA)	16.00	23.00	17.00	21.00	16.00	14.00	13.23	23.00
Nb(XRF)	17	22	23	23	19	19	17	31
La(INAA)								
Ce(INAA)								
Sr(XRF)	103	79	70	80	125	196	165	12
Nd(ID)								
Sm(INAA)								
Zr(XRF)	88	87	164	174	101	122	114	76
Hf(INAA)								
Eu(INAA)								
Y(XRF)	22	22	25	24	22	21	21	24
Yb(INAA)								
Lu(INAA)								
Sc(INAA)								
Tb(INAA)								
Cr(XRF)					26	41	47	
Ni(XRF)					10	15	17	
<sup>87</sup> Sr/ <sup>86</sup> Sr <sub>(i)</sub>	0.71007		0.70954					0.70820
<sup>143</sup> Nd/ <sup>144</sup> Nd								
<sup>147</sup> Sm/ <sup>144</sup> Nd								
ε Nd	-9.56		-10.09					-10.00
T <sub>DM</sub>								
<sup>206</sup> Pb/ <sup>204</sup> Pb	18.10		18.01					18.03
<sup>207</sup> Pb/ <sup>204</sup> Pb	15.58		15.56					15.58
<sup>208</sup> Pb/ <sup>204</sup> Pb	38.95		38.89					38.83

Table A-3: Normative mineralogy of the DSV rocks.

Sample #	Tra-3	Tra-4	Tra-57	Tra-31	Tra-43	Tra-6	Tra-27
quartz	0.00	5.89	8.53	7.40	8.63	9.67	6.89
orthoclase	12.73	28.23	27.43	18.16	26.32	22.60	25.90
albite	29.08	34.74	26.20	23.96	30.98	31.15	38.10
anorthite	27.15	18.55	13.46	19.98	15.52	18.22	12.76
corundum	0.00	0.00	0.00	0.00	0.00	0.00	0.00
diopside	14.22	0.79	9.28	13.09	6.23	5.60	5.01
hypersthene	6.52	6.28	9.51	11.68	7.00	8.04	6.30
olivine	3.85	0.00	0.00	0.00	0.00	0.00	0.00
magnetite	3.04	2.56	2.77	2.85	2.64	2.44	2.52
ilmenite	1.93	1.29	1.58	1.63	1.40	1.12	1.26
hematite	0.00	0.00	0.00	0.00	0.00	0.00	0.00
titanite	0.00	0.00	0.00	0.00	0.00	0.00	0.00
apatite	1.48	1.67	1.25	1.24	1.27	1.17	1.24
rutile	0.00	0.00	0.00	0.00	0.00	0.00	0.00
%anorthite	48.29	34.82	33.95	45.48	33.38	36.90	25.09
color index	29.56	10.93	23.13	29.26	17.27	17.20	15.10

Sample #	Tra-52	Tra-54	Tra-55	Tra-38	Tra-66	Tra-60	Tra-72
quartz	3.13	8.68	7.65	8.73	1.33	5.84	0.00
orthoclase	27.22	26.61	26.42	25.79	31.48	28.37	28.35
albite	33.80	35.83	37.43	31.19	39.65	41.65	31.71
anorthite	13.31	14.05	13.06	14.38	15.08	11.35	14.62
corundum	0.00	0.00	0.00	0.00	0.00	0.00	0.00
diopside	7.96	3.80	4.65	10.88	1.74	4.28	10.89
hypersthene	9.25	6.00	5.78	3.85	5.31	3.33	4.25
olivine	0.00	0.00	0.00	0.00	0.00	0.00	4.28
magnetite	2.65	2.53	2.54	2.61	2.64	2.58	2.83
ilmenite	1.38	1.23	1.27	1.31	1.37	1.32	1.62
hematite	0.00	0.00	0.00	0.00	0.00	0.00	0.00
titanite	0.00	0.00	0.00	0.00	0.00	0.00	0.00
apatite	1.31	1.27	1.21	1.24	1.39	1.28	1.44
rutile	0.00	0.00	0.00	0.00	0.00	0.00	0.00
%anorthite	28.25	28.17	25.86	31.56	27.55	21.42	31.56
color index	21.23	13.55	14.24	18.66	11.06	11.51	23.88

Table A-3: Normative mineralogy of the DSV rocks, continued.

Sample #	Tra-33	Tasa-82	Tasa-83	Tasa-74	Ttmt-18	Tcr-9310	Tcr-80
quartz	16.40	5.28	0.00	1.07	20.53	28.25	29.62
orthoclase	30.50	19.70	31.00	22.44	36.70	27.23	33.17
albite	34.15	29.11	27.38	33.29	34.22	30.46	31.39
anorthite	11.43	18.24	7.89	13.29	2.51	7.26	3.16
corundum	0.15	0.00	0.00	0.00	0.00	2.69	1.20
diopside	0.00	9.80	19.31	13.90	3.31	0.00	0.00
hypersthene	3.58	11.98	5.95	10.10	0.00	1.34	0.32
olivine	0.00	0.00	1.86	0.00	0.00	0.00	0.00
magnetite	1.99	2.92	3.19	2.90	0.00	2.03	0.00
ilmenite	0.84	1.74	2.08	1.76	0.08	0.55	0.08
hematite	0.14	0.00	0.00	0.00	1.25	0.00	0.80
titanite	0.00	0.00	0.00	0.00	0.66	0.00	0.00
apatite	0.80	1.23	1.34	1.24	0.21	0.22	0.13
rutile	0.00	0.00	0.00	0.00	0.00	0.00	0.13
%anorthite	25.08	38.51	22.37	28.54	6.84	19.24	9.16
color index	6.56	26.43	32.39	28.67	4.65	3.91	1.20

Sample #	Tct2-37	Tct2-41	Tpa-78	Tpa-931	Tpa-46	Tpa-69	Tpa-48
quartz	35.21	37.24	0.00	6.76	4.20	3.07	4.46
orthoclase	32.31	34.45	15.05	20.38	19.38	20.24	20.40
albite	23.40	23.09	25.95	26.45	30.36	33.20	30.56
anorthite	5.73	2.64	18.74	22.15	16.59	15.62	16.18
corundum	0.00	1.25	0.00	0.00	0.00	0.00	0.00
diopside	2.08	0.00	20.55	9.32	13.36	11.05	11.04
hypersthene	0.17	0.55	3.58	8.94	10.37	11.11	11.59
olivine	0.00	0.00	10.36	0.00	0.00	0.00	0.00
magnetite	0.00	0.00	2.81	2.90	2.84	2.83	2.86
ilmenite	0.07	0.08	1.64	1.71	1.67	1.67	1.71
hematite	0.52	0.53	0.00	0.00	0.00	0.00	0.00
titanite	0.14	0.00	0.00	0.00	0.00	0.00	0.00
apatite	0.38	0.13	1.31	1.40	1.22	1.24	1.20
rutile	0.00	0.04	0.00	0.00	0.00	0.00	0.00
%anorthite	19.66	10.26	41.94	45.58	35.33	31.99	34.62
color index	2.84	1.16	38.95	22.86	28.24	26.64	27.20

Table A-3: Normative mineralogy of the DSV rocks, continued.

Sample #	Tpa-11	Tpa-68	Tpa-51	Tpa-50	Ttmb-7	Ttmb-8	Ttmb-25
quartz	4.95	6.41	6.31	5.87	0.00	0.00	0.00
orthoclase	20.35	20.09	25.32	22.39	7.08	6.59	7.14
albite	29.01	27.75	29.86	28.42	27.25	27.22	26.43
anorthite	17.37	17.89	13.43	15.14	26.38	26.79	24.60
corundum	0.00	0.00	0.00	0.00	0.00	0.00	0.00
diopside	10.75	10.81	12.24	10.95	15.95	15.86	16.62
hypersthene	11.73	11.25	7.49	12.00	7.43	8.91	18.51
olivine	0.00	0.00	0.00	0.00	9.79	8.41	0.35
magnetite	2.87	2.92	2.68	2.64	3.20	3.24	3.29
ilmenite	1.71	1.73	1.46	1.42	2.15	2.20	2.26
hematite	0.00	0.00	0.00	0.00	0.00	0.00	0.00
titanite	0.00	0.00	0.00	0.00	0.00	0.00	0.00
apatite	1.27	1.15	1.20	1.16	0.76	0.76	0.81
rutile	0.00	0.00	0.00	0.00	0.00	0.00	0.00
%anorthite	37.45	39.19	31.03	34.76	49.19	49.60	48.21
color index	27.06	26.71	23.88	27.02	38.52	38.63	41.03

Sample #	Ttmb-14	Ttmb-15	Ttmb-16
quartz	0.00	0.00	0.04
orthoclase	8.02	8.47	8.20
albite	26.93	28.15	27.91
anorthite	24.89	25.38	23.66
corundum	0.00	0.00	0.00
diopside	14.27	15.82	16.76
hypersthene	17.17	12.99	16.39
olivine	2.09	2.39	0.00
magnetite	3.34	3.41	3.49
ilmenite	2.33	2.39	2.48
hematite	0.00	0.00	0.00
titanite	0.00	0.00	0.00
apatite	0.95	1.01	1.06
rutile	0.00	0.00	0.00
%anorthite	48.03	47.41	45.87
color index	39.20	36.99	39.12

Table A-4: Normative mineralogy of Morikawa data (1993 and unpublished data).

Sample#	Td2-1.1	Td2-5.1	Tcr-6.5	Td2-6.6	Td2-7.1	Td2-7.2	Td2-7.3	Td2-4.1
quartz	35.73	41.85	39.17	38.25	32.89	30.22		45.58
orthodase	32.79	32.75	36.04	37.03	32.54	27.80		31.45
albite	21.76	15.48	15.65	15.88	26.33	29.64		15.32
anorthite	7.99	6.42	3.71	3.70	5.06	7.35		2.87
corundum	0.00	2.01	3.98	4.04	0.54	0.00		3.91
diopside	0.00	0.00	0.00	0.00	0.00	2.04		0.00
hypersthene	0.96	0.51	0.00	0.03	1.48	1.15		0.00
olivine	0.00	0.00	0.00	0.00	0.00	0.00		0.00
magnetite	0.00	0.00	0.00	0.00	0.00	0.00		0.00
ilmenite	0.06	0.08	0.14	0.08	0.07	0.08		0.08
hematite	0.62	0.84	1.23	0.86	0.86	1.17		0.70
titanite	0.02	0.00	0.00	0.00	0.00	0.38		0.00
apatite	0.00	0.00	0.00	0.00	0.13	0.18		0.04
rutile	0.07	0.05	0.09	0.12	0.10	0.00		0.04
%anorthite	26.86	29.30	19.18	18.91	16.13	19.86		15.80
color index	1.64	1.43	1.37	0.97	2.41	4.44		0.78

## **Appendix B**

### **Analytical Techniques**

Thirty-eight samples were processed for major and trace element chemistry. Table B-1 summarizes the number of samples from each stratigraphic unit and the analytical techniques applied. The freshest samples possible were collected and broken into small chip sized fragments (1-5 cm) in the field and then stored in ziplock bags. Visible alteration was avoided as much as was practical but some noticeably altered samples had to be collected to provide adequate coverage of all stratigraphic units across the entire field area. Weathering rhines and filled vesicles were discarded in the field.

Rock chips were crushed in a Bico Chipmunk rock crusher down to < 5 mm. Crushed samples were examined and secondary minerals were removed. The samples were then powdered to < 325 mesh in a Bico Shatter Box. The Chipmunk and the Shatter Box both have tungsten-carbide crushing surfaces.

### **Major and Selected Trace Elements analysis with X-ray Fluorescence**

Thirty-eight samples were analyzed for major and certain trace elements (Zr, Rb, Sr, Nb, Y, Ba) with X-ray Fluorescence spectrometry (XRF). All XRF analyses were performed on a Rigaku 3030 spectrometer at the

University of Nevada, Las Vegas. Table B-2 presents the accuracy for the XRF major elements with replicate analyses of BIR-1 a USGS standard. Table B-3 presents the accuracy for the trace elements analyzed with XRF with replicate analyses of DR-N, also USGS standard. Fused glass disks were used for the major element analysis and pressed pellets for the trace elements. The fused glass discs were created by melting 9.00 g lithium tetra-borate ( $\text{Li}_2\text{B}_4\text{O}_7$ ), 0.16 g ammonium nitrate ( $\text{NH}_4\text{NO}_3$ ), and 1.00 g of powdered sample at  $1100^\circ\text{C}$  in Au-Pt crucibles. After 30 minutes of heating the melt was cooled slowly in an Au-Pt mold. The pressed pellets were created using 3.00 g of sample mixed with 0.60 g of methyl cellulose. The mixture was pressed to a methyl-cellulose backing in an Ashcroft hydraulic pellet press for 90 seconds at 3,000 psi. All ingredients were weighed to 0.0002 g. The pellets and discs were stored in a desiccator.

Loss on Ignition (LOI) was conducted on two of the mafic units (Table B-1) and on two of the felsic units (a tuff and rhyolite from the Culdesac complex). Approximated 3 g of sample was added to a previously dried and weighed ceramic crucible. The samples were then heated to  $1000^\circ\text{C}$  for two hours and gradually cooled in the oven and then desiccator until they could be weighed again.

#### **Rare-earth and trace element analysis (INAA)**

Thirty-one samples (Table B-1) were analyzed for rare-earth and trace elements using Instrumental Neutron Activation Analysis (INAA). Samples weighing approximately 0.2000 g were loaded in 8 cm lengths of Suprasil silica



tubing that were then weighed and melted closed. Tubes were first cleaned in a heated solution of 50% (by volume)  $\text{HNO}_3$  and then checked for leaks in the same solution after being sealed. The analyses were performed at the Phoenix Memorial Laboratory, Ann Arbor, Michigan. Precision and accuracy data for the INAA elements are found in Table B-4 (Yogodzinski, in review).

### **Isotopic Analysis (TIMS)**

Fifteen samples were analyzed for Nd, Sr, and Pb isotopic ratios by Thermal Ionization Mass Spectrometry (TIMS). Approximately 5 g of sample was sent to the lab in a glass screw-top vial. The analyses were performed on a VG Sector 54 mass spectrometer at the University of Kansas, Lawrence. A thorough description of the procedure can be found in Feuerbach et al. (1993).

Table B-1: Analytical procedures.

Summary of Analytical Procedures				
Unit	XRF	LOI	INAA	Isotopes
basalt of Table Mtn	6		3	2
andesite of Powerline Rd	10	1	9	4
rhyolite of Culdesac Wash	4	2	2	2
andesite of Alta Spring	4		4	2
tuff of Table Mtn	1		1	1
andesite of Rodeo Grounds	13	1	12	5
<b>Total</b>	<b>38</b>	<b>4</b>	<b>31</b>	<b>16</b>

Table B-2: Accuracy for major elements.

element	Published values for BIR-1	Average of 21 analyses	Percent error
SiO <sub>2</sub>	47.77	47.08	1%
Al <sub>2</sub> O <sub>3</sub>	15.65	15.09	4%
TiO <sub>2</sub>	0.96	0.95	1%
Fe <sub>2</sub> O <sub>3</sub>	11.26	11.13	1%
CaO	13.24	13.05	1%
K <sub>2</sub> O	0.03	0.03	3%
MnO	0.17	0.17	0%
P <sub>2</sub> O <sub>5</sub>	0.05	0.05	18%
Na <sub>2</sub> O	1.75	1.65	6%
MgO	9.68	9.61	1%
<b>Total</b>	<b>100.55</b>	<b>98.82</b>	<b>2%</b>

Table B-3: Accuracy of the XRF trace elements.

element	# of analyses	DR-N Published	Average	%error
Zr	11	125	143	14%
Sr	11	400	410	2%
Nb	14	8	9	7%
Y	10	28	30	7%
Rb	10	73	75	2%
Ba	10	385	334	13%

## References

- Anderson, R. E., 1971, Thin skin extension in Tertiary rocks of southeastern Nevada: Geological Society of America Bulletin, v. 82, p. 43-58.
- Anderson, R. E., Longwell, C. R., Armstrong, R. L., and Marvin, R. F., 1972, Significance of K-Ar ages of Tertiary rocks from the Lake Mead region, Nevada-Arizona: Geological Society of America Bulletin, v. 83, p. 273-288.
- Arndt, N. T. and Christensen, U., 1992, The role of lithospheric mantle in continental flood volcanism: Thermal and geochemical constraints: Journal of Geophysical Research, v. 97, p. 10,967-10,981.
- Bennet, V. C., and DePaolo, D. J., 1987, Proterozoic crustal history of the western United States as determined by neodymium isotopic mapping: Geological Society of America Bulletin, v. 99, p. 974-685.
- Bradshaw, T. K., 1991, Tectonics and magmatism in the Basin and Range province of the western United States' [Ph.D. Thesis]: Milton Keynes, Open University, 240 p.
- Bradshaw, T. K., Hawkesworth, C. J., and Gallagher, K., 1993, Basaltic volcanism in the Southern Basin and Range: No role for a mantle plume: Earth and Planetary Science Letters, v. 116, p. 45-62.
- Bridwell, H. L., 1991, The Sloan Sag: A mid-Miocene volcanotectonic depression, north-central McCullough Mountains, southern Nevada [M.S. Thesis]: Las Vegas, University of Nevada, 147 p.
- Cascadden, T., 1991, Style of volcanism and extensional tectonics in the eastern Basin and Range province, northern Mohave County, Arizona [M.S. Thesis]: Las Vegas, University of Nevada, p. 156.
- Calderone, G. J., Butler, R. F. and Acton, G. D., 1991, Paleomagnetism of Middle Miocene volcanic rocks in the Mojave-Sonora desert region of western Arizona and southeastern California: Journal of Geophysical Research, v. 95, 625-647 p.
- Carmichael, I. S. E., Turner, F. J., and Verhoogen, J., 1974, Igneous petrology: New York, McGraw Hill Book Company, 739 p.
- Daley, E. E., and DePaolo, D. J., 1992, Isotopic evidence for lithospheric

thinning during extension: Southeastern Great Basin: *Geology*, v. 20, p. 104-108.

Dalrymple, G. B., 1979, Critical tables for the conversion of K-Ar ages from old to new constants: *Geology*, v. 7, no. 11, p. 558-560.

DePaolo, D. J., 1981, Neodymium isotopes in the Colorado Front Range and crust-mantle evolution in the Proterozoic: *Nature*, v. 291, p. 193-196.

Dudas, F. O., Carlson, R. W., and Eggler, D. H., 1987, Regional middle Proterozoic enrichment of the subcontinental mantle source of igneous rocks from central Montana: *Geology*, v. 15, p. 22-25.

Duebendorfer, E. M., Sewall, A. J., and Smith, E. I., 1990, The Saddle Island detachment; An evolving shear zone in the Lake Mead area, Nevada *in* Wernicke, B. P. ed., Basin and Range extensional tectonics near the latitude of Las Vegas, Nevada: Geological Society of America Memoir 176, p. 77-97.

Falkner, C., 1993, History and petrogenesis of the Aztec Wash pluton, Eldorado Mountains, Nevada [M.S. Thesis]: Nashville, Tennessee, Vanderbilt University, 204 p.

Falkner, C. M., Miller, C. F., Wooden, J. L., and Heizler, M. T., 1995, Petrogenesis and tectonic significance of the calc-alkaline, bimodal Aztec Wash pluton, Eldorado Mountains, Colorado River extensional corridor: *Journal of Geophysical Research*, v. 100, No. B7, p. 10,453-10,476.

Faulds, J. E., 1993a, The Mt. Perkins block, northwestern Arizona: An exposed cross-section of a synextensional volcano in highly extended terrane: *Geological Society of America Abstracts with Programs*, v. 25(5), p. A36.

Faulds, J. E., 1993b, Miocene stratigraphy of the central Black Mountains, Northwestern Ariz.: Variations across a major accommodation zone *in* Sherrod, D. R. and Nielson, J. E. eds., Tertiary stratigraphy of highly extended terranes, California, Arizona, and Nevada: U.S. Geological Survey, U.S. Geological Survey Bulletin 2053, p. 37-43.

Faulds, J. E., Geissman, J. W., and Mawer, C. K., 1990, Structural development of a major extensional accommodation zone in the Basin and Range Province, northwestern Arizona and southern Nevada; Implications for kinematic models of continental extension *in* Wernicke, B. P. eds.,

Basin and Range extensional tectonics near the latitude of Las Vegas, Nevada: Geological Society of America Memoir 176, 37-76 p.

- Faulds, J. E., Gans, B., and Smith, E. I., 1994, Spatial and temporal patterns of extension in the northern Colorado River extensional corridor, northwestern Arizona and southern Nevada: Geological Society of America Abstracts with Programs, v. 26(2), p. A51.
- Faulds, J. E., Feuerbach, D. L., Reagan, M. K., Metcalf, R. V., Gans, P., and Walker, J. D., 1995, The Mt. Perkins Block, northwestern Arizona: An exposed cross section of an evolving, pre- to synextensional magmatic system: Journal of Geophysical Research, v. 100, p. 15,249-15,266.
- Faure, G., 1986, Principles of isotope geology, Second Edition: New York, John Wiley & Sons, p. 589.
- Feuerbach, D. L., Smith, E. I., Shfiqullah, M., and Damon, P. E., 1991, New K-Ar dates for late Miocene to early Pliocene mafic volcanic rocks in the Lake Mead area, Nevada and Arizona: Isochron/West, v. 57, p. 17-20.
- Feuerbach, D. L., Smith, E. I., Walker, J. D., and Tangeman, J. A., 1993, The role of the mantle during crustal extension: Constraints from geochemistry of volcanic rocks in the Lake Mead area, Nevada and Arizona: Geological Society of America Bulletin, v. 105, p. 1561-1575.
- Fisher, R.V. and Schmincke, H.V., 1984, Pyroclastic Rocks: Springer-Verlag, New York, 472 p.
- Fitton, J. F., James, D., and Leeman, W. P., 1991, Basic magmatism associated with Late Cenozoic extension in the Western United States: Compositional variations in space and time: Journal of Geophysical Research, v. 96, p. 13,693-13,711.
- Frey, F. A., and Printz, M., 1978, Ultramafic inclusions from San Carlos, Arizona: Petrologic and geochemical data bearing on their petrogenesis: Earth and Planetary Science Letters, v. 38, p. 129-176.
- Gallagher, K. and Hawkesworth, C. J., 1992, Dehydration melting and the generation of continental flood basalts: Nature, v. 358, p. 57-59.
- Glazner, A. F., 1990, Recycling of continental crust in Miocene volcanic rocks from the Mojave block, southern California in Anderson, J. L. eds., The nature and origin of Cordilleran magmatism: Geological Society

of America Memoir 174, 147-168 p.

- Glazner, A. F., and Bartley, J. M., 1984, Timing and tectonic setting of Tertiary low-angle normal faulting and associated magmatism in the southwestern United States: *Tectonics*, v. 3, p. 385-396.
- Glazner, A. F., and Farmer, G. L., 1991, Production of isotopic variability in continental basalts by cryptic crustal contamination: *Science*, v. 255, p. 72-74.
- Glazner, A. F., Farmer, G. L., Hughes, W. T., Wooden, J. L., and Pickthorn, W., 1991, Contamination of basaltic magma by mafic crust at Amboy and Pishah Craters, Mojave Desert, California: *Journal of Geophysical Research*, v. 96, No. B8, p. 13,673-13,691.
- Hofmann, A. W., 1988, Chemical differentiation of the Earth: the relationship between mantle, continental crust, and oceanic crust: *Earth and Planetary Science Letters*, v. 90, p. 297-314.
- Howard, K. A., and John, B. E., 1987, Crustal extension along a rooted system of imbricate low-angle faults: Colorado River extension corridor, California and Arizona in Coward, M. P., Dewey, J. F. and Hancock, P. L. eds., *Continental Extensional Tectonics*: Geological Society of London Special Publication, 28, p. 299-311.
- Ionov, D. A., Kramm, U., and Stosch, H.-G., 1992, Evolution of the upper mantle beneath the southern Baikal rift zone: and Sr-Nd isotope study of xenoliths from the Bartoy volcanoes: *Contributions to Mineralogy and Petrology*, v. 111, p. 235-247.
- Irvine, T. N., and Baragar, W. R. A., 1971, A guide to the chemical classification of the common volcanic rocks: *Canadian Journal of Earth Sciences*, v. 8, p. 523-548.
- Kempton, P. D., Fitton, J. G., Hawkesworth, C. J., and Ormerod, D. S., 1991, Isotopic and trace element constraints on the composition and evolution of the lithosphere beneath the southwestern United States: *Journal of Geophysical Research*, v. 96, No. B8, p. 13,713-13,735.
- Larsen, L. L., and Smith, E. I., 1990, Mafic enclaves in the Wilson Ridge pluton, Northwestern Arizona: Implications for the generation of a calc-alkaline intermediate pluton in an extensional environment: *Journal of Geophysical Research*, v. 95, p. 17,693-17,716.

- McDonough, W. F., 1990, Constraints on the composition of the continental lithospheric mantle: *Earth and Planetary Science Letters*, v. 101, p. 1-18.
- McKenzie, D. and Bickle, M. J., 1988, The volume and composition of melt generated by extension of the lithosphere: *Journal of Petrology*, v. 29, p. 625-679.
- Metcalf, R. V., Smith, E. I., and Mills, J. G., 1993, Magma mixing and commingling in the northern Colorado River extensional corridor; Constraints on the production of intermediate magma - Part I in Lahen, M. M., Trexler, J.H., and Spinoza, C. eds., *Crustal evolution of the Great Basin and Sierra Nevada: Cordilleran/Rocky Mountain Section, Geological Society of America Guidebook: Department of Geological Sciences, University of Nevada, Reno*, p. 35-55.
- Metcalf, R., Smith, E. I., Walker, J. D., Reed, R. C., and Gonzalez, D. A., 1995, Isotopic disequilibrium among commingled hybrid magmas: Evidence for a two-stage magma mixing-commingling process in the Mt. Perkins pluton, Arizona: *Journal of Geology*, v. 103, p. 509-527.
- Meyers, I. A., 1984, *Geology and mineralization at the Cyclopic Mine, Mohave County, Arizona [M.S. Thesis]: University of Nevada, Las Vegas*, 64 p.
- Morikawa, S. A., 1994, *The Geology of the mid-Miocene Tuff of Bridge Spring: Southern Nevada and northwestern Arizona [M.S. Thesis]: Las Vegas, University of Nevada*, 175 p.
- Ormerod, D. S., Rogers, N. W., and Hawkesworth, C. J., 1991, Melting of the lithospheric mantle: Inverse modeling of alkali-olivine basalts from the Big Pine Volcanic Field, California: *Contributions to Mineralogy and Petrology*, v. 108, p. 305-317.
- Reynolds, S. J., 1988, *Geologic Map of Arizona, Map 26: Arizona Geological Survey, Scale 1:1,000,000*.
- Smith, E. I., and Faulds, J. E., 1994, Patterns of Miocene magmatism in the northern Colorado River extensional corridor, Nevada, Arizona, and California: *Geological Society of America Abstracts with Programs*, v. 26(2), p. A93.
- Smith, E. I., Feuerbach, D., Naumann, T. R., and Mills, J. G., 1990, Mid-Miocene volcanic and plutonic rocks in the Lake Mead area of Nevada

- and Arizona; Production of intermediate igneous rocks in an extensional environment *in* Anderson, J. L. ed., The nature and origin of Cordilleran magmatism: Geological Society of America Memoir 174, p. 163-193.
- Smith, R. B., Nagy, W. C., Julande, K. A., Viveiros, J. J., and Barker, C. A., 1989, Geophysical and tectonic framework of the eastern Basin and Range-Colorado River region, California, Arizona, and Nevada *in* Pakiser, L. C. and Mooney, W. D. eds., Geophysical framework of the continental United States: Geological Society of America Memoir 172, p. 205-233.
- Sun, S.-s., and McDonough, W. F., 1989, Chemical and isotopic systematics of oceanic basalts: implications for mantle composition and processes *in* Saunders, A. D. and Norry, M.J. eds., Magmatism in the Ocean Basins: Geological Society Special Publications, no. 42, p. 313-345.
- Takahashi, E., and Kushiro, I., 1983, Melting of a dry peridotite at high pressures and basalt magma genesis: *American Mineralogist*, v. 68, p. 859-879.
- Thompson, K. G., 1985, Stratigraphy and petrology of the Hamblin-Cleopatra volcano, Clark County, Nevada [M.S. Thesis]: Austin, Texas, University of Texas, 306 p.
- Theodore, T. G., Blair, W. G., Nash, J. T., McKee, E. H., Antweiler, J. C. and Campbell, W. L., 1982, Geology and gold mineralization of the Gold Basin-Lost Basin mining districts, Mohave County, Arizona: U.S. Geological Survey Open File Report 82-1052, 167 p.
- Turner, R. D., and Glazner, A. F., 1991, Miocene volcanism, folding, and faulting in the Castle Mountains, southern Nevada and eastern California *in* Wernicke, P. B. eds., Basin and Range extensional tectonics at the latitude of Las Vegas: Geological Society of America Memoir 176, 23-35 p.
- Weber, M. E., and Smith, E. I., 1987, Structural and geochemical constraints on the reassembly of disrupted mid-Miocene volcanoes in the Lake Mead-Eldorado Valley area of southern Nevada: *Geology*, v. 15, p. 553-556.
- Wendlandt, E., DePaolo, D. J., and Baldrige, W. S., 1993, Nd and Sr isotope chronstratigraphy of the Colorado Plateau lithosphere: Implications for magmatic and tectonic underplating of the continental crust: *Earth and*



Planetary Science Letters, v. 116, p. 23-43.

Wernicke, B., Axen, G. J., and Snow, J. K., 1988, Basin and Range extensional tectonics at the latitude of Las Vegas, Nevada: Geological Society of America Bulletin, v. 100, p. 1738-1757.

Wilson, M., 1989, Igneous petrogenesis: A global tectonic approach: London, Unwin Hyman, 465 p.

Yogodzinski, G. M., Naumann, T.R., Smith, E.I., Bradshaw, T.K., Walker, J.D., in review, Crustal assimilation by alkalic basalt, and the evolution of a mafic volcanic field in the central Great Basin, South-Central Nevada: Journal of Geophysical Research.

Yogodzinski, G. M., Volynets, O. N., Koloskov, A. V., Seliverstov, N. I. and Matvenkov, V. V., 1994, Magnesian andesites and the subduction component in a strongly calc-alkaline series at Piip Volcano, Far Western Aleutians: Journal of Petrology, v. 35, p. 163-204.